1967

A theoretical investigation of elastic and Voigt transient spherical waves, and plane three-element viscoelastic waves

Edward Hornsey
Missouri University of Science and Technology

Department: Physics

A THEORETICAL INVESTIGATION OF ELASTIC AND VOIGT TRANSIENT SPHERICAL WAVES, AND PLANE THREE-ELEMENT VISCOELASTIC WAVES

by

EDWARD EUGENE HORNSEY -1937

A DISSERTATION

Presented to the Faculty of the Graduate School of the

UNIVERSITY OF MISSOURI AT ROLLA

In Partial Fulfillment of the Requirements for the Degree

DOCTOR OF PHILOSOPHY

1967

George B. Clark
Advisor

Peter J. Henderson

Roger A. Raffield

Charles E. Antle

R. J. Davidson

ABSTRACT

A mathematical model of explosive generated waves in rock is needed in many areas of engineering endeavor. Investigations to date have been unsuccessful in obtaining a model that satisfactorily represents real wave phenomena at all radial distances and in all of the important characteristics.

In this investigation, spherical waves in elastic and Voigt media were investigated. Series solutions for plane waves in a three-element viscoelastic medium were obtained. A dual exponential pressure pulse, $P(t) = P_o(e^{-\alpha t}-e^{-\beta t})$, was assumed because it can exhibit significant features of real pressure pulses while avoiding instantaneous rise time, which is an objectionable feature of some of the models frequently employed in the literature.

The most significant correlation of elastic and real waves was their similar decay rates for peak values of particle velocity and displacement at large radial distances. At intermediate distances, Voigt waves exhibited pulse lengthening and peak value attenuation rates similar to those reported for real waves, but the arrival time was much too early.

It was concluded that elastic and Voigt spherical waves, and three-element viscoelastic plane waves are not sufficient to represent explosive generated waves in rock. On the basis of this and other investigations cited in the literature it appears that a mechanism for attenuation other than, or in addition to, viscosity will be needed to satisfactorily represent waves in rock.

ACKNOWLEDGEMENTS

The author wishes to express his gratitude first to his wife, for her patience throughout this research and the graduate studies which preceded it. He is especially indebted to Dr. George B. Clark, his dissertation supervisor, for his encouragement, guidance, and financial support through summer research appointments; and to Prof. R. F. Davidson, Chairman of the Engineering Mechanics Dept., for his encouragement and support. He is also indebted to James Jamison for checking some of the mathematical developments of Chapter V, and who in conjunction with James Wade of the Computer Center was responsible for the original programming of the Voigt spherical waves of which the computer program used in this investigation was a modification. Appreciation is also expressed to Mrs. Annette Anderson for typing the manuscript.

TABLE OF CONTENTS

LIST OF FIGURES

LIST OF SYMBOLS

a = effective cavity radius

$a\alpha$ = product of a and α

A = acceleration

$[A]$ = polonomial in the transform variable s

b_m = constants

c = dilatational wave velocity = $[(\lambda+2\mu)/\rho]^{\frac{1}{2}}$

c = longitudinal wave velocity = $(E/\rho)^{\frac{1}{2}}$

$D_{-n}(Y)$ = parabolic cylinder function of the negative integral order

$D_{i,j}(Z)$ = $\frac{d^i}{dZ^i}(Z^{j-1} e^{-Z})$ $\quad i \geq 0$

$DE_{i,j}(Z)$ = combined notation, represents $D_{i,j}(Z)$ for $i \geq 0$, represents $E_{i,j}(Z)$ for $i \leq 0$

e = exponential

$E_{i,j}(Z)$ = $\int_0^Z \int_0^{t_2} \cdots \int_0^{t_i} \tau^{j-1} e^{-\tau} \, d\tau, \, dt_i, \ldots, dt_2$ $\quad i \geq 0$

E = modulus of elasticity (Young's modulus)

Ee = equivalent modulus of elasticity

EXP = $\exp(-T-R^{-2}/8T)$

$F(\nu,n)$ = $\dfrac{(-1)^{\nu}(2\nu-n-1)!}{2^{2\nu-n}(\nu-n)!(\nu)!(n-1)!(\nu-1)!}$

$H(t-t_o)$ = unit step function (Heaviside's step function)

k = scale factor or summation index

K = constant

L = constant

m = summation index

M = constant

n = summation index

p = subscript indicating peak value

p_o = constant

$P(t)$ = pressure pulse function

P_o = constant

q_o = constant

q_1 = constant

r = radial distance

R = dimensionless radial distance = $\omega_o(r-a)/c$

s = Laplace transform variable

t = time

t_o = constant (time)

T = dimensionless time = $\omega_o t$

u = radial displacement or longitudinal displacement

v = particle velocity

x = longitudinal distance

X = dimensionless distance = $\omega_o x/c$

z = summation parameter, integer

Z = $T-X = \omega_o(t-x/c)$

α = constant (pressure pulse parameter)

β = constant (pressure pulse parameter)

γ = constant = $1-\alpha/\omega_o$

$\delta(t-t_o)$ = unit impulse (Dirac delta function)

ε = normal strain

η = damping coefficient = E/ω_o

λ = Lame's constant (elastic)

λ' = corresponding viscoelastic modulus

μ = elastic shear modulus

μ' = corresponding viscoelastic modulus

ν = Poisson's ratio or summation index

ρ = density

Σ = summation

σ = normal stress

τ = time = $t-(r-a)/c$

ϕ = displacement potential ($u = \partial\phi/\partial r$)

χ = constant = E_1/E_2

ω = circular frequency

ω_o = transition frequency

$\doteqdot$ = symbol connecting a function and its transform

$\overline{\ }$ = transform of the variable when appearing as a bar over a variable

CHAPTER I

INTRODUCTION

Real Earth Waves. Many areas of engineering endeavor are affected either directly or indirectly by the effects of explosive generated waves in rock masses. The civil engineer and the mining engineer are concerned not only with the breakage and removal of materials with explosives, but must also concern themselves with undesirable side effects in surrounding areas such as foundation and structural damage, and damage to utilities. Mine and tunnel supports of all types are vulnerable to blast damage, particularly where they are subjected to repeated blasting effects. Explosive generated waves can fracture and weaken natural rock pillars and roof, and may lead to spalling or slabbing if the blast is of sufficient intensity or repeated often enough.

Geophysicists are also concerned with wave motion through rock masses. The seismologist interested in seismic prospecting utilizes explosive generated waves in his investigations and the earthquake seismologist studies naturally occurring and man-made waves in the crust of the earth.

Engineers involved with the design of underground and above ground protective structures are intimately concerned with the problem of wave propagation through rock masses. Military engineers are frequently faced with the opposite problem, that of destroying underground fortifications and tunnels.

Theoretical analyses of wave motion in solid media have generally been made starting with the assumption that the wave front is either plane or spherical.

The simplest mathematical model, the elastic, has been investigated in considerable detail. The plane wave elastic problem is relatively simple, and is found in many mathematics texts on partial differential equations and transform calculus. The elastic plane waves offer a first approximation of wave shape in real materials, but no mechanism for attenuation; therefore, the wave shape and amplitude remain constant with travel distance.

Literature Review. The spherical elastic problem has been investigated extensively. Sharpe (1) used the Fourier integral to obtain the displacement caused by a unit step pressure pulse; he then obtained the displacement for several other pressure pulses using the solution for the unit step in conjunction with Duhamel's integral. Duvall (2) investigated spherical elastic waves caused by a dual exponential pressure pulse of the form $P(t) = P_o \left[e^{-\alpha t} - e^{-\beta t} \right]$. He compared theoretically predicted strain waves with experimentally determined values. Goldsmith (3) made an extensive investigation of spherical elastic waves generated by a single decay exponential pressure pulse, $P(t) = P_o\, e^{-\alpha t}$. Experimental evidence shows that waves generated by explosive sources are not adequately described by elastic wave theory, particularly at small distances from the explosion.

Since the elastic model has been shown to be inadequate, many other models have been proposed which include mechanisms for damping or attenuation. In addition to his extensive discussion of elastic wave phenomena, Kolsky (4) discusses internal friction mechanisms including viscoelastic and plastic theory. Bland (5) investigated the linear viscoelastic models and discusses the correspondence principle between the elastic and linear viscoelastic solutions. Clark (6) summarizes the progress to date on elastic, solid friction, and viscoelastic wave phenomena. Much of the effort to obtain a better model has centered around the viscoelastic models. These models can be represented physically by parallel and series combinations of linear springs and dashpots (Appendix A).

Most of the published literature dealing with viscoelastic models has been concerned with plane wave propagation. Most of this work has been purely mathematical and solutions were generally left in terms of complicated integral transforms or convolution integrals.

Some of the most significant work, involving theoretical solutions and numerical evaluation, on the Voigt model (a spring in parallel with a dashpot) has been done by Collins (7) in his study of plane Voigt waves; Rupert (8), Clark and Rupert (9) and Clark, Rupert, and Jamison (10) in their studies of plane and spherical Voigt waves.

Other studies of plane wave propagation in a linear

viscoelastic medium include the investigations of the Maxwell model (a spring and a dashpot in series) by Lee and Kanter (11) using Laplace transforms and the method of images to solve finite rod problems. Hanin (12) obtained single infinite series solutions for displacement in a plane Voigt medium, assuming a unit impulse displacement function. The Voigt and three-element viscoelastic models were investigated by Morrison (13), and integral solutions for the velocity and stress were obtained. Glauz and Lee (14) employed the method of characteristics to obtain numerical solutions for the four element model sometimes called the Burger model (a Maxwell model in series with a Voigt model). They determined stresses, strains, and velocities for a semi-infinite bar subjected to a constant velocity at one end.

Lee and Morrison (15) obtained integral solutions for stresses in viscoelastic rods of semi-infinite extent subjected to constant velocity and constant stress conditions at the free end. Their investigations include elastic, viscous, and two, three, and four element viscoelastic models using Laplace transforms in the solutions. Uniaxial wave propagation in a three element linear viscoelastic material was investigated by Arenz (16) using an extension of the Schapery collocation inversion method. He states that such a simple model is not sufficient to represent real viscoelastic properties of materials such as polyurethane. Berry and Hunter (17) discuss the general viscoelastic model and give integral solutions for several boundary conditions for finite

and semi-infinite rods. Allen and Robinson (18) investigated the problem of a plane wave interacting with a spherical cavity. They assumed both elastic and viscoelastic media and used a numerical inversion similar to the method of Papoulis.

The spherical viscoelastic wave problem has been investigated to a much lesser extent than has the plane wave problem. In addition to the references previously cited on the spherical Voigt model, Lee (19) investigated the Voigt model but altered it by the introduction of a 'constant loss factor'. Berry (20) obtained an integral solution for the displacement for the spherical symmetric wave problem using as his model 'a kind of Maxwell solid'. Lockett (21) investigated the general viscoelastic model for spherical wave propagation and obtained solutions by numerical integration.

There has been very little effort, reported in the literature, correlating theoretical and real wave phenomena in rock. None of the investigators has reported a model which satisfactorily represents real wave phenomena in rock, except under very restricted conditions.

Objectives of the Investigation. The objectives of this investigation were essentially four fold: (a) to select a mathematical model for an explosive generated pressure pulse that is desirable both from a mathematical and experimental point of view; (b) to conduct a parameter study of spherical symmetric elastic waves generated by that pressure pulse; (c) to conduct a

parameter study of spherical waves in a Voigt medium generated by the same pressure pulse and to compare Voigt waves with elastic and real earth waves and; (d) to develop series solutions for plane waves in a three-element viscoelastic medium (an elastic element in series with a Voigt model) for unit impulse, unit step, single and dual decay exponential pressure pulses.

A detailed discussion of pressure pulses and the selection of a mathematical model that conforms reasonably well with observed phenomena, while avoiding the mathematical objection of instantaneous rise time, is given in Chapter II.

The parameter studies of the elastic and Voigt spherical waves include studies of the effects of variation of pressure pulse parameters, elastic and viscoelastic properties, cavity radius, radial distance, and time. Five radial properties of the wave motion were studied: displacement, particle velocity, acceleration, stress, and strain. A parameter study of spherical elastic wave propagation is desirable from the standpoint of better understanding theoretical wave phenomena and to give a basis for comparison for the viscoelastic models, particularly the Voigt. The elastic parameter study is given in Chapter III and the Voigt spherical study in Chapter IV.

Chapter V is devoted to the solution of the three-element plane wave problem. Double series solutions for the unit impulse and unit step pressure pulses are given. Triple series solutions were required for the single decay exponential pressure pulse.

Solutions for the dual exponential pressure pulse were obtained by superposition of two single decay exponential pressure pulse solutions.

The figures have been included at the end of the respective chapters in which they are discussed.

CHAPTER II

MATHEMATICAL MODELS OF EXPLOSIVE GENERATED PRESSURE PULSES

Requirements of the Model. One of the first problems encountered in the study of waves originating from an explosive or other transient source is that of finding a suitable mathematical model to represent the pressure pulse. This selection is governed by the physical phenomena, as well as by the degree of difficulty encountered in solving the resulting boundary value problem. Solutions of wave equations in the transform plane, using Laplace transforms, are relatively easy to obtain, but inversion to the time plane is generally quite difficult. The selection of a mathematical model has frequently been made on the basis of the path of least resistance, from a mathematical point of view.

The problem reduces to that of finding as simple a mathematical model as is possible while still representing the pressure pulse to an acceptable degree of accuracy.

The selection is hampered by lack of knowledge about the pressure time relationship very near an explosive source. Physical measurements show that the general characteristics of an explosive generated pressure pulse include an extremely rapid rise time to peak pressure and a much slower decay rate. Cole (22) gives several examples of experimentally determined pressure pulses caused by underwater explosions.

The selection of a pressure pulse model is further

complicated by the fact that very near a high explosive or nuclear explosive detonation the medium is vaporized, and at larger distances it is crushed. Elastic or viscoelastic wave phenomena, therefore, would not apply at distances very near the detonation but might be applicable at distances greater than an effective cavity radius a. The pressure pulse at the effective cavity radius is therefore needed in the study of elastic and viscoelastic wave phenomena generated by an explosive source. The effective cavity radius is also needed and it probably depends on the properties of the medium, and the type, size, and geometry of the explosive. Very little research has been done in determining effective cavity radius.

Unit Impulse Function. Frequently in the literature, the unit impulse (Dirac delta function) has been used to represent a very sharp pressure pulse. Collins (23), for example, used the unit impulse to represent a hammer blow. Tse, Morse, and Hinkle (24) state that the unit impulse can be used to represent phenomena such as impact, provided the duration of the impact is very short compared with the natural frequency of the system. It can be formally defined as a 'function' with the properties:

$$\delta(t - t_o) = 0 \qquad t \neq t_o$$

$$\int_{-\infty}^{\infty} \delta(t - t_o)\,dt = 1 \tag{1}$$

$$\left\{ \delta(t - t_o) \right\} \doteq e^{-t_o s}$$

Unit Step Function. The unit impulse is closely related to another discontinuous function, the unit step function (Heaviside's step function). The unit step function has the properties:

$$H(t - t_o) = \begin{cases} 0 & t < t_o \\ 1 & t > t_o \end{cases}$$

$$\left\{ H(t - t_o) \right\} = \frac{e^{-t_o s}}{s} \qquad (2)$$

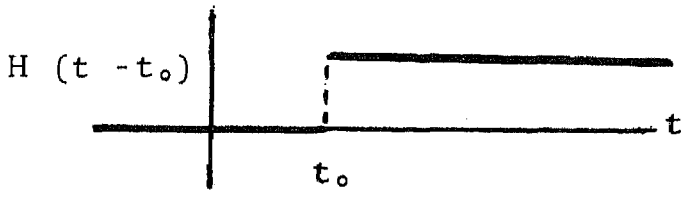

It can be shown that the unit impulse function is the first derivative of the unit step function with respect to time.

$$\delta(t - t_o) = H'(t - t_o) \qquad (3)$$

The first derivative of the unit impulse with respect to time is sometimes encountered in the literature and it is generally referred to, in mechanics applications, as a doublet of unit movement. Higher derivatives are seldom encountered in engineering literature.

The unit step function and the unit impulse function both belong to a generalization of functions called distributions. Rigorous treatments of the properties and transforms of these

'functions' are lengthy and involved, and considerable mathematical controversy has been connected with the unit impulse. These 'functions' are discussed in most operational mathematics books, vibrations books, and many other books dealing with applied mathematics. [Ref. Churchill (25)].

The unit impulse is often the simplest mathematical model to use for representing a pressure pulse when operational methods are employed. It is, however, not always a desirable model because of the instantaneous rise and fall times. This instantaneous rise time leads to some undesirable effects in the mathematical models for wave propagation; for example, an instantaneous finite value of particle velocity with the arrival of the wave front in the elastic wave problem.

Solutions based on the unit impulse and unit step 'functions' are useful however, as they can be employed to obtain the solutions for other forcing functions by means of convolution.

Single Decay Exponential. The single decay exponential, $P(t) = P_o\, e^{-\alpha t}$, comes somewhat closer to representing the type pressure pulse that experimental evidence and intuition would lead one to expect. Probably the greatest objection to this model is the instantaneous rise time that was found in the previous two models.

Sharpe (26) employed the single decay exponential to represent a pressure pulse, and then let $\alpha = 0$ to obtain the solutions for the unit step function. Goldsmith (27) represented an explosive pressure pulse by a single decay exponential, in his study

of spherical elastic wave propagation.

Examples of the single decay exponential are given in Figure 1, with P_o equal to one. The decay exponential can be scaled timewise by dividing α by a scale factor $\underline{k}$, which simply expands the time scale by the factor $\underline{k}$.

Dual Decay Exponential. A combination of two decay exponentials of the form

$$P(t) = P_o \left(e^{-\alpha t} - e^{-\beta t}\right) \qquad \beta > \alpha \tag{4}$$

gives a reasonable pressure pulse shape with considerable flexibility. This function has the advantage of being relatively simple mathematically, continuous, and easily scaled timewise. It has no instantaneous rise or fall time as did the models previously discussed. This model is compatible with observed phenomena, as it may have a relatively fast rise time and a slower decay time. The rise time can be made any desired value simply by choosing the proper combination of α and β. Hereafter this model will be referred to as the dual exponential. Some examples are given in Figure 2.

Time scaling can be accomplished as in the case of the single decay exponential, by dividing the constants α and β by the scale factor $\underline{k}$.

Duvall (28) represented an explosive generated pressure pulse by the dual exponential in his studies of spherical elastic wave propagation.

Figures 3, 4, and 5 show some of the interesting and useful

properties of the dual exponential pressure function. Figure 3 gives the relationship between the β/α ratio and the time to the peak amplitude for several different values of α. Mathematically, the time to the peak amplitude is

$$t_p = \ln(\beta/\alpha) \; / \; [\, \alpha \; (\beta/\alpha - 1)]. \qquad (5)$$

Figures 4 and 5 give information that is useful in analyzing the rate of decay of the dual exponential pressure pulse. Figure 4 is a graph of the ratio of the time for the function to deteriorate to one-half of its maximum value to the time to maximum amplitude versus the β/α ratio. The elapsed times to one-half the maximum amplitude were taken from computed values of the dual exponential and therefore were only approximate. Figure 5 is similar to Figure 4 except that the time for the function to reach one-fifth of its maximum amplitude was used. Curves of the type in Figures 3, 4, and 5 would be useful for fitting a dual exponential to an experimentally measured pressure pulse. The functions represented in Figures 4 and 5 appear to be straight line functions and were approximated as such.

The slope of the pressure pulse at $t = 0$ is also of interest, and it is quite easily shown that its value is $\beta-\alpha$. The maximum value of the pressure pulse is

$$P(t)_p = P_o \left\{ (\beta/\alpha)^{-\left[\frac{1}{\beta/\alpha - 1}\right]} - (\beta/\alpha)^{-\left[\frac{\beta/\alpha}{\beta/\alpha - 1}\right]} \right\}. \qquad (6)$$

It is therefore convenient to choose

$$P_o = 1/ \left\{ (\beta/\alpha)^{-\left[\frac{1}{\beta/\alpha - 1}\right]} - (\beta/\alpha)^{-\left[\frac{\beta/\alpha}{\beta/\alpha - 1}\right]} \right\} \qquad (7)$$

so that the maximum value of the dual exponential pressure pulse will be unity. In all of the investigations in this thesis, the value of P_o was chosen such that the maximum value of the pressure function was equal to unity, in order to facilitate comparisons.

In addition to the afore mentioned properties of the dual exponential pressure pulse, it can be made to approach the unit impulse by making both α and β/α large. It approaches the unit step function for α equal to zero and large β.

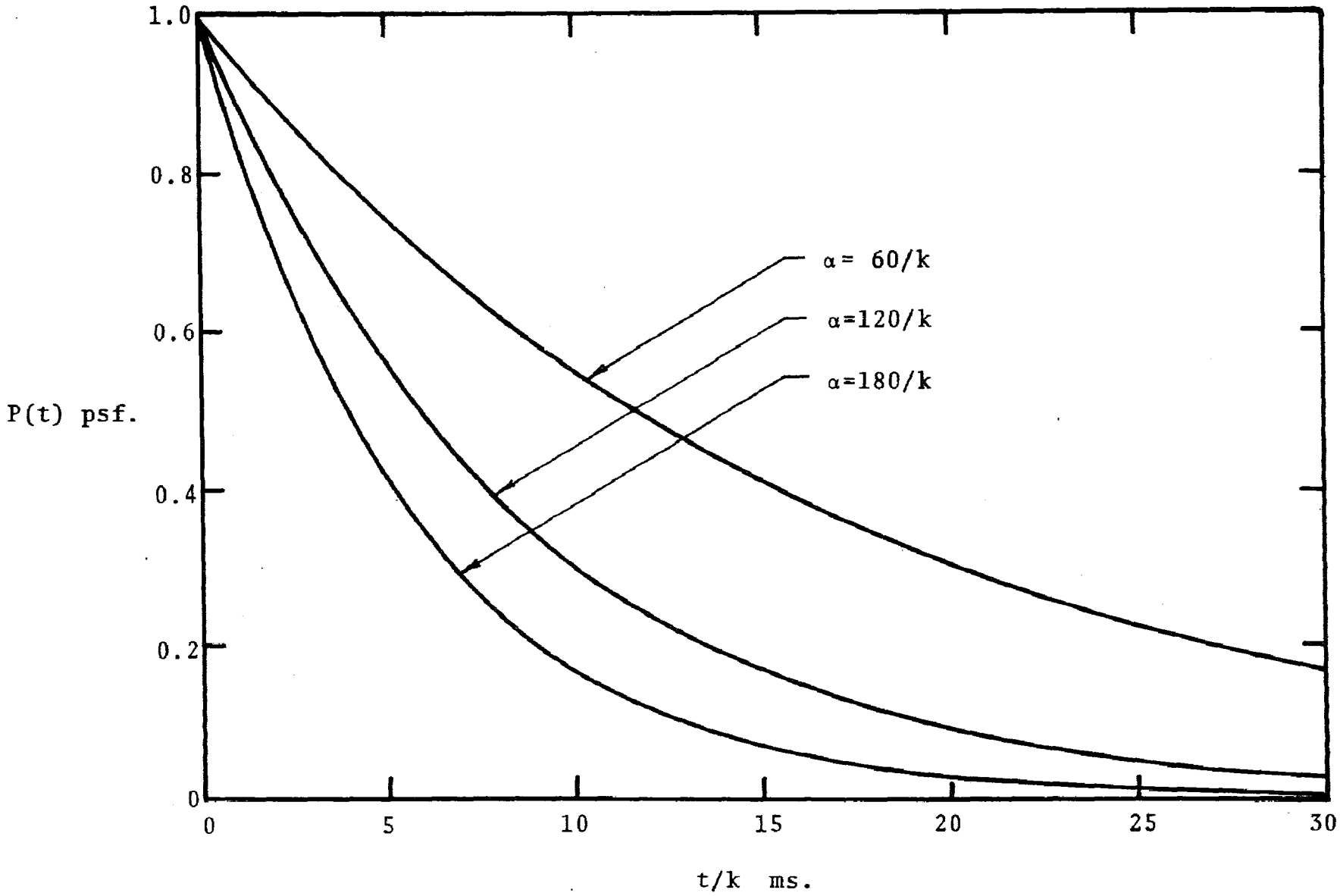

Figure 1. Pressure vs. time for the single decay exponential pressure pulse, $P(t)=e^{-\alpha t}$.

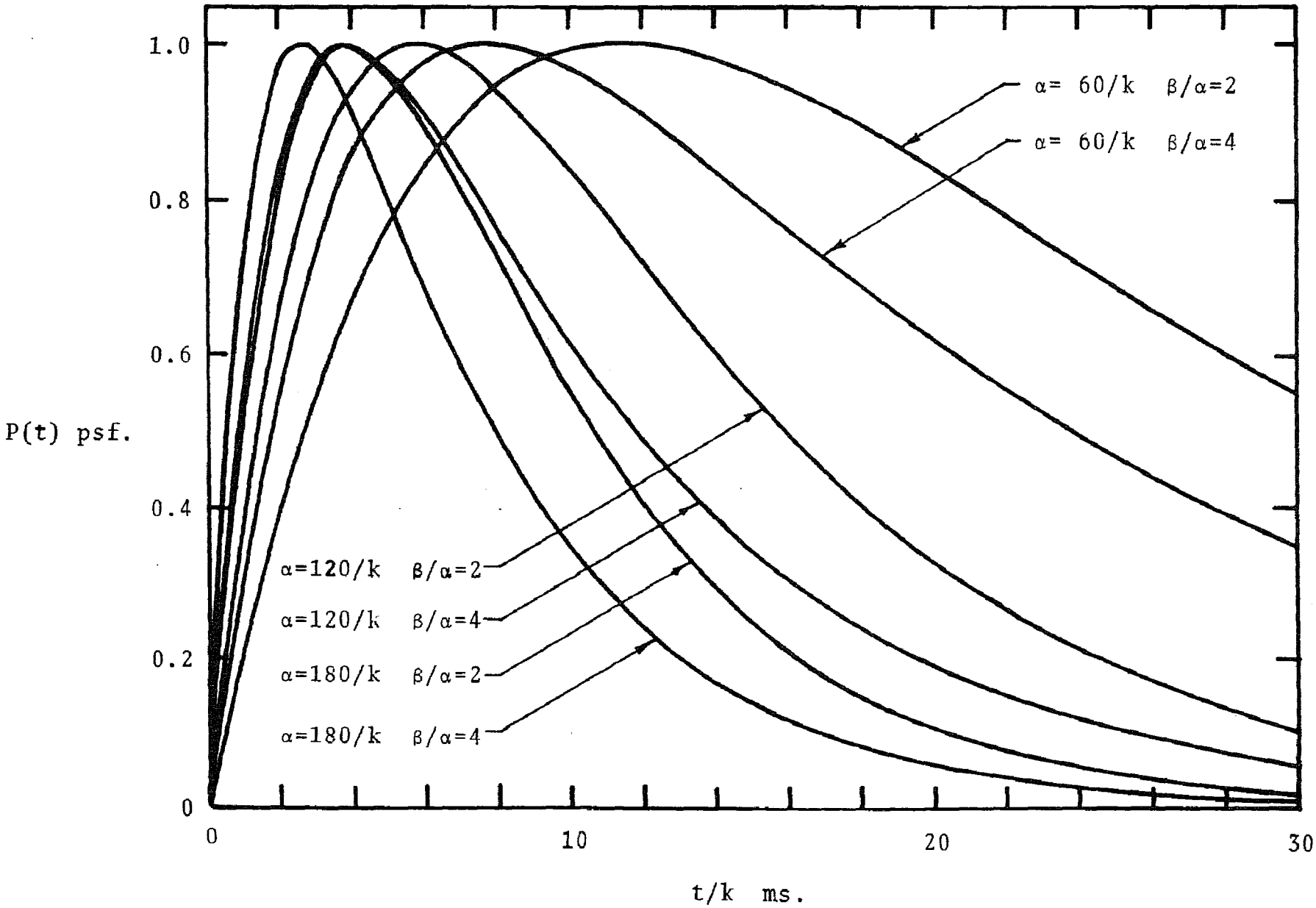

Figure 2. Pressure vs. time for the normalized dual exponential pressure pulse, $P(t)=P_o(e^{-\alpha t}-e^{-\beta t})$.

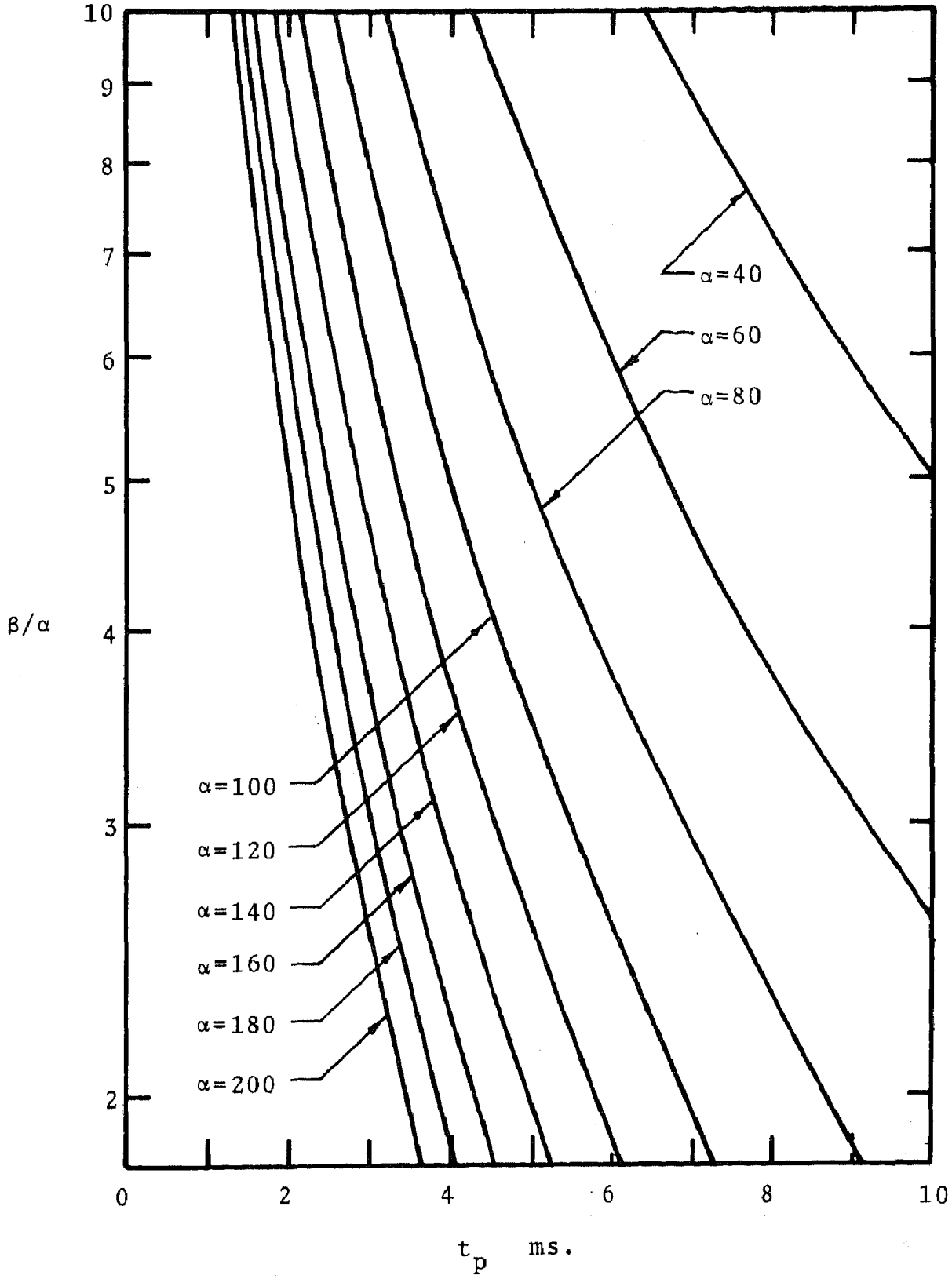

Figure 3. The β/α ratio vs. time to peak amplitude for the dual exponential pressure pulse.

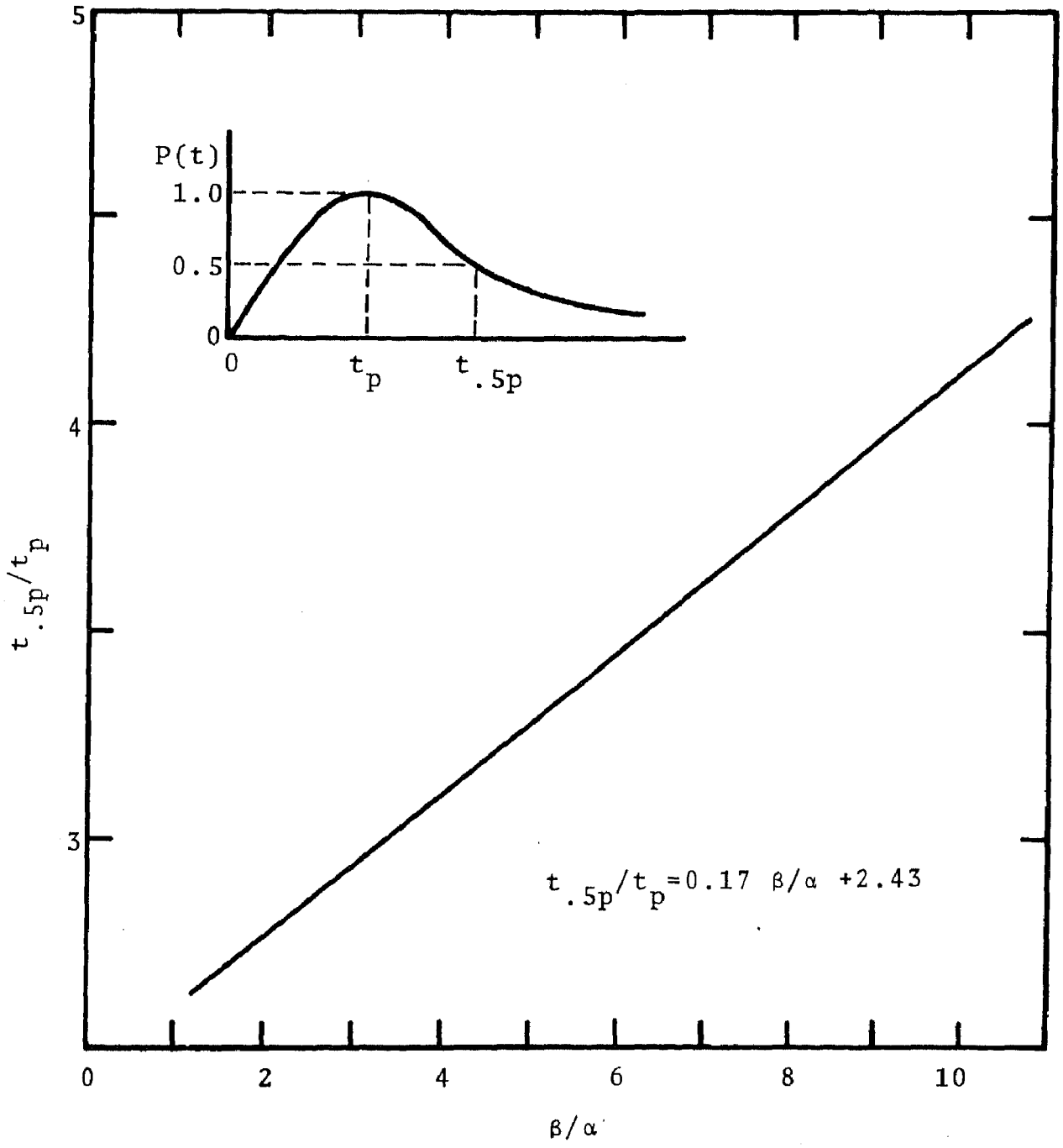

Figure 4. Fifty percent decay time ratio vs. β/α for the dual exponential pressure pulse.

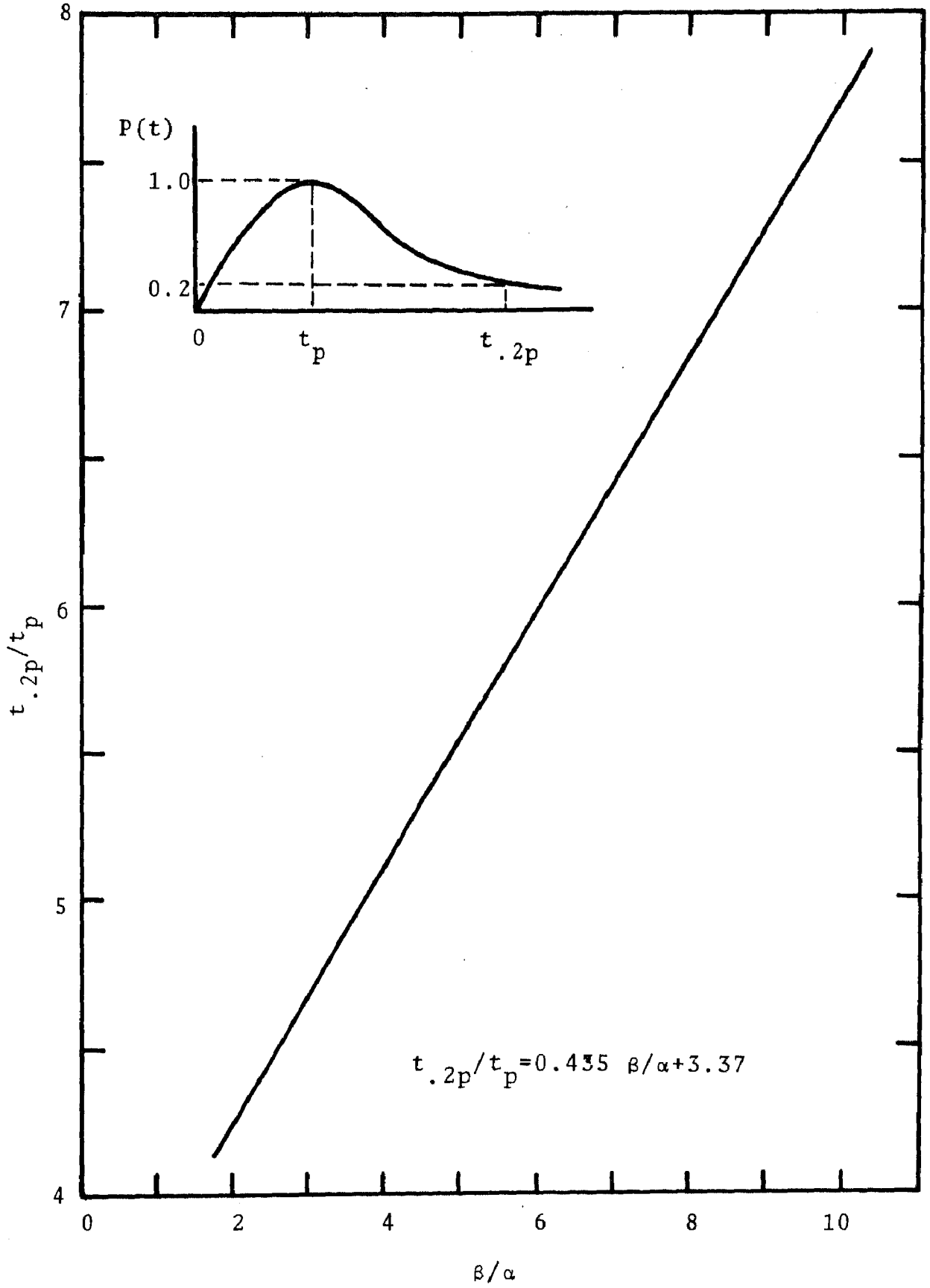

Figure 5. Eighty percent decay time ratio vs. β/α for the dual exponential pressure pulse.

CHAPTER III

TRANSIENT SPHERICAL WAVES IN AN ELASTIC MEDIUM

Scope of the Investigation. Transient spherical waves were investigated in detail in an attempt to gain understanding of wave propagation originating from a spherical explosive source in an elastic medium. It is well known that the elastic model is not, in general, an exact model for wave propagation. A more thorough understanding of transient elastic waves is desirable, however, from the standpoint of gaining insight into explosive wave phenomena. It can also be employed as a basis of comparison for the more complex and hopefully more realistic models, such as the Voigt model, or others which will simulate real earth waves.

It is necessary to carefully define the limits of an investigation of this nature since there is an infinity of parameter combinations that could be investigated. An examination of the parameters involved will illustrate the problem. A choice of wave parameters (eg. particle velocity, displacement, etc.) and wave parameter characteristics (eg. peak value, pulse length, rise time, etc.) to be investigated, must be made. For each of the wave parameters investigated, the effects of variation of pressure pulse parameters, elastic constants and density of the medium, cavity radius, radial distance, and time can be studied.

In order to keep the investigation within reasonable bounds, the study was concentrated primarily on the peak values

of the radial wave parameters: displacement, particle velocity, acceleration, stress and strain. There are other parameters that are sometimes of interest that were not investigated, such as tangential stress and strain, dilatation, and strain rate.

For purposes of this investigation, the radial parameters of the wave motion caused by the pressure pulse

$$P(t) = P_o \left[e^{-\alpha t} - e^{-\beta t} \right] \qquad \beta > \alpha \tag{8}$$

were obtained by superimposing the solutions for the pressure pulses $P(t) = P_o e^{-\alpha t}$ and $P(t) = -P_o e^{-\beta t}$. The reasons for this choice of pressure pulse are given in Chapter II. The constant P_o was chosen such that the maximum value of the pressure pulse was equal to unity (equation 7). All of the numerical calculations were made using an IBM model 360 digital computer.

In order to obtain meaningful comparisons, four realistic media were chosen to be studied:

Medium	Poisson's Ratio	Dilatational Wave Velocity fps.	Density slug/ft^3
Tuff	0.09	6,262	4.00
Sandstone	0.00	9,314	4.98
Granite	0.15	12,284	5.24
Limestone	0.19	15,248	5.10

These media were chosen because they represent a wide range of realistic elastic properties. The properties of the sandstone, granite, and limestone were based on some average properties for these materials obtained from Wuerker's tables (29). The

properties of the tuff are those of the Rainier tuff and were obtained from Johnson, et. al. (30). Most of the study was made using granite as the medium. The choice was arbitrarily made. Comparisons of the peak values for the other media were then made with the peak values for the granite. The peak values of the wave parameters were, in general, taken from data sets where a 0.5 millisecond time interval and a fifty foot effective cavity radius were assumed.

Radial Wave Parameters. Sharpe (31) determined the displacement potential for spherical waves in an elastic medium generated by a single decay exponential pressure pulse. He assumed a Poisson's ratio of 0.25. Duvall (32) used Sharpe's solution and superposition to study spherical elastic waves generated by a dual exponential pressure pulse. Rupert (33) has the spherical elastic problem worked out in detail for a unit impulse pressure function. The solutions which follow are slightly more general than those given by Sharpe and Duvall, as no restriction has been placed on the value of Poisson's ratio.

The displacement potential for spherical elastic waves generated by a single decay exponential pressure pulse $P(t) = P_o e^{-\alpha t}$ is (Appendix B)

$$\phi = \frac{K}{r} \left\{ -e^{-\alpha\tau} + e^{-M\tau} \left[\cos \omega\tau + L \sin \omega\tau \right] \right\} \qquad (9)$$

where

$$K = \frac{aP_o}{\rho\left[\alpha^2 - \frac{4\alpha c\mu}{a(\lambda+2\mu)} + \frac{4c^2\mu}{a^2(\lambda+2\mu)}\right]}$$

$$\tau = t - (r-a)/c$$

$$M = \frac{2c\mu}{a(\lambda+2\mu)}$$

$$\omega = \frac{2c\left[(\lambda+\mu)\mu\right]^{\frac{1}{2}}}{a(\lambda+2\mu)}$$

and

$$L = \left[\frac{\mu}{(\lambda+\mu)}\right]^{\frac{1}{2}} - \frac{\alpha}{\omega} .$$

The radial parameters of the wave motion can be found from the displacement potential and they are:

$$u(r,t) = \frac{\partial\phi}{\partial r} = \frac{K}{r^2}\left\{e^{-\alpha\tau} - e^{-M\tau}\left[\cos\omega\tau + L\sin\omega\tau\right]\right\}$$

$$+ \frac{K}{rc}\left\{-\alpha e^{-\alpha\tau} + e^{-M\tau}\left[(M-\omega L)\cos\omega\tau + (ML+\omega)\sin\omega\tau\right]\right\} \quad (10)$$

$$v(r,t) = \frac{\partial u}{\partial t} = \frac{K}{r^2}\left\{-\alpha e^{-\alpha\tau} + e^{-M\tau}\left[(M-\omega L)\cos\omega\tau\right.\right.$$

$$\left.\left. + (ML+\omega)\sin\omega\tau\right]\right\} + \frac{K}{rc}\left\{\alpha^2 e^{-\alpha\tau} + e^{-M\tau}\right.$$

$$\left.\left[(\omega^2+2M\omega L-M^2)\cos\omega\tau + (\omega^2 L-2M\omega-M^2 L)\sin\omega\tau\right]\right\} \quad (11)$$

$$A(r,t) = \frac{\partial v}{\partial t} = \frac{K}{r^2}\left\{\alpha^2 e^{-\alpha\tau} + e^{-M\tau}\left[(\omega^2+2M\omega L-M^2)\right.\right.$$

$$\left.\left.\cos\ \omega\tau + (\omega^2 L-2M\omega-M^2 L)\ \sin\ \omega\tau\right]\right\}$$

$$+\frac{K}{rc}\left\{-\alpha^3 e^{-\alpha\tau} + e^{-M\tau}\left[(M^3-3M^2\omega L-3M\omega^2 + \omega^3 L)\right.\right.$$

$$\left.\left.\cos\ \omega\tau + (M^3 L-3M\omega^2 L+3M^2\omega-\omega^3)\ \sin\ \omega\tau\right]\right\} \qquad (12)$$

$$\varepsilon(r,t) = \frac{\partial u}{\partial r} = \frac{2K}{r^3}\left\{-e^{-\alpha\tau} + e^{-M\tau}\left[\cos\ \omega\tau + L\ \sin\ \omega\tau\right]\right\}$$

$$-\frac{2K}{r^2 c}\left\{-\alpha e^{-\alpha\tau} + e^{-M\tau}\left[(M-\omega L)\ \cos\ \omega\tau + (ML+\omega)\ \sin\ \omega\tau\right]\right\}$$

$$-\frac{K}{rc^2}\left\{\alpha^2 e^{-\alpha\tau} + e^{-M\tau}\left[(\omega^2+2M\omega L-M^2)\ \cos\ \omega\tau\right.\right.$$

$$\left.\left.+ (\omega^2 L-2M\omega-M^2 L)\ \sin\ \omega\tau\right]\right\} \qquad (13)$$

and

$$\sigma(r,t) = (\lambda+2\mu)\ \varepsilon + 2\lambda u/r \qquad (14)$$

Scaling Laws. Analysis of the equations and the numerical data has shown that elastic wave parameters obey the scaling laws predicted by dimensional analysis. [Ref. Hubbert (34), and Clark (35)]. If the cavity radius is scaled by a scale factor k and the pressure pulse is scaled timewise by the same factor k, a simple relationship exists between the parameters before and after scaling. If the elastic constants and density of the

medium, and the pressure parameter P_o are held constant, the scaling laws can be written:

$$\begin{aligned} v(r,t,a,\alpha,\beta/\alpha) &= v(kr,kt,ka,\alpha/k,\beta/\alpha) \\ \sigma(r,t,a,\alpha,\beta/\alpha) &= \sigma(kr,kt,ka,\alpha/k,\beta/\alpha) \\ \varepsilon(r,t,a,\alpha,\beta/\alpha) &= \varepsilon(kr,kt,ka,\alpha/k,\beta/\alpha) \\ A(r,t,a,\alpha,\beta/\alpha) &= k\ A(kr,kt,ka,\alpha/k,\beta/\alpha) \\ u(r,t,a,\alpha,\beta/\alpha) &= \frac{1}{k}\ u(kr,kt,ka,\alpha/k,\beta/\alpha) \end{aligned} \qquad (15)$$

The division of α by $\underline{k}$, and the holding constant of the β/α ratio, scales the dual exponential pressure pulse timewise by the factor $\underline{k}$. It was found convenient to use the product of the cavity radius $\underline{a}$ and the pressure pulse parameter α in this investigation since the scaling laws are applicable for a given medium provided the product $\underline{a\alpha}$ is held constant along with the β/α ratio.

Cole (36) states that the 'principle of similarity' requires that the pressure remain the same if the charge size, distance, and time are scaled by the factor $\underline{k}$. He further states that this principle is borne out by physical tests as well as theory, but that it applies only for the shock wave and not for later phenomena.

Analysis of Wave Parameters. Typical curves displaying the radial wave parameters as functions of time for several radial distances are given in Figures 6 through 10. The peak values of these parameters for a granite medium are given (Figures 11 thru

15) as functions of radial distance for several combinations of $\underline{a}\alpha$ and β/α. Peak wave parameter values for tuff, sandstone, granite, and limestone are compared in Figures 16 thru 20.

The peak values of displacement (Figures 11 and 16) were found to be highly dependent on the cavity radius $\underline{a}$, and increase with an increase in cavity radius. A study of displacements caused by unit step and dual exponential pressure pulses showed the peak displacements to be affected relatively little by the pressure pulse parameters α and β/α. The decay of the peak displacement with radial distance approaches an inverse first power relationship ($u_p \propto r^{-1}$) at large radial distances.

The peak particle velocity decay is also approximately inversely proportional to the radial distance (Figures 12 and 17). The decay rate is affected very little by radial distance, $\underline{a}\alpha$, β/α, or the properties of the medium. The decay rate is, however, slightly greater than the inverse first power of the distance for small radial distances and small $\underline{a}\alpha$. The peak value increases with decreasing rise time of the pressure pulse. The limiting case is given by the single decay exponential pressure pulse, which has an instantaneous rise time at the pressure pulse arrival. The peak values of the particle velocity for the single decay exponential pressure pulse were found to be independent of α, and to decay exactly as the inverse first power of the radial distance ($v_p \propto r^{-1}$). The peak particle velocity curve for the single decay exponential pressure pulse was shown (Figure 12)

in order to establish an upper limit to the values obtained from the dual exponential pressure pulse.

The peak values of acceleration (Figures 13 and 18) for the dual exponential pressure pulse were found to decay at a rate exactly inversely proportional to the radial distance ($A_p \propto r^{-1}$), independent of the pressure pulse parameters and the medium. The magnitude, however, depends on α and β/α, for a given medium. The peak acceleration increases with an increase in α and β/α. It increases directly proportional to α if the β/α ratio is held constant. The peak acceleration occurs at $\tau = 0$, which corresponds to the arrival time of the wave front in an elastic medium at $t = (r-a)/c$.

The decay rate of the peak values of stress (Figures 14 and 19) becomes inversely proportional to the radial distance as the time to the peak value of the pressure pulse decreases (ie. as α and β/α increase). The decay rate also approaches the inverse first power of the distance as the cavity radius and radial distance become large. The limiting value, as in the case of peak velocity, is given by the single decay exponential pressure pulse (Figure 14). The peak stress was found to be independent of the value of α for the single decay exponential pressure pulse and it results in a decay rate inversely proportional to the radial distance, independent of α.

Peak strains (Figures 15 and 20) are approximately proportional to the peak stresses at radial distances greater than two

or three cavity radii. The peak strains, as the peak stresses, approach a decay rate inversely proportional to the radial distance with large $a\alpha$, β/α, and radial distance. The upper limiting values of peak strains are given (Figure 15) by the curve for the single decay exponential pressure pulse. At radial distances greater than two cavity radii the peak strain decays inversely proportional to the radial distance, independent of α, for the single decay exponential pressure pulse.

Studies of the effects of varying the dilatational wave velocity and Poisson's ratio, showed the peak wave parameters to be affected greatly by changes in the wave velocity but relatively little by changes in Poisson's ratio. A decrease in the dilatational wave velocity caused an increase in all of the peak wave parameters investigated. An increase in Poisson's ratio caused an increase in the peak values of displacement, particle velocity, and strain, but caused no change in the peak values of acceleration.

Peak values of particle velocity, strain, and stress were found to be in phase with one another for large radial distances (about two or three cavity radii and beyond for the cases studied). The peak stresses are not nearly as dependent on the properties of the medium as are the other wave parameters, but they are primarily dependent on those of the pressure pulse. The peak strain is highly dependent on the medium.

The oscillatory nature of the wave parameters was found to

increase with radial distance; an observation in agreement with Duvall (37). The elapsed time from the arrival of the wave front until the wave parameter crosses the zero axis (pulse length) is a function of the pressure pulse shape, radial distance, cavity radius, and the properties of the medium. The pulse length decreases with an increase in radial distance and wave velocity.

The properties of the medium have little affect on the decay rate of the peak values of the displacement and particle velocity, and no affect on the decay rate of the acceleration. The decay rate of the peak strain is affected considerably by the properties of the medium at small radial distances but not significantly at larger distances. The peak stress is also influenced considerably at very small radial distances, with more rapid decay rates for larger values of wave velocity.

Comparison with Real Waves. Explosive generated waves in rock are not, in general, adequately described by spherical elastic wave theory. At large radial distances, however, the attenuation of peak particle velocity and peak displacement for elastic waves approached that reported for real waves. [Ref. Sauer (38)] .

Investigations, reported by Sauer, of waves generated by high explosive and nuclear explosive detonations show that at small to intermediate distances the attenuation rates of the peak values of displacement, particle velocity, and acceleration are considerably greater than those predicted by elastic theory.

Some data on real wave phenomena and peak value attenuation rates are given in Appendix D.

In addition to the differences in attenuation rates; elastic wave pulse lengths exhibit shortening with travel distance whereas real waves lengthen. Elastic waves show abrupt arrivals of the wave front (slope of the wave parameter with time) compared to real waves.

Elastic wave theory might legitimately be used as a first approximation of real waves at large radial distances provided appropriate values of $\underline{a}$ and P_o could be found. In view of the relatively small affect of changes in Poisson's ratio and the fact that most rocks do not differ too significantly in density, analysis could be made on the basis of average values of these parameters. In view of the afore mentioned, changes in elastic waves from one medium to another could be considered to be functions of only the wave velocity of the medium.

The figures which follow (Figures 6 through 20) were discussed in this chapter and were obtained from equations 10 through 14.

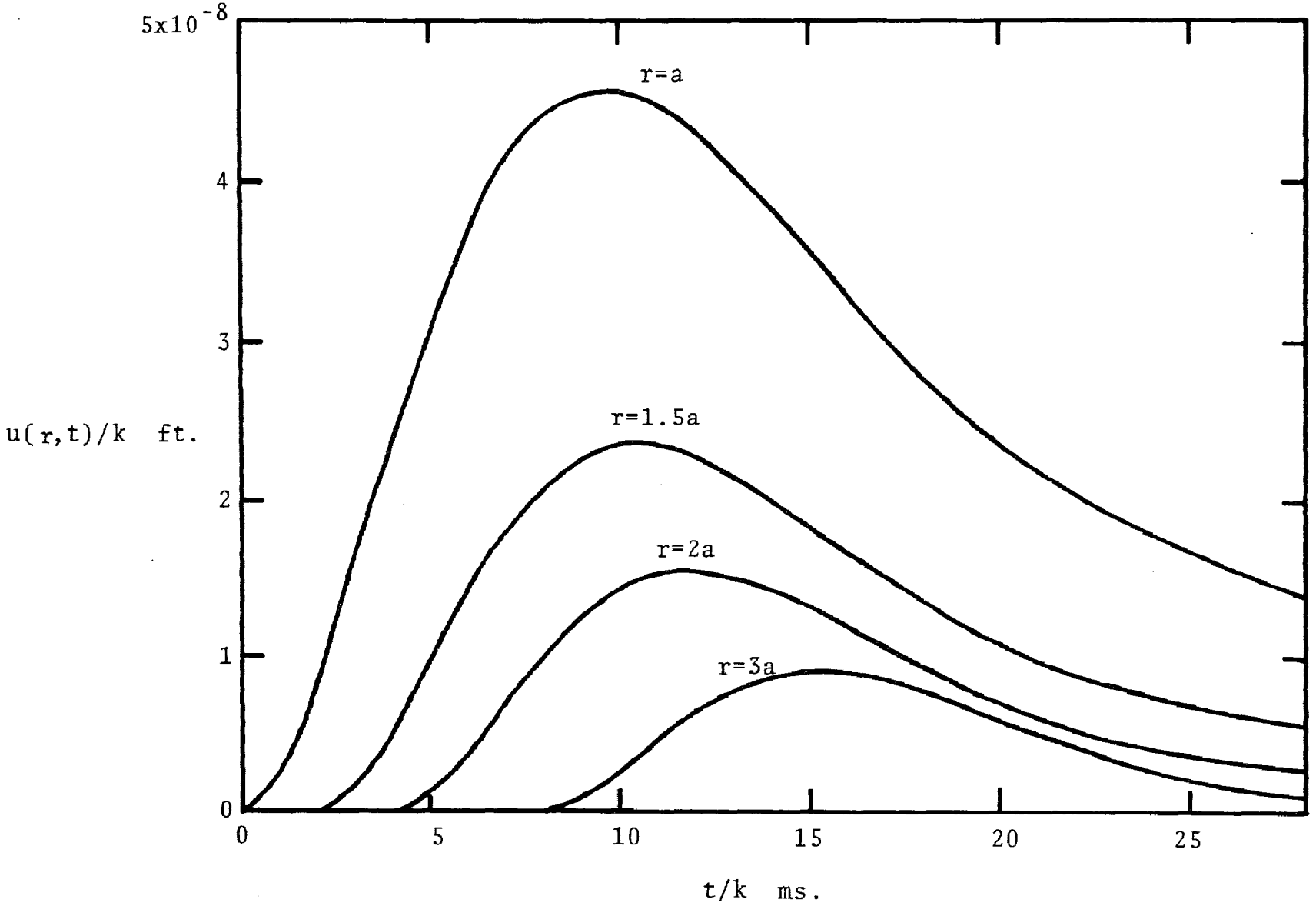

Figure 6. Displacement vs. time for spherical waves in a granite elastic medium for a normalized dual exponential pressure pulse, $a\alpha=3,000$, $\beta/\alpha=4$, $k=60/\alpha$.

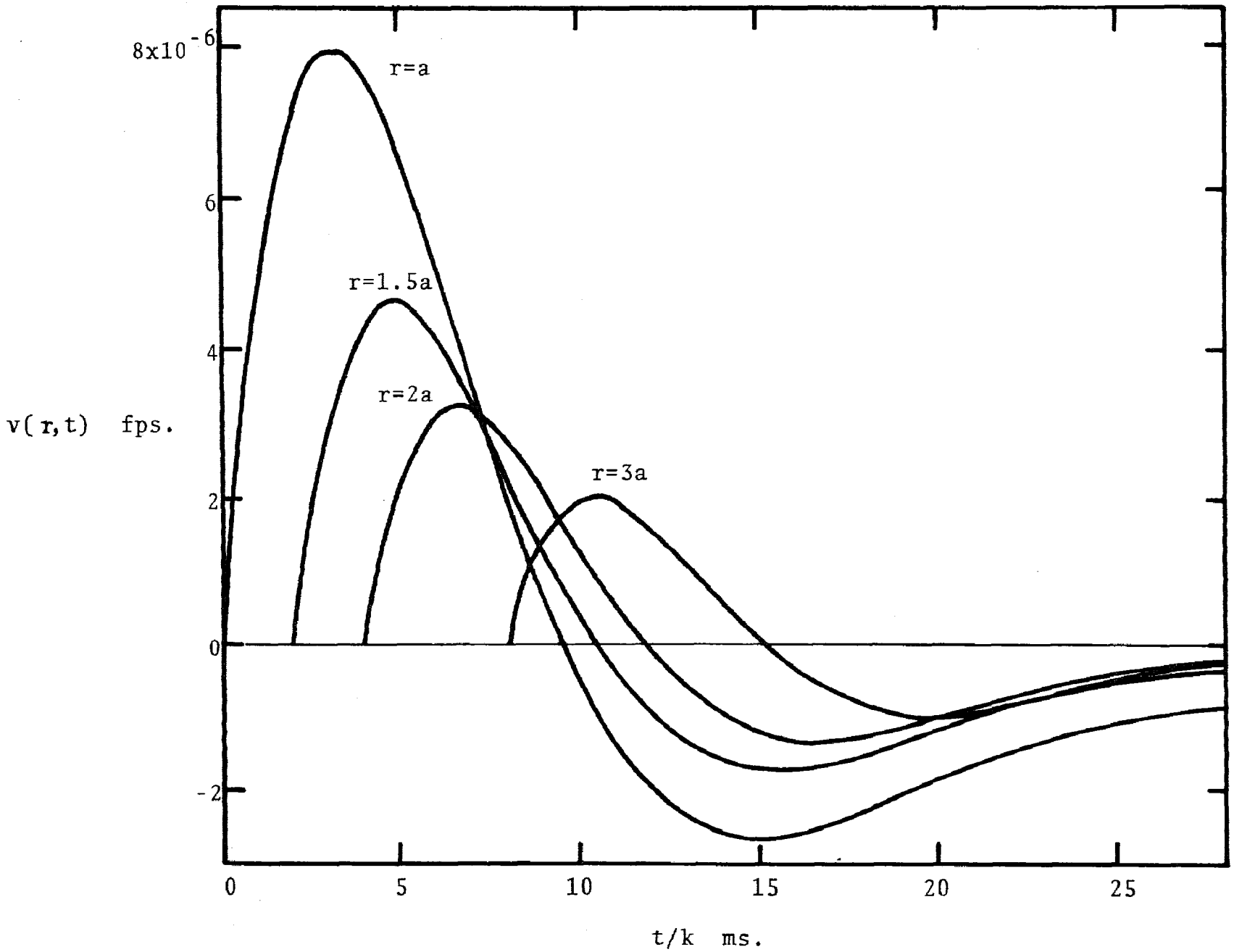

Figure 7. Particle velocity vs. time for spherical waves in a granite elastic medium for a normalized dual exponential pressure pulse, $a\alpha=3{,}000$, $\beta/\alpha=4$, $k=60/\alpha$.

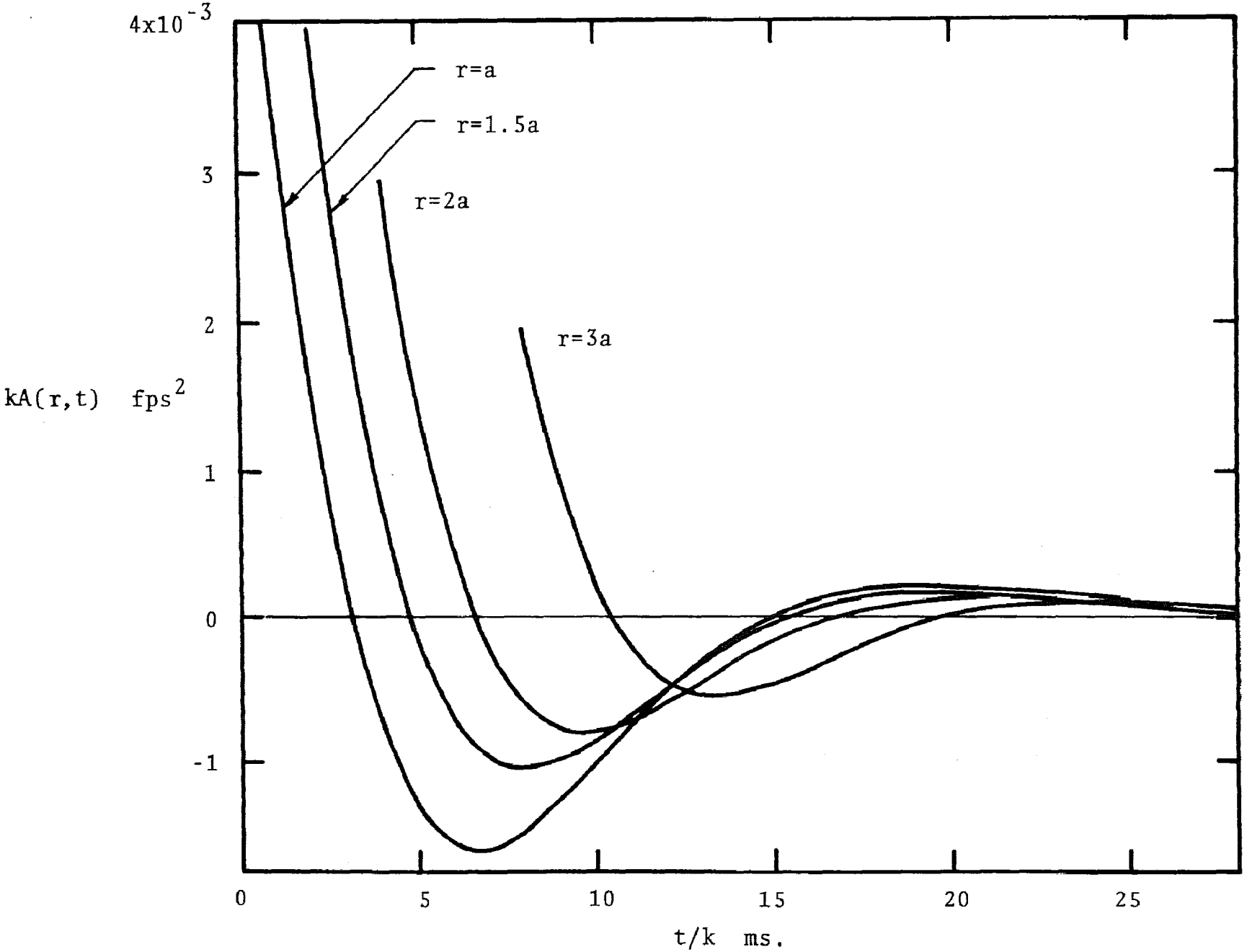

Figure 8. Acceleration vs. time for spherical waves in a granite elastic medium for a normalized dual exponential pressure pulse, $a\alpha=3,000$, $\beta/\alpha=4$, $k=60/\alpha$.

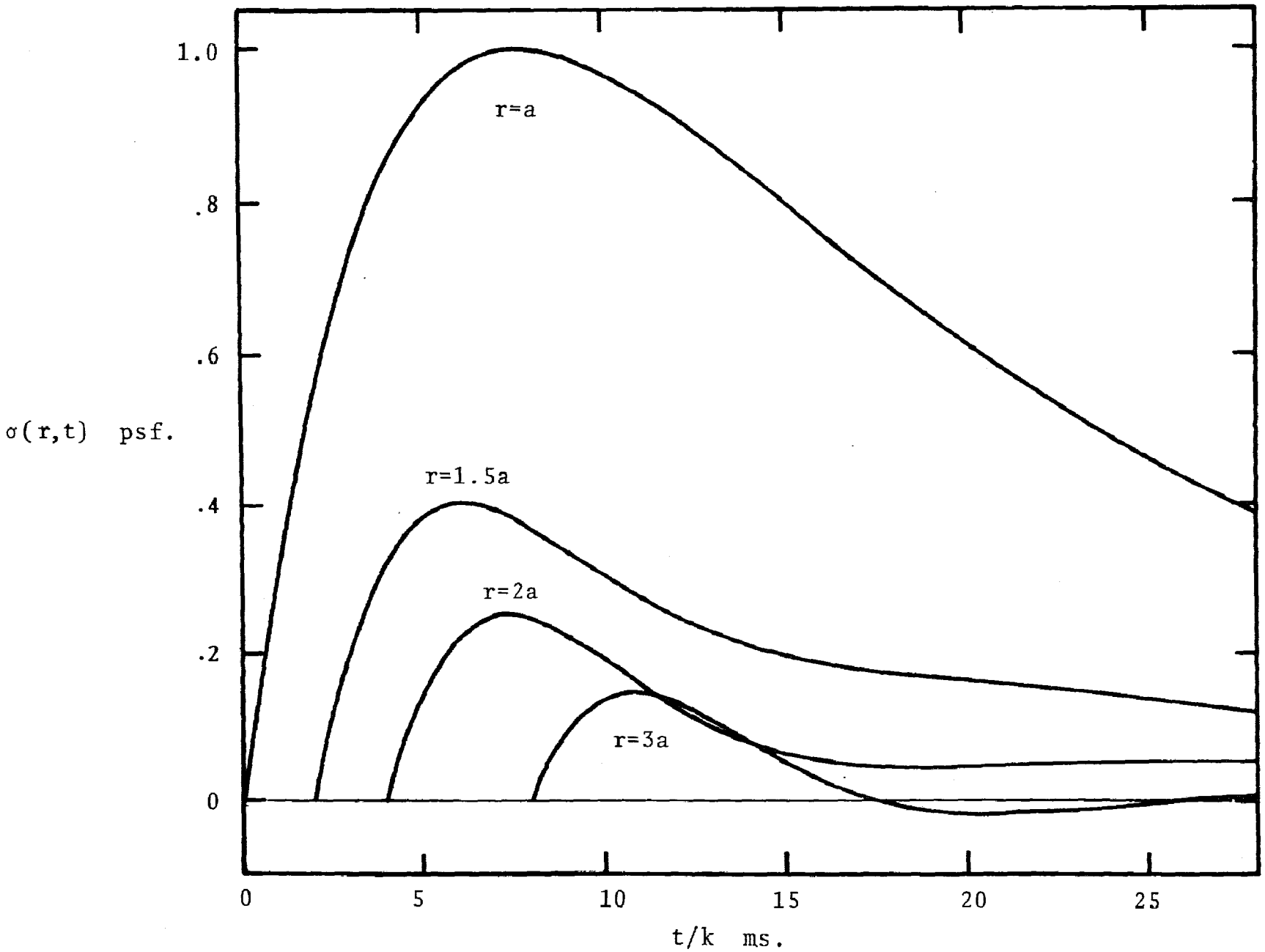

Figure 9. Stress vs. time for spherical waves in a granite elastic medium for a normalized dual exponential pressure pulse, $a\alpha=3,000$, $\beta/\alpha=4$, $k=60/\alpha$.

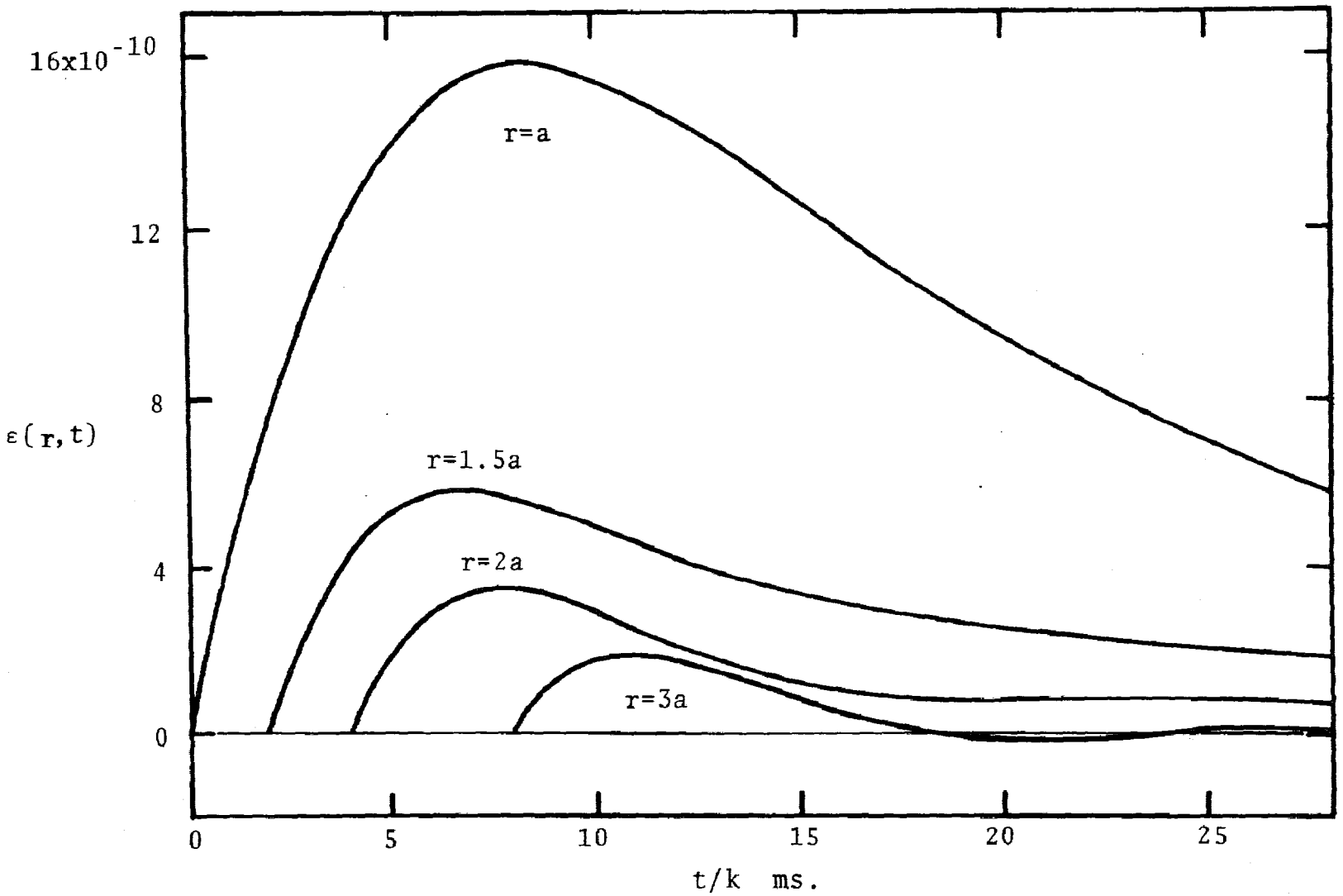

Figure 10. Strain vs. time for spherical waves in a granite elastic medium for a normalized dual exponential pressure pulse, $a\alpha=3,000$, $\beta/\alpha=4$, $k=60/\alpha$.

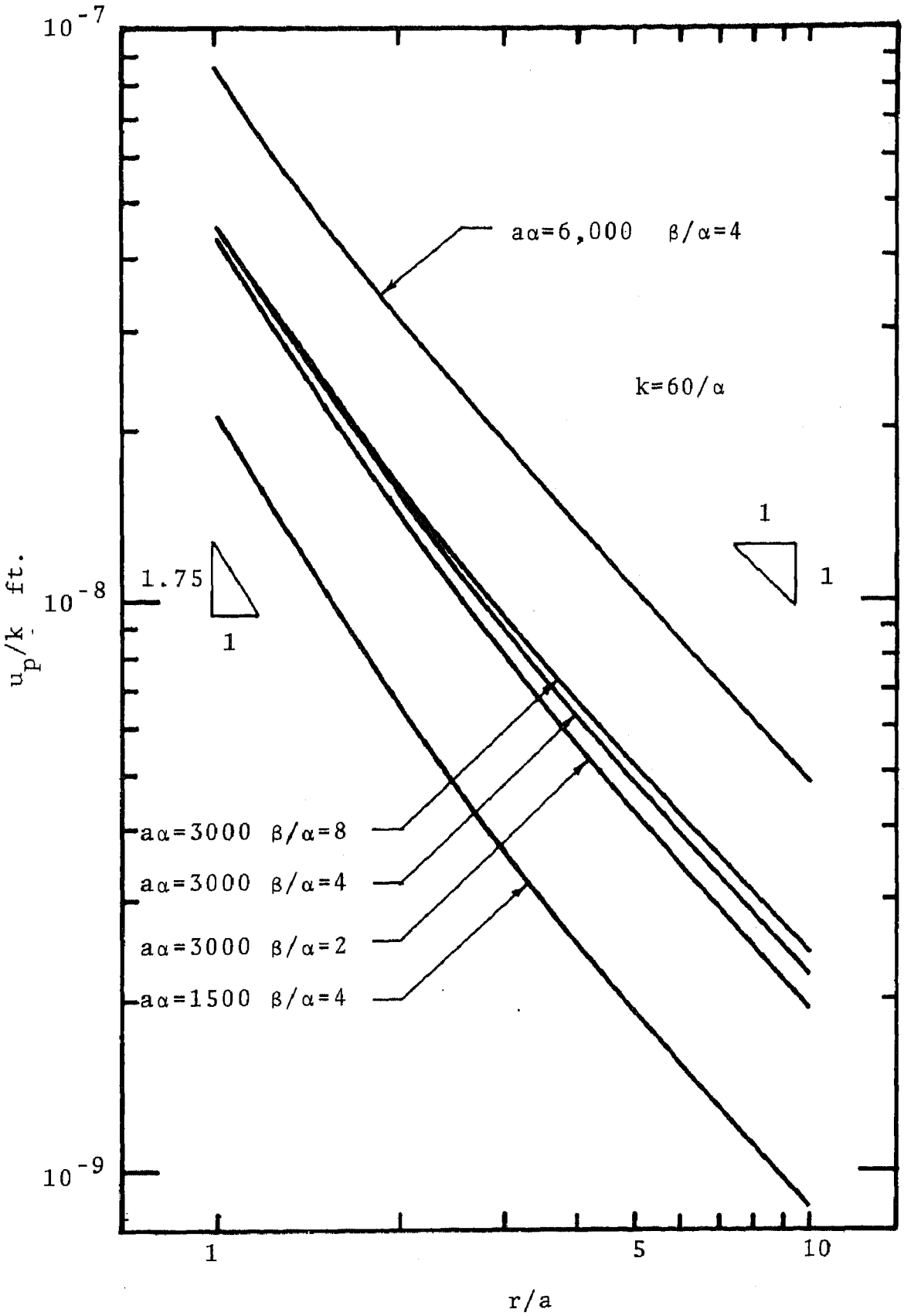

Figure 11. Peak displacement vs. radial distance for spherical waves in a granite elastic medium for normalized dual exponential pressure pulses.

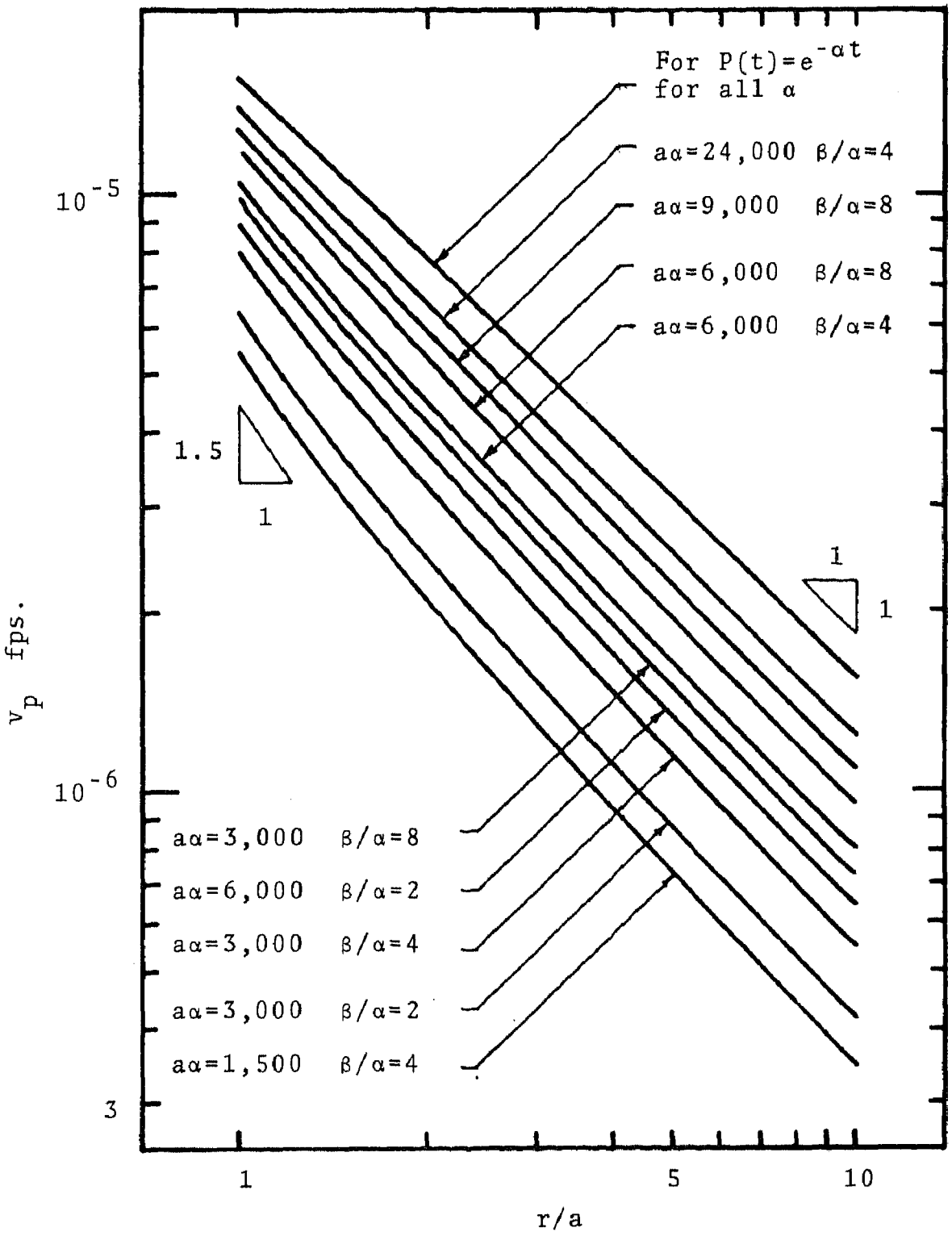

Figure 12. Peak particle velocity vs. radial distance for spherical waves in a granite elastic medium for normalized dual exponential pressure pulses.

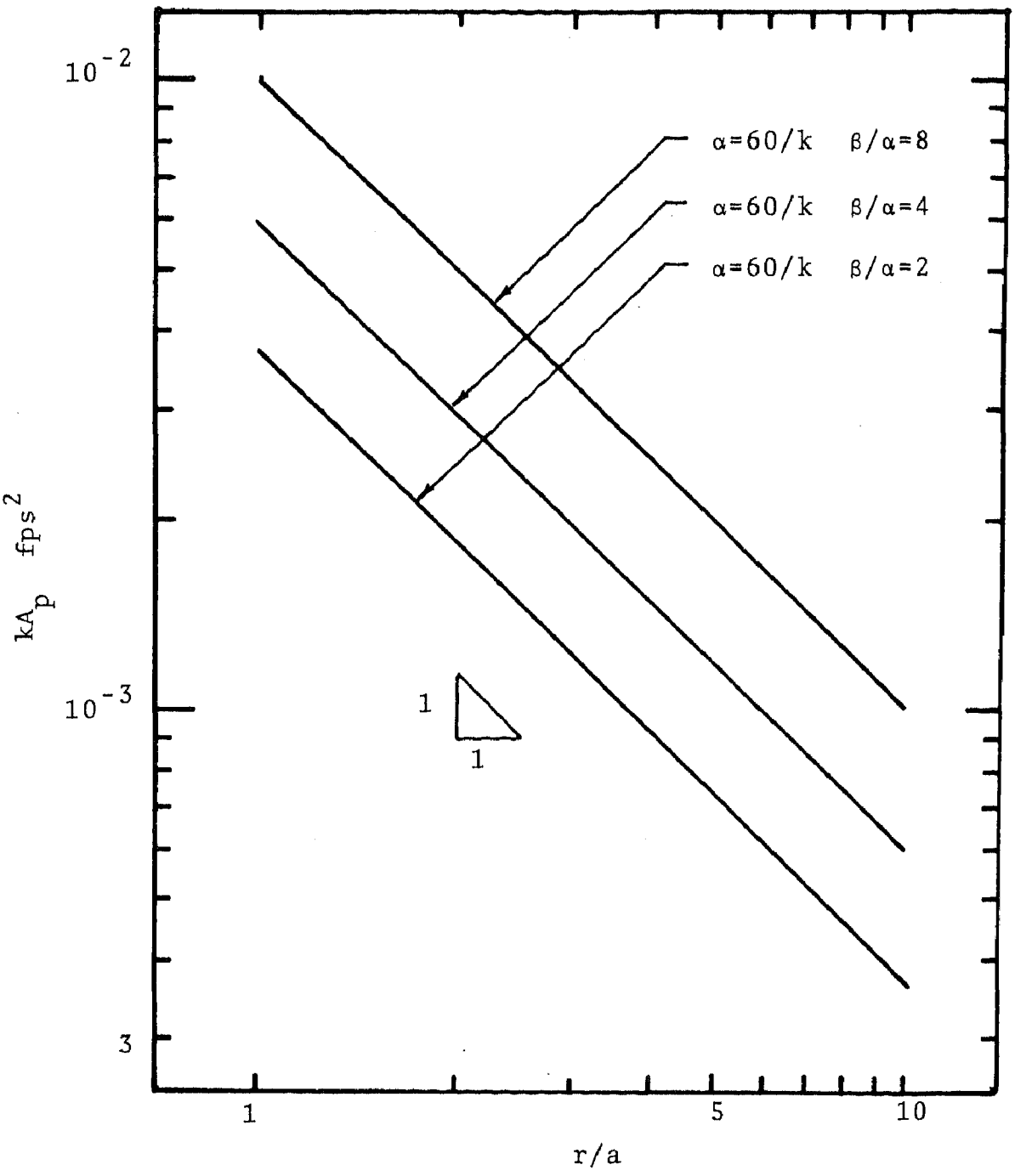

Figure 13. Peak acceleration vs. radial distance for spherical waves in a granite elastic medium for normalized dual exponential pressure pulses.

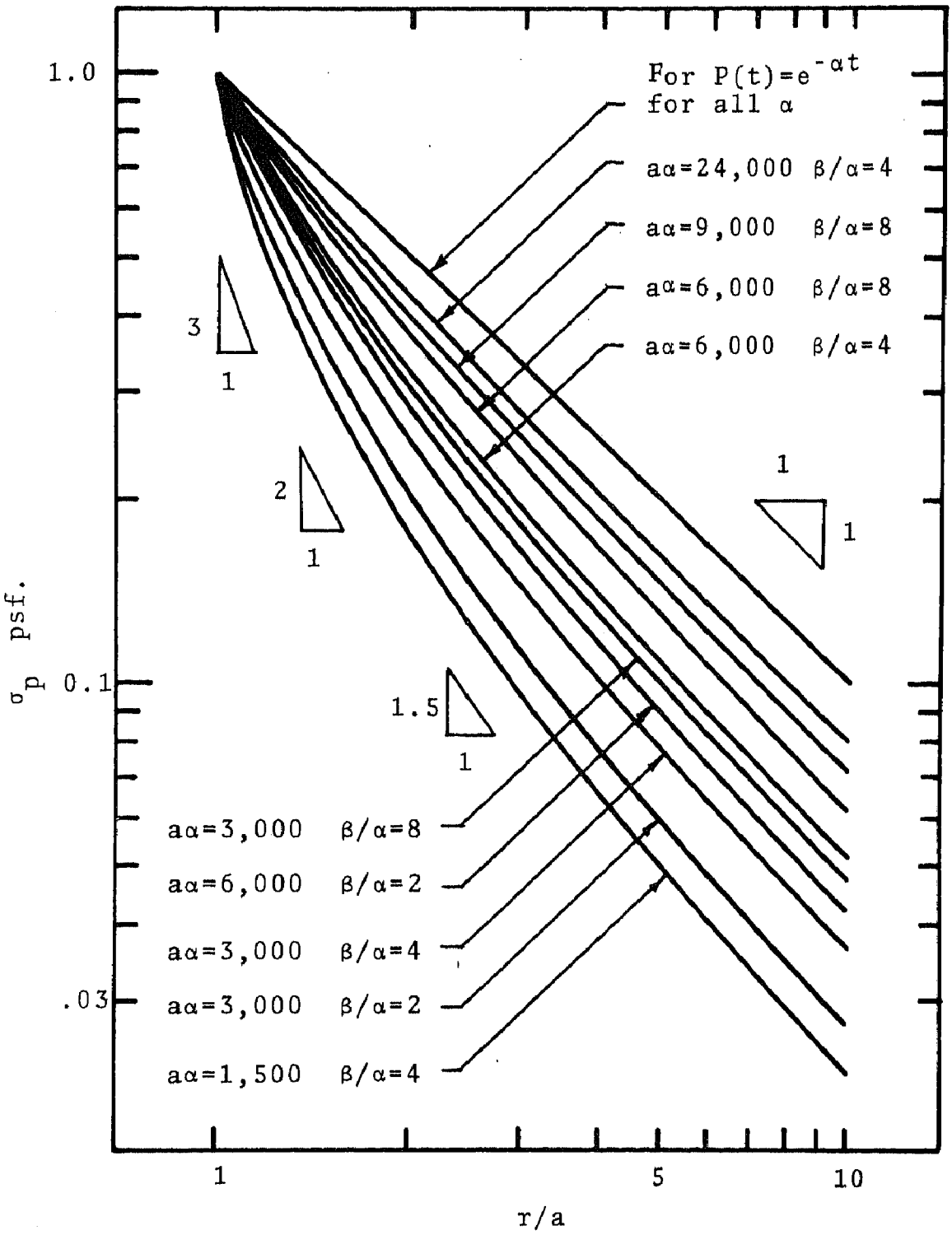

Figure 14. Peak stress vs. radial distance for spherical waves in a granite elastic medium for normalized dual exponential pressure pulses.

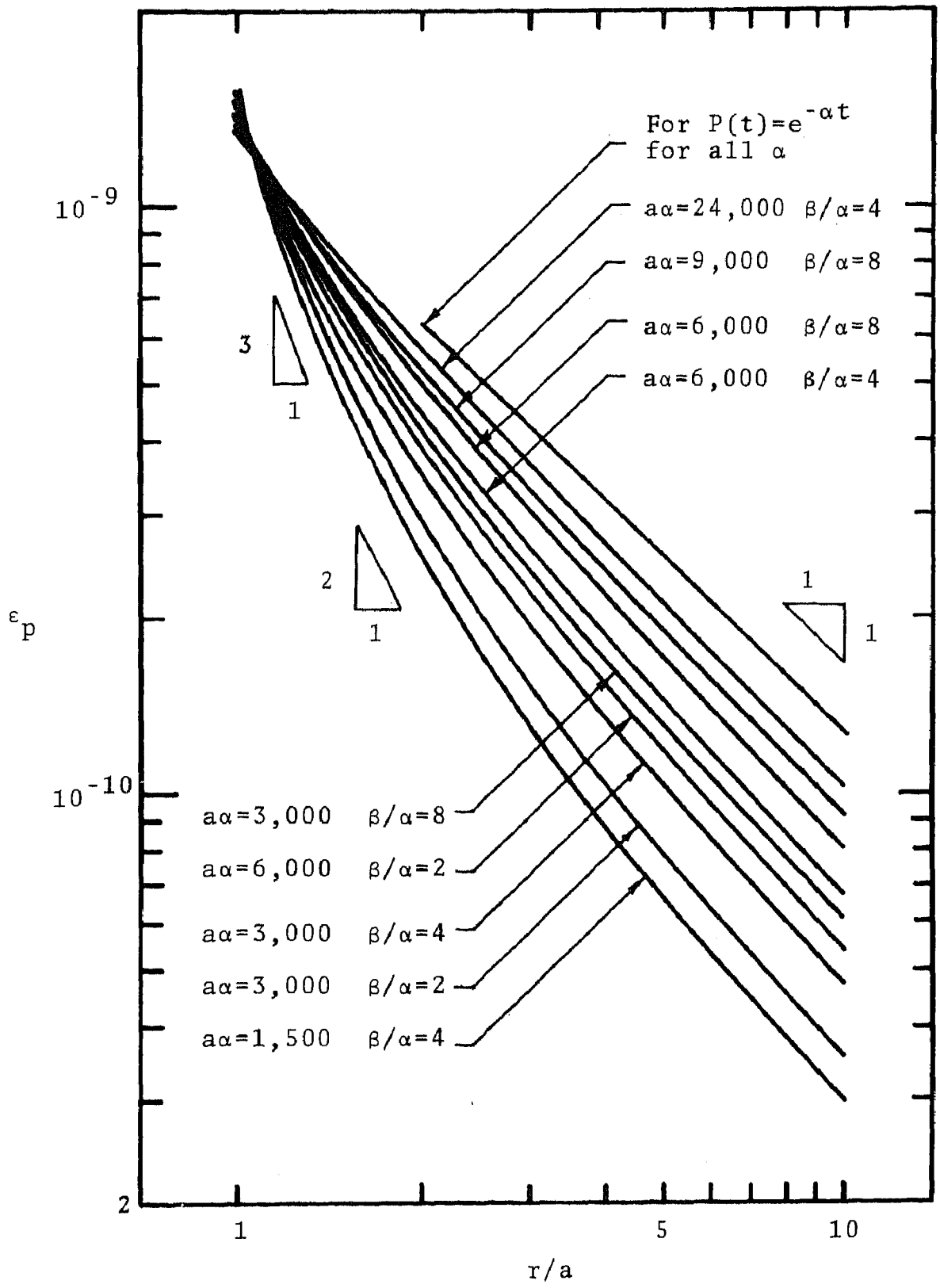

Figure 15. Peak strain vs. radial distance for spherical waves in a granite elastic medium for normalized dual exponential pressure pulses.

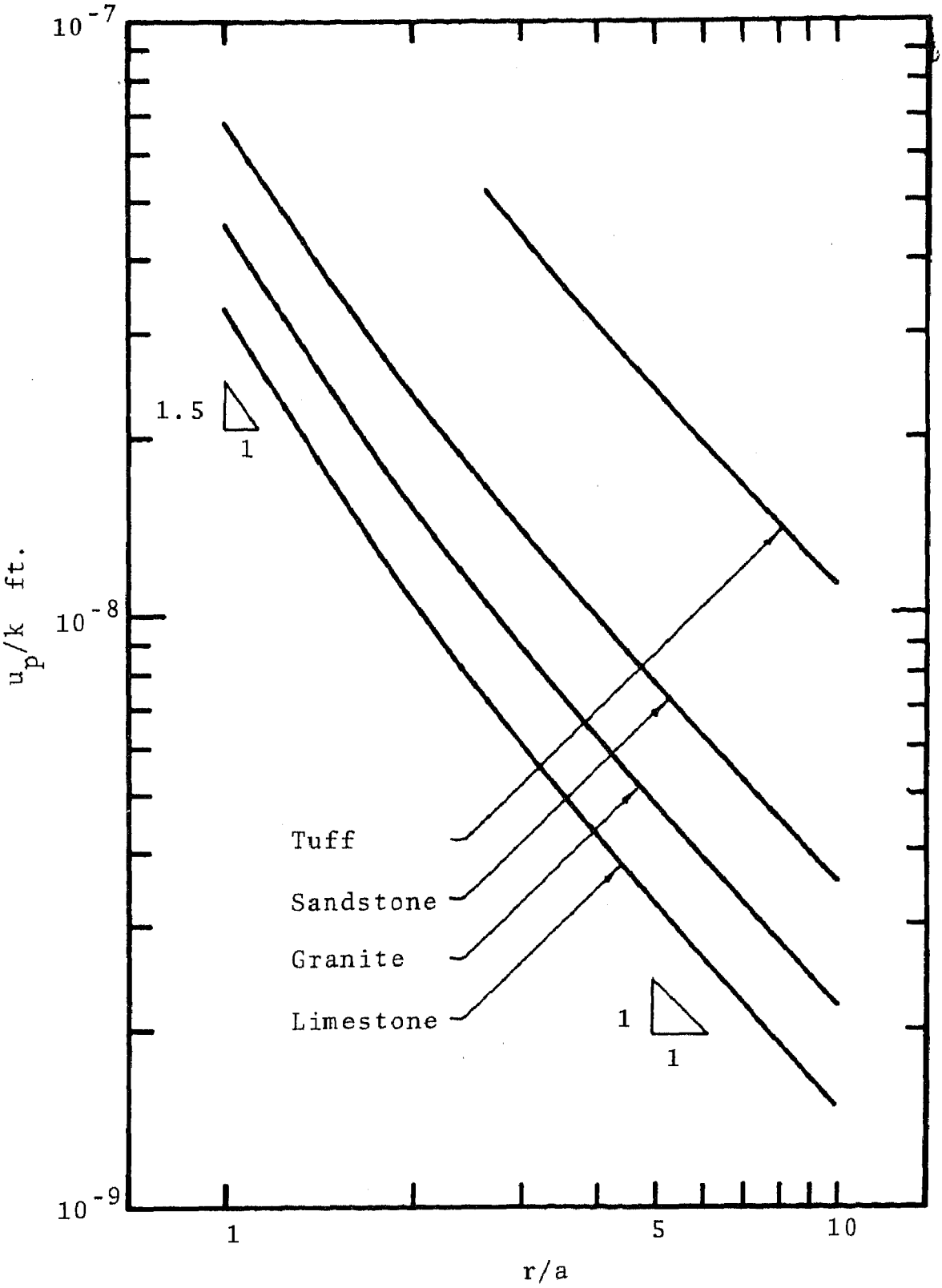

Figure 16. Peak displacement vs. radial distance for spherical elastic waves in tuff, sandstone, granite, and limestone for a normalized dual exponential pressure pulse, $a\alpha=3,000$, $\beta/\alpha=4$, $k=60/\alpha$.

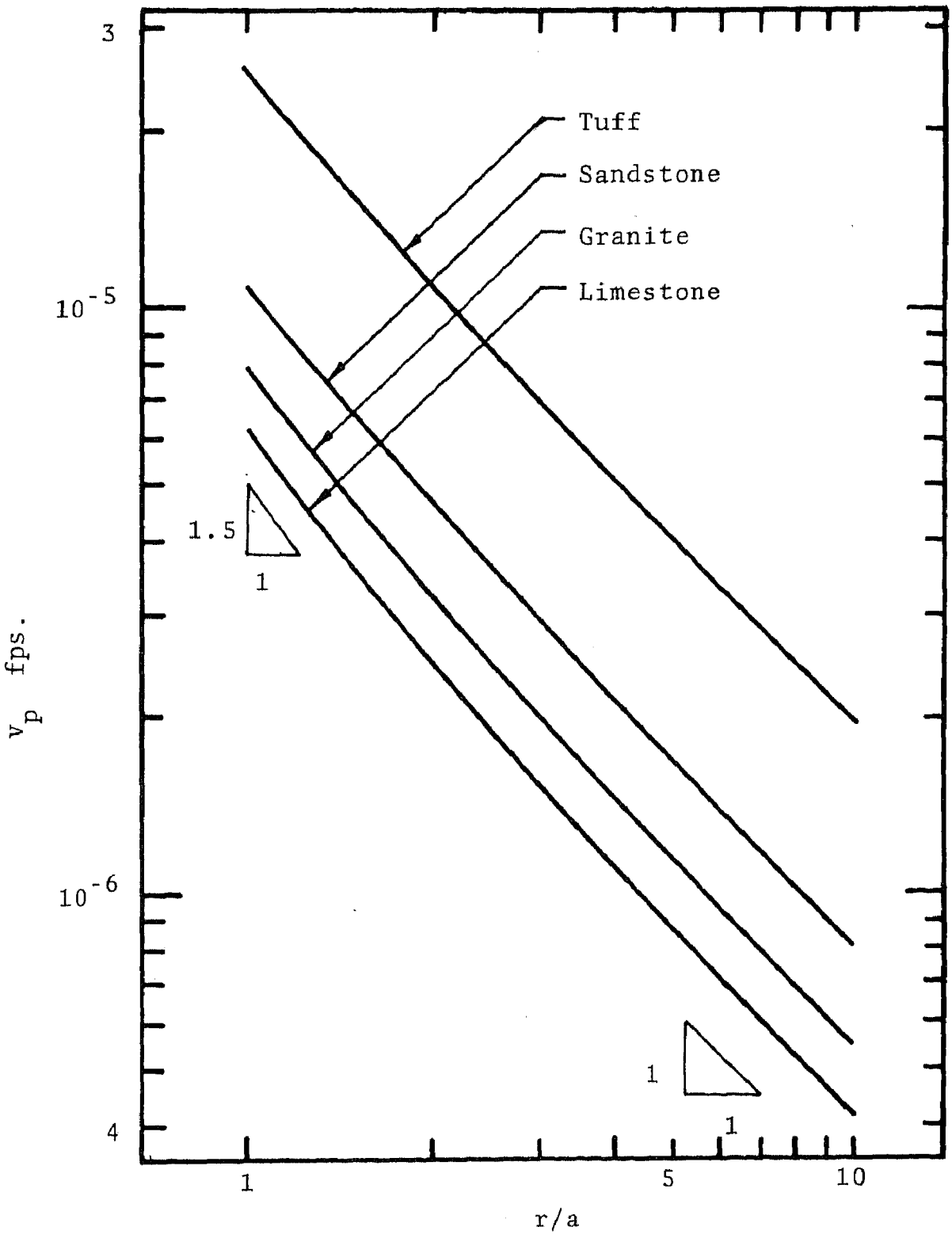

Figure 17. Peak particle velocity vs. radial distance for spherical elastic waves in tuff, sandstone, granite, and limestone for a normalized dual exponential pressure pulse, $a\alpha=3,000$, $\beta/\alpha=4$.

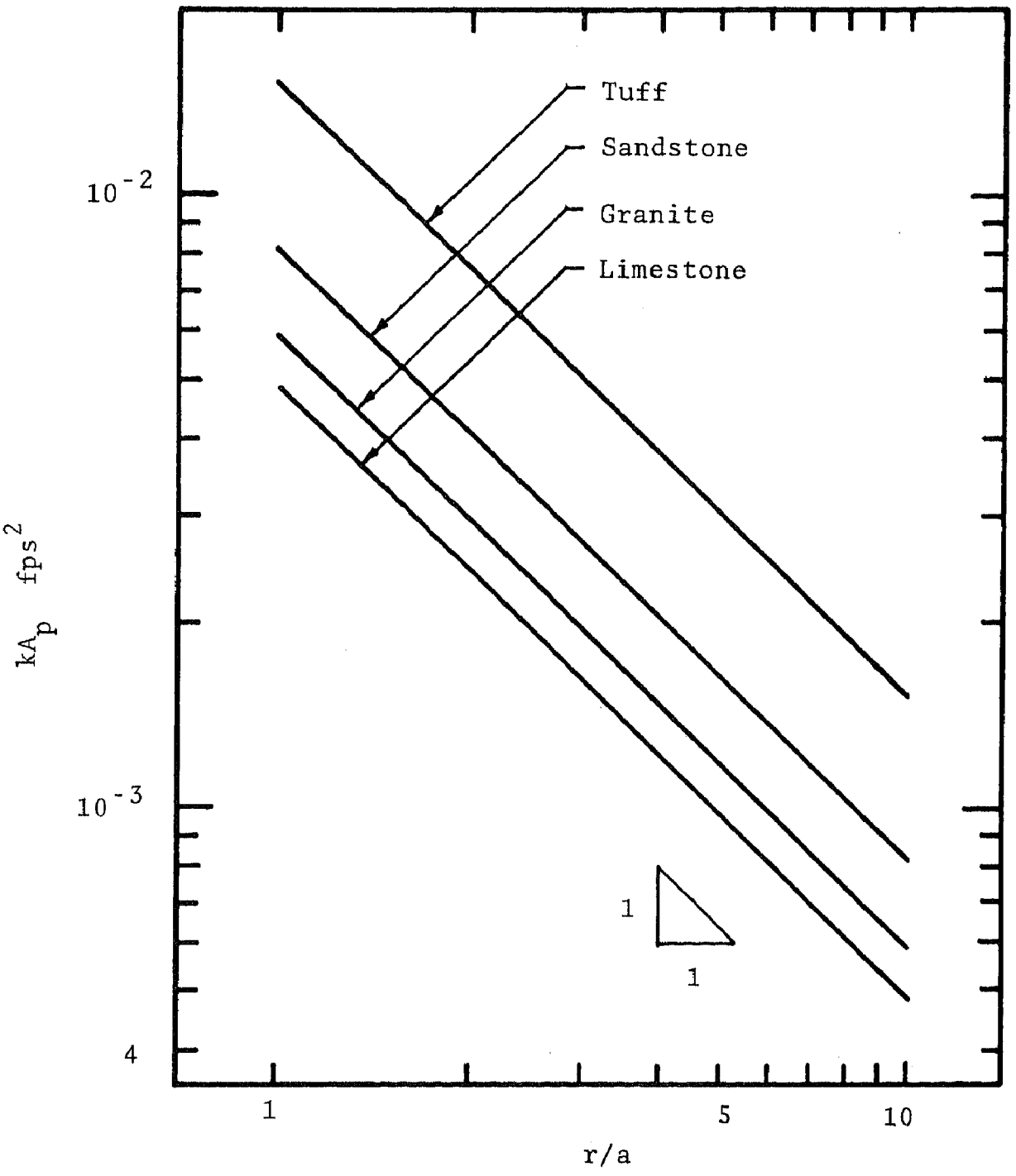

Figure 18. Peak acceleration vs. radial distance for spherical elastic waves in tuff, sandstone, granite, and limestone for a normalized dual exponential pressure pulse, $\beta/\alpha=4$, $k=60/\alpha$.

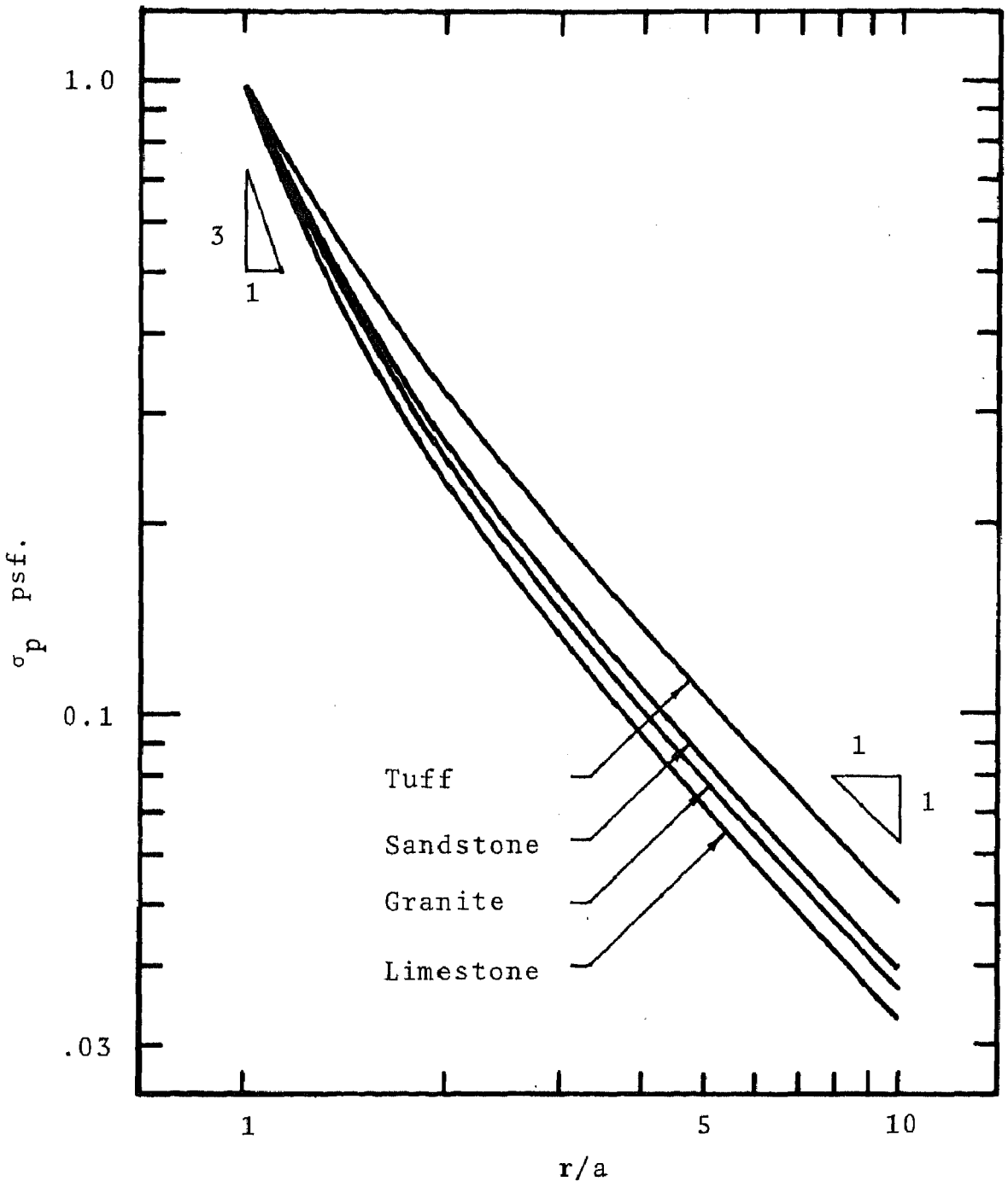

Figure 19. Peak stress vs. radial distance for spherical elastic waves in tuff, sandstone, granite, and limestone for a normalized dual exponential pressure pulse, $a\alpha=3,000$, $\beta/\alpha=4$.

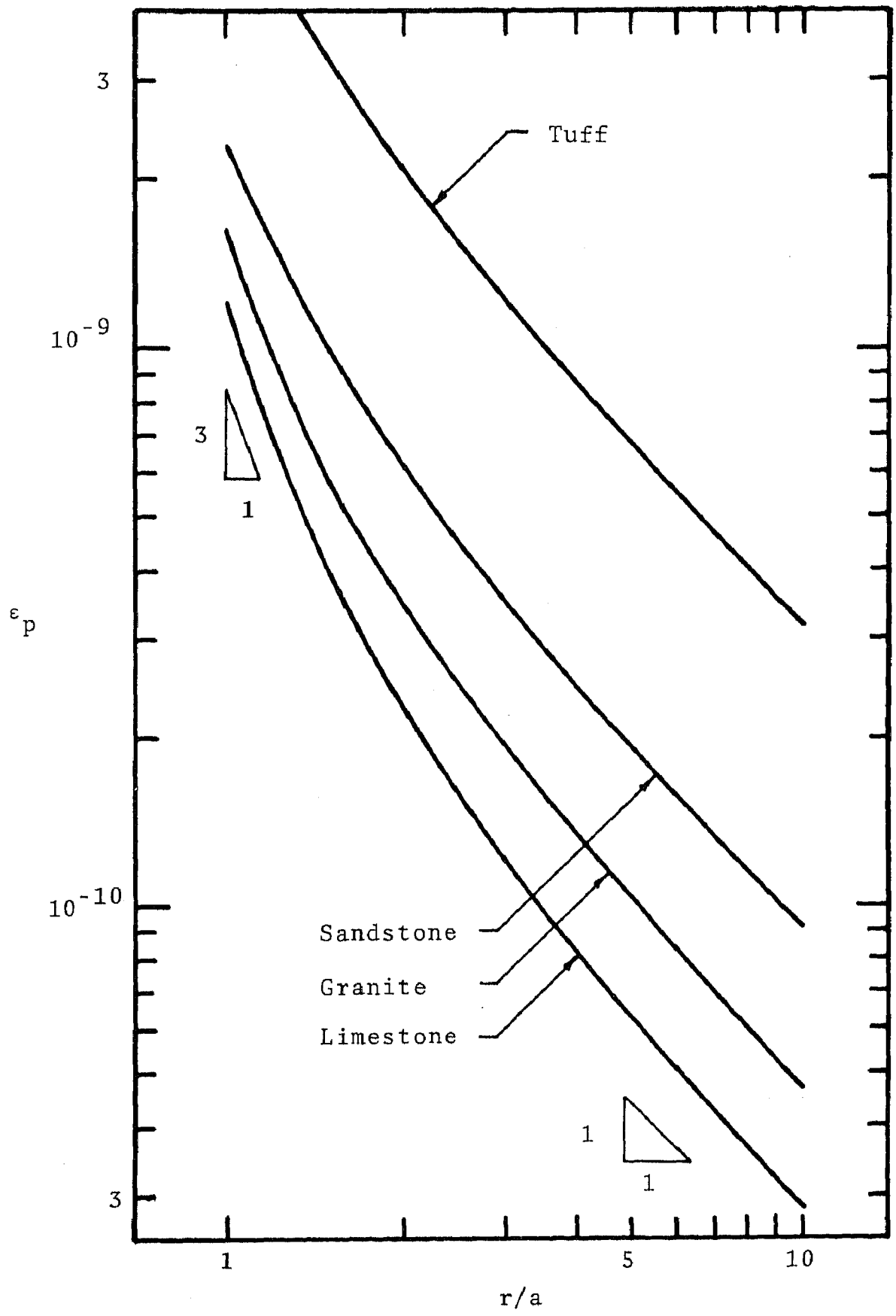

Figure 20. Peak strain vs. radial distance for spherical elastic waves in tuff, sandstone, granite, and limestone for a normalized dual exponential pressure pulse, $a\alpha=3,000$, $\beta/\alpha=4$.

CHAPTER IV

TRANSIENT SPHERICAL WAVES IN A VOIGT MEDIUM

Introduction and Objectives. The uniaxial stress-strain relationship for the Voigt model is

$$\sigma = E\left(1 + \frac{1}{\omega_o}\frac{\partial}{\partial t}\right)\varepsilon \qquad (16)$$

where E/ω_o is the damping coefficient. If the elastic modulus E is held constant, changes in the damping coefficient depend only on ω_o. As ω_o becomes large the Voigt model approaches the elastic model.

One of the purposes of this phase of the investigation was to determine some of the significant properties of spherical wave parameters; particularly, how damping affects the decay of the peak values of the wave parameters with radial distance. Voigt waves were compared to elastic and real waves in order to ascertain the applicability of the Voigt model in predicting wave phenomena. In order to facilitate comparisons with the elastic solutions of Chapter III, the elastic properties of granite were used. The comparisons of Voigt and elastic waves illustrate the effects of damping.

Only approximate values of ω_o for rocks have been published in the literature; therefore, no attempt was made to use values of ω_o corresponding to any particular real material. Values of ω_o were chosen on the basis of the work of Clark, et al. (39) to be 600,1200, and 6000. These values of ω_o were found to be sufficient

to give an understanding, and to demonstrate the limited applicability of the Voigt model in simulating real wave phenomena.

Because of the large amount of computer time required, only one set of elastic parameters (granite) and only one value of $a\alpha$ and β/α were investigated. The studies appear to be sufficient to provide an understanding of wave propagation in a Voigt medium, when taken in conjunction with the investigation of elastic waves (Chapter III), since the Voigt model reduces to the elastic for large ω_o.

Radial Wave Parameters. The spherical Voigt wave equation can be written in terms of the displacement potential ϕ:

$$\left(1 + \frac{1}{\omega_o} \frac{\partial}{\partial t}\right) \frac{\partial^2 r\phi}{\partial r^2} = \frac{1}{c^2} \frac{\partial^2 r\phi}{\partial t^2} \qquad (17)$$

Clark, et al. (40) give the solutions for Voigt spherical waves generated by a single decay exponential pressure pulse. They make the assumption that $\lambda=\mu$ and $\lambda'=\mu'$, which is equivalent to the assumption that the viscoelastic equivalent of Poisson's ratio is equal to the elastic Poisson's ratio, and that its value is 0.25. This restriction assumes that the viscoelastic equivalent of Poisson's ratio is not time dependent.

In the solutions which follow, the notation used is similar to that of Clark. Poisson's ratio in the Voigt problem is assumed to be independent of time, but no restriction has been placed on its value. The solutions are the same as those given by Clark except for the b_m terms, which depend on the choice of Poisson's ratio.

In order to simplify the equations, the following summation notation was adopted:

$$\sum\sum_z = \sum_{m=o}^{\infty} \sum_{n=o}^{\infty} b_m \frac{R^n}{n!} 2^{(m+n+z)/2} T^{(m+n+z-1)/2}$$

$$D_{-n-m-z}\left[R/(2T)^{\frac{1}{2}}\right] \quad EXP \tag{18}$$

where

$$EXP = \exp(-T-R^2/8T)$$

$$R = \omega_o(r-a)/c$$

$$T = \omega_o t$$

$D_{-n-m-z}\left[R/(2T)^{\frac{1}{2}}\right]$ = parabolic cylinder function of order $(-n-m-z)$ [Refs. Collins (41) and Appendix C].

The b_m's are the only terms influenced by the choice of pressure pulse and Poisson's ratio. If the pressure pulse is the single decay exponential $P(t) = P_o e^{-\alpha t}$, the b_m's are the coefficients in the expansion

$$\frac{1}{(s-\gamma)[A]} = \frac{1}{S^3} \sum_{m=o}^{\infty} b^m/s^{m/2} \tag{19}$$

where

$$\gamma = \left(1-\frac{\alpha}{\omega_o}\right)$$

and

$$[A] = s^2 + \left\{\frac{4\mu}{\rho a c \omega_o}\right\} s^{3/2} + \left\{\frac{4\mu}{\rho a^2 \omega_o^2} - 2\right\} s$$

$$-\left\{\frac{4\mu}{\rho a c \omega_o}\right\} s^{1/2} + 1.$$

The radial wave parameters written in terms of the summation notation of equation 18 are:

$$u(r,t) = \frac{P_o a}{\rho \omega_o^2 \sqrt{\pi}} \left\{ \frac{1}{r^2} \sum\sum_5 + \frac{\omega_o}{rc} \left[\sum\sum_4 - \sum\sum_6 \right] \right\} \tag{20}$$

$$v(r,t) = \frac{P_o a}{\rho \omega_o \sqrt{\pi}} \left\{ \frac{1}{r^2} \left[\sum\sum_3 - \sum\sum_5 \right] + \frac{\omega_o}{rc} \left[\sum\sum_2 - 2\sum\sum_4 + \sum\sum_6 \right] \right\} \tag{21}$$

$$A(r,t) = \frac{P_o a}{\rho \sqrt{\pi}} \left\{ \frac{1}{r^2} \left[\sum\sum_1 - 2\sum\sum_3 + \sum\sum_5 \right] + \frac{\omega_o}{rc} \left[\sum\sum_o - 3\sum\sum_2 + 3\sum\sum_4 - \sum\sum_6 \right] \right\} \tag{22}$$

$$\varepsilon(r,t) = \frac{-P_o a}{\rho \omega_o^2 \sqrt{\pi}} \left\{ \frac{2}{r^3} \sum\sum_5 + \frac{2\omega_o}{r^2 c} \left[\sum\sum_4 - \sum\sum_6 \right] + \frac{\omega_o^2}{rc^2} \left[\sum\sum_3 - 2\sum\sum_5 + \sum\sum_7 \right] \right\} \tag{23}$$

$$\sigma(r,t) = \frac{-P_o a \mu}{\rho \omega_o^2 \sqrt{\pi}} \left\{ \frac{4}{r^3} \sum\sum_3 + \frac{4\omega_o}{r^2 c} \left[\sum\sum_2 - \sum\sum_4 \right] + \frac{\rho \omega_o^2}{r\mu} \left[\sum\sum_1 - 2 \sum\sum_3 + \sum\sum_5 \right] \right\} \tag{24}$$

In this investigation of spherical waves in a Voigt medium, as in the investigation of spherical elastic waves (Chapter III), solutions for the dual exponential pressure pulse were obtained by superposition of the solutions for the pressure pulses $P(t) = P_o\, e^{-\alpha t}$ and $P(t) = -P_o\, e^{-\beta t}$. This superposition is justified by the Boltzmann superposition principle [Ref. Kolsky (42)]. It can also be justified mathematically in a manner similar to that for the spherical elastic problem (Appendix B). The transform of the displacement potential for any of the linear viscoelastic models can be obtained directly from the transformed elastic solution. The elastic moduli are simply replaced by the transforms of the corresponding viscoelastic moduli (correspondence principle). The superposition discussed in Appendix B should therefore hold for any linear viscoelastic medium.

Scaling Laws. Analysis of the equations of the radial wave parameters and numerical verification lead to the conclusion that Voigt waves obey the same scaling laws as elastic waves (equations 15), provided ω_o is also scaled by the factor $\underline{k}$. The constant ω_o must be divided by the scale factor $\underline{k}$. This change in ω_o changes the viscoelastic character of the medium. No simple scaling laws apply to this model if the elastic and viscoelastic characteristics of the medium are unaltered. These conclusions are easily verified by dimensional analysis.

If the elastic constants, P_o, and the density of the medium are held constant, and a dual exponential pressure pulse is assumed, the scaling laws can be written:

$$
\begin{aligned}
v(r,t,a,\alpha,\beta/\alpha,\omega_o) &= v(kr,kt,ka,\alpha/k,\beta/\alpha,\omega_o/k) \\
\sigma(r,t,a,\alpha,\beta/\alpha,\omega_o) &= \sigma(kr,kt,ka,\alpha/k,\beta/\alpha,\omega_o/k) \\
\varepsilon(r,t,a,\alpha,\beta/\alpha,\omega_o) &= \varepsilon(kr,kt,ka,\alpha/k,\beta/\alpha,\omega_o/k) \\
A(r,t,a,\alpha,\beta/\alpha,\omega_o) &= k\, A(kr,kt,ka,\alpha/k,\beta/\alpha,\omega_o/k) \\
u(r,t,a,\alpha,\beta/\alpha,\omega_o) &= \frac{1}{k}\, u(kr,kt,ka,\alpha/k,\beta/\alpha,\omega_o/k)
\end{aligned}
\qquad (25)
$$

These scaling laws were verified for the single decay exponential and the dual exponential pressure pulses, but similar scaling laws should hold for other pressure pulse shapes provided they are scaled timewise.

Comparison with Elastic Waves. Typical curves showing the radial displacement, particle velocity, acceleration, stress, and strain as functions of time are given in Figures 21 through 25. These curves are for arbitrarily chosen values of $a\alpha$ = 3,000 and $\beta/\alpha = 4$. If ω_o becomes large, Voigt wave characteristics and magnitude approach those of elastic waves (Figures 6 through 10). Comparisons of waves in elastic and Voigt media, for one value of radial distance ($r = 1.5$ a), are given in Figures 26 through 30.

At relatively small radial distances, one to three cavity radii for the cases studied, the peak values of the wave parameters for the elastic waves occur earlier than the corresponding peaks for the Voigt waves. At larger radial distances, four to six cavity radii, the peak values of particle velocity and stress in a Voigt medium were found to be approximately in phase with the corresponding elastic wave parameter peak values.

The acceleration peaks were observed to occur at decreasing values of time as the damping increases. Particle velocity peaks were also observed to occur earlier as the damping was increased, for radial distances greater than three cavity radii.

The peak values of the wave parameters (Figures 31 through 35) are always less for Voigt waves than for the corresponding elastic waves, but they approach those of elastic waves as the damping approaches zero (ω_o becomes large). This fact is illustrated well in Figure 27, for particle velocity.

Voigt wave parameters have the same general shape as elastic wave parameters, while differing in several important respects. The most obvious departure of Voigt waves from elastic waves is found in the case of accelerations at small values of time. Elastic wave acceleration peak value occurs instantaneously with the arrival of the wave front and decays quite rapidly with time; whereas, the acceleration in a Voigt medium starts at zero, builds up quite rapidly to a peak value, and deteriorates rapidly. Accelerations in the two media have approximately the same shape, a short time after the peak values have been reached.

One of the most significant differences between the wave parameters for Voigt and elastic waves is the gradual arrival of Voigt waves compared to the relatively abrupt arrival of elastic waves. This is most strikingly illustrated in the case of particle velocity wave front arrivals, the slopes (with respect to time) of which are the accelerations discussed in the previous paragraph.

The peak values of the wave parameters were found to attenuate at approximately constant rates as functions of radial distance, out to six cavity radii for the parameters investigated. Damping has its largest affect on the peak values of acceleration, and its least overall affect on displacement.

Radial stress at one cavity radius is equal to the applied pressure pulse. At small radial distances the stresses and strains naturally differ very little between the two media. At distances greater than two cavity radii these parameters are much smaller for the Voigt medium than for the elastic.

Peak values of radial wave parameters were compared for elastic and Voigt media (Figures 31 through 35) out to a radial distance of six cavity radii, for $\omega_o = 600$, $\underline{a\alpha} = 3000$, and $\beta/\alpha = 4$. The peak values of displacement were found to decay at a rate of approximately -1.7 ($u_p \propto r^{-1.7}$) in a Voigt medium compared to an average decay rate in an elastic medium of about -1.4 over the same radial range. These decay rates are dependent somewhat on the elastic properties of the medium.

Voigt particle velocity peak values decay at a rate, -1.9 compared to -1.2 for elastic waves. The acceleration peak value attenuation rate for elastic medium is a constant -1.0 independent of the properties of the medium and the pressure pulse parameters; whereas, Voigt acceleration peaks deteriorate at a rate of -2.6 over a distance from one to six cavity radii. The peak values of stress and strain in a Voigt medium decay at a rate of -2.3 compared to rates of -1.5 and -1.6 for stress

and strain respectively in an elastic medium.

The decay rates given in the previous two paragraphs might be considered representative for displacement, particle velocity, and acceleration since the decay rates of those wave parameters were found, in the elastic problem, to be affected very little by changes in elastic constants, $a\alpha$, and β/α. The decay rates for stress and strain peak values were found to be significantly affected by changes in $a\alpha$ and β/α for small distances, therefore, Figures 34 and 35 could not be considered representative if the parameters were changed greatly. They do, however, illustrate the qualitative effects of damping in the Voigt model.

The slow rise time for the Voigt waves at small values of time is illustrated for the particle velocity in Figures 36 and 37. The wave parameters approach zero as the time approaches zero. This property of the Voigt model causes the arrival time of the wave front in theory to be at $t = 0$. For practical purposes of course, the effective arrivals occur much later for large radial distances. Effective arrivals have not been defined but they might realistically be defined as arrivals of amplitudes in excess of some arbitrarily chosen value or some fixed percentage of the peak value.

Comparison With Real Waves. Sauer, et al. (43) report attenuation rates for peak displacements that are greater than -2.0 at small distances and approach -1.0 at large distances. The Voigt

model with ω_o = 600, $\underline{a\alpha}$ = 3,000, and β/α = 4, gives an attenuation rate averaging about -1.7 out to radial distance of six cavity radii. Larger attenuation rates would require considerably larger values of the damping coefficient (smaller ω_o), and smaller rates approaching -1.0 at large distances would require that the Voigt model degenerate to the elastic model.

Sauer, et al. (44) also give a composite correlation of peak particle velocity versus two logarithmic decades of scaled range, which shows an average attenuation rate of -1.65. The Voigt model gave an attenuation rate of -1.7 at small radial distance for ω_o = 1,200, $\underline{a\alpha}$ = 3,000, and β/α = 4, (Figure 32). At small radial distances real waves were reported to attenuate at rates greater than -3.0, with rates decreasing to -1.0 at large distances. [Ref. Sauer (45)]

A composite correlation of first radial acceleration peaks for real waves, shows attenuation rates of -5.0 at small distances, -3.0 at intermediate and -2.0 at large distances [Ref. Sauer (46), and Appendix D]. The Voigt model gave attenuation rates comparable to those of real waves in the intermediate to large distance range, for the parameter values investigated. Apparently, very large values of damping would be required in order to obtain attenuation rates for the Voigt model that approach those reported for peak acceleration at small radial distances.

Voigt waves arrive much sooner than elastic or real waves. This early arrival time was noted by Clark, et al. (47) in

their investigation of Voigt waves generated by a single decay exponential pressure pulse. Clark attributed the early arrival of the wave front to the abrupt rise in magnitude of the pressure pulse (instantaneous rise time) and the rigid response of the Voigt model to abrupt changes in force. The early arrival of the wave front was found to be only slightly changed by employing the dual exponential pressure pulse, which exhibits no instantaneous rise time. The effective wave front arrivals obtained for the dual exponential pressure pulse arrived much earlier than elastic waves, but only slightly later than Voigt waves for the single exponential pressure pulse.

Voigt waves exhibit significant pulse lengthening with travel distance as do real waves. They differ, however, in their pulse lengthening characteristics from those of real waves, in that they spread out in both directions from the arrival time predicted by elastic wave velocity.

Conclusions. Comparison of theoretical wave propagation with real wave propagation is hampered by insufficient knowledge of the effective cavity radius.

It appears that Voigt waves exhibit significant correlation with real waves at intermediate radial distances. The attenuation rates can apparently be made to agree fairly well in the intermediate range of radial distances, and the Voigt waves show pulse lengthening. Probably the most significant difference occurs in the early arrival of Voigt waves.

A change in pressure pulse shape from the single decay exponential to the dual decay exponential apparently satisfies few if any of the objections to the Voigt model reported by Clark, et al. (48).

At very small distances, the Voigt model would require an extremely large damping coefficient to give attenuation rates of the magnitude reported for real waves. At large radial distances the damping would have to become very small to give attenuation rates corresponding to those of real waves. In the latter case the Voigt model approaches the elastic, which no longer exhibits pulse lengthening.

At best it appears that the Voigt model would be applicable only over relatively small range of radial distance. No combinations of damping and pressure pulse shape are expected to give significantly better correlation with real waves over a large range of radial distance.

No simple scaling laws are applicable to Voigt waves if the elastic and viscoelastic properties of the medium are unaltered.

The validity of the series solutions (equations 20 through 24) are attested to by the fact that they approach the appropriate elastic cases as ω_o becomes large (Figures 26 through 30). Their validity is further supported by the close agreement with results obtained by numerical inversion (Appendix F).

The Voigt curves which follow (Figures 21 through 37) were obtained from equations 20 through 24.

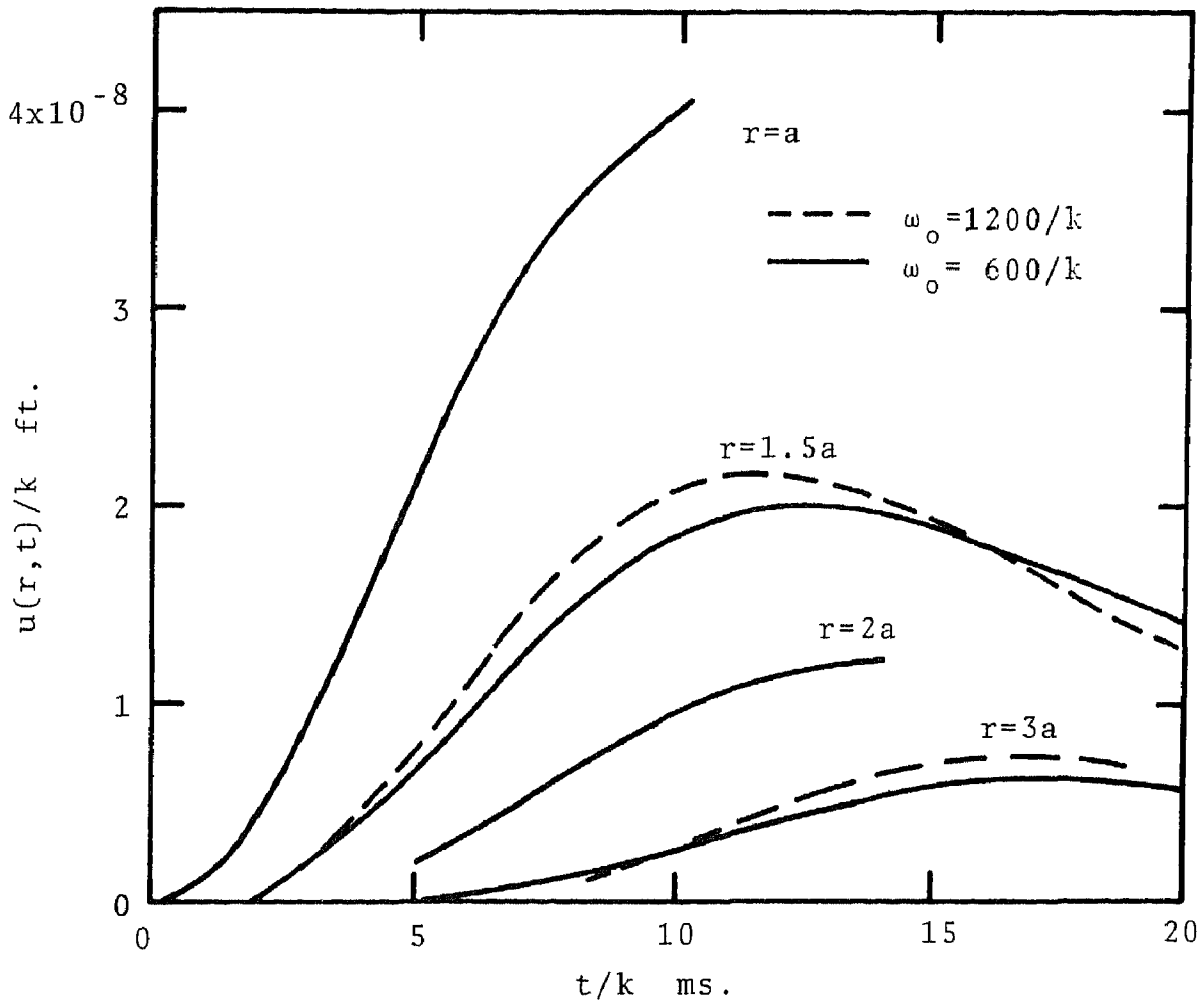

Figure 21. Displacement vs. time for spherical waves in a granite Voigt medium for a normalized dual exponential pressure pulse, $a\alpha=3,000$, $\beta/\alpha=4$, $k=60/\alpha$.

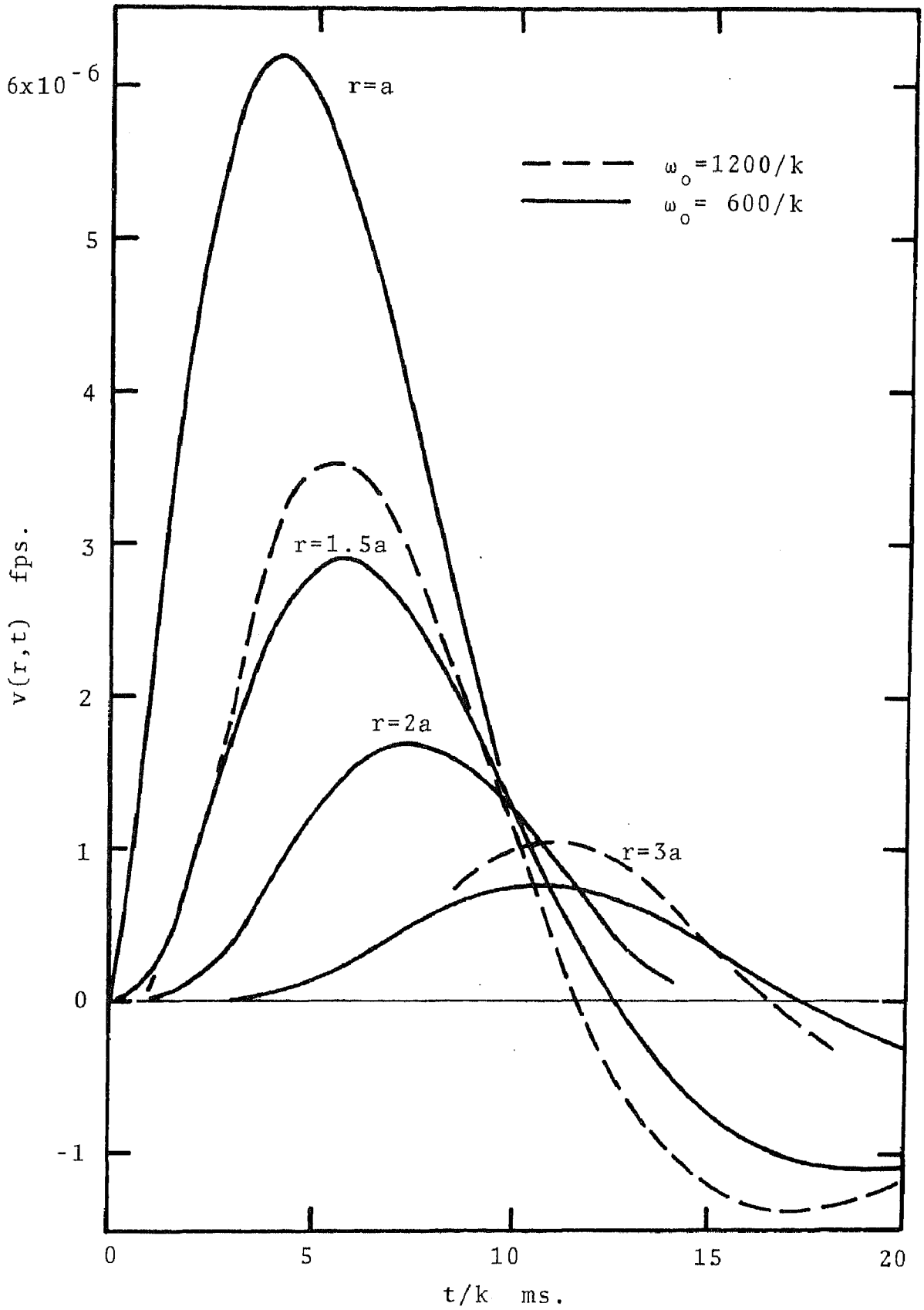

Figure 22. Particle velocity vs. time for spherical waves in a granite Voigt medium for a normalized dual exponential pressure pulse, $a\alpha=3,000$, $\beta/\alpha=4$, $k=60/\alpha$.

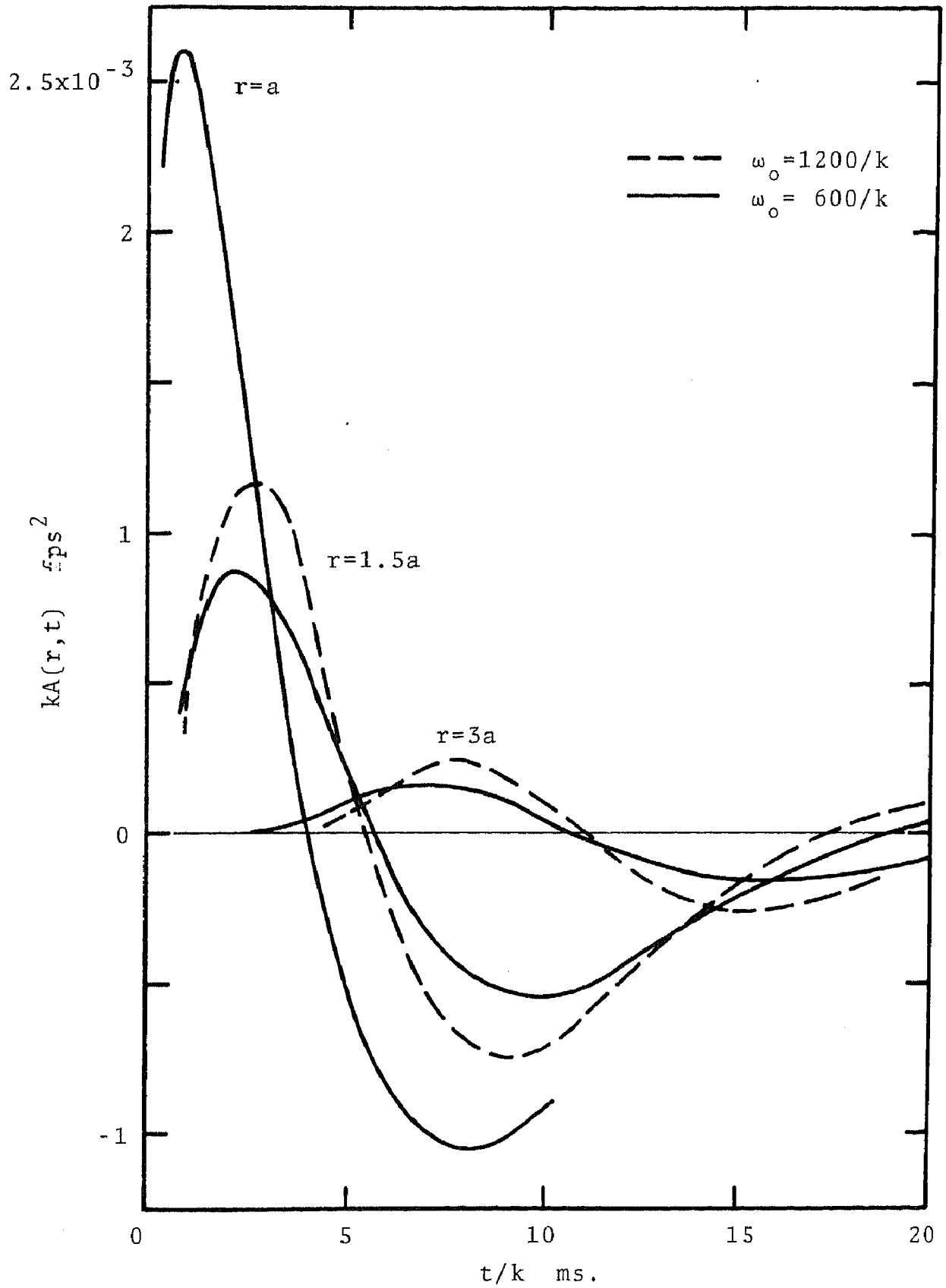

Figure 23. Acceleration vs. time for spherical waves in a granite Voigt medium for a normalized dual exponential pressure pulse, $a\alpha=3,000$, $\beta/\alpha=4$, $k=60/\alpha$.

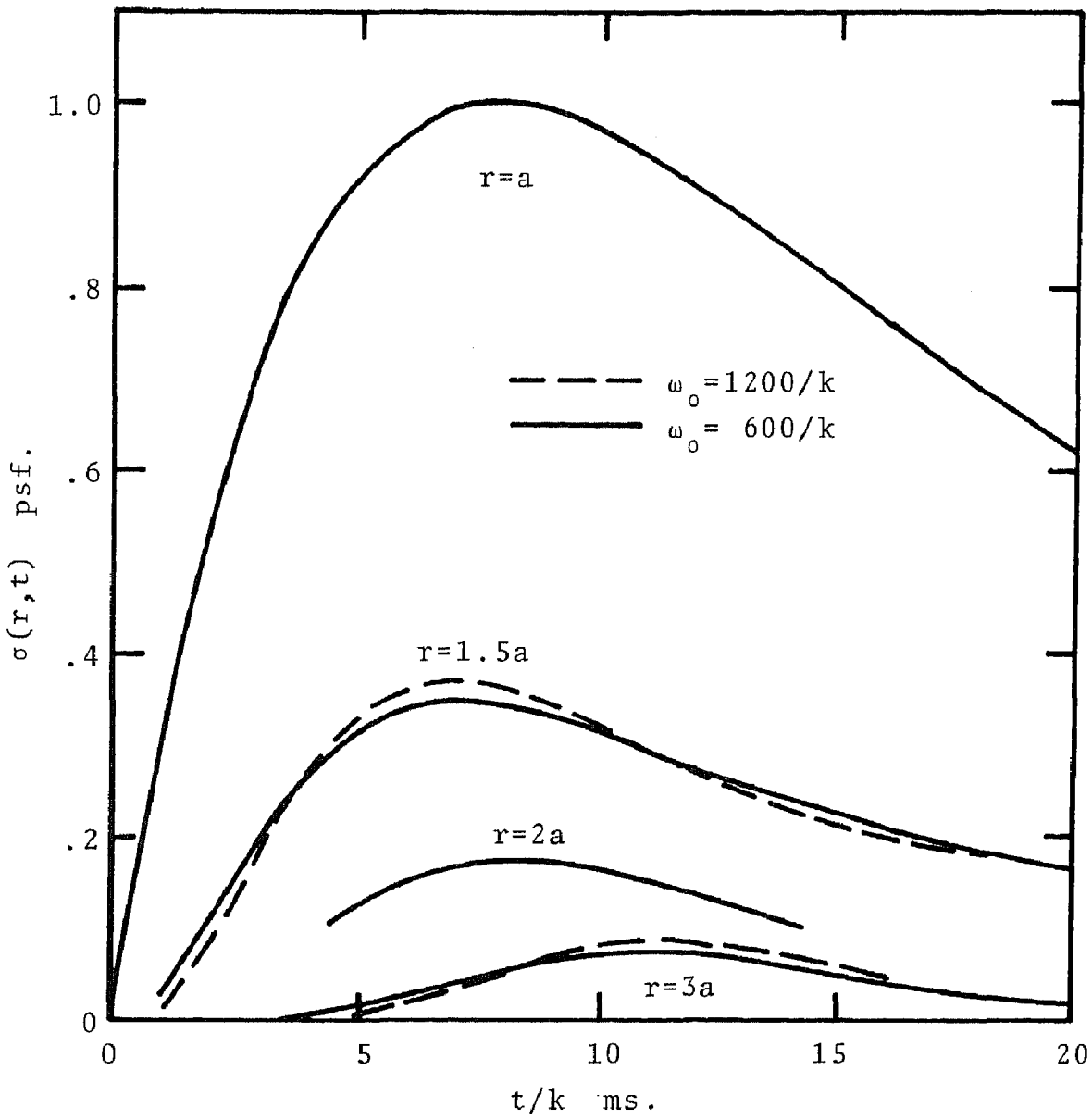

Figure 24. Stress vs. time for spherical waves in a granite Voigt medium for a normalized dual exponential pressure pulse, $a\alpha=3{,}000$, $\beta/\alpha=4$, $k=60/\alpha$.

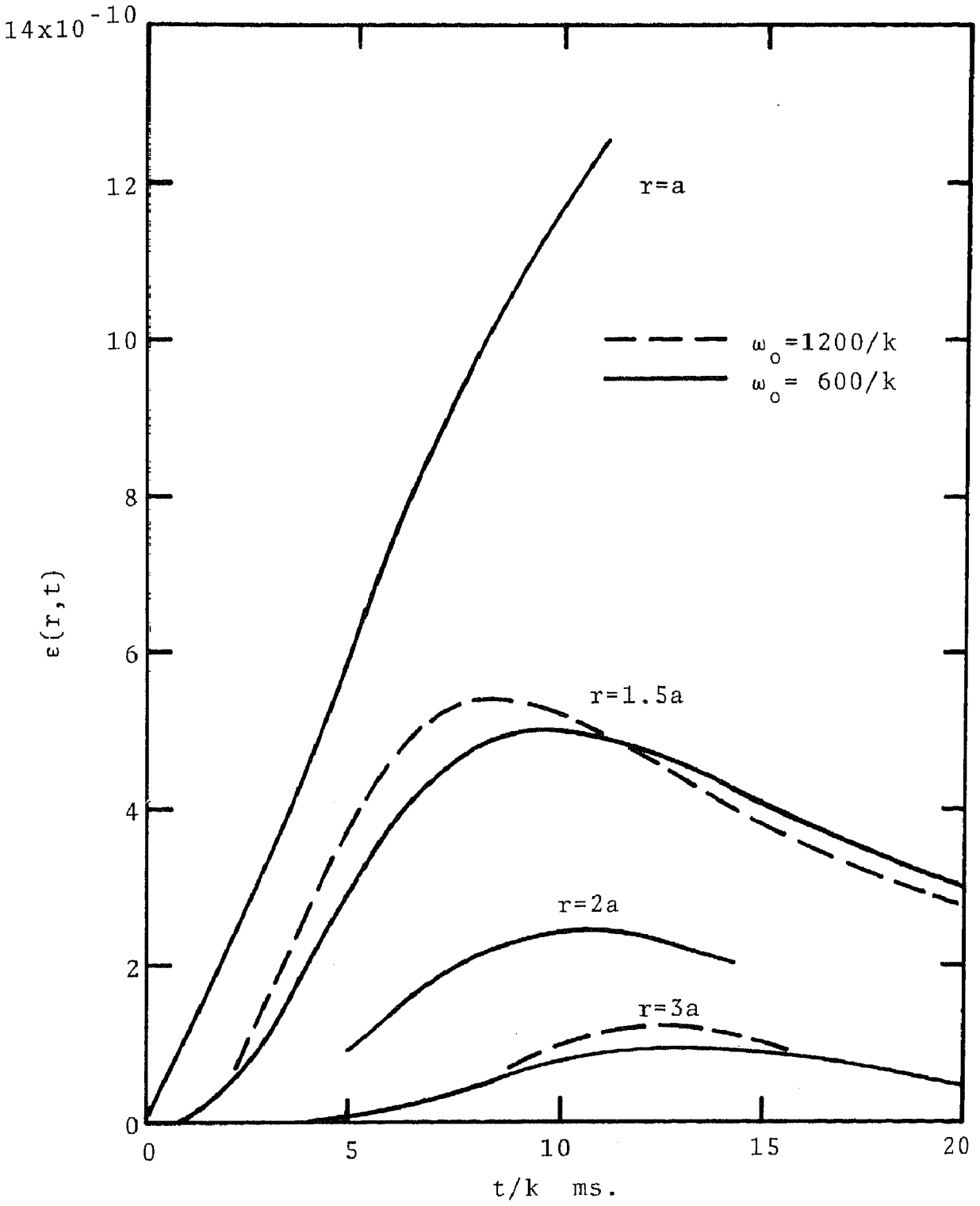

Figure 25. Strain vs. time for spherical waves in a granite Voigt medium for a normalized dual exponential pressure pulse, $a\alpha=3,000$, $\beta/\alpha=4$, $k=60/\alpha$.

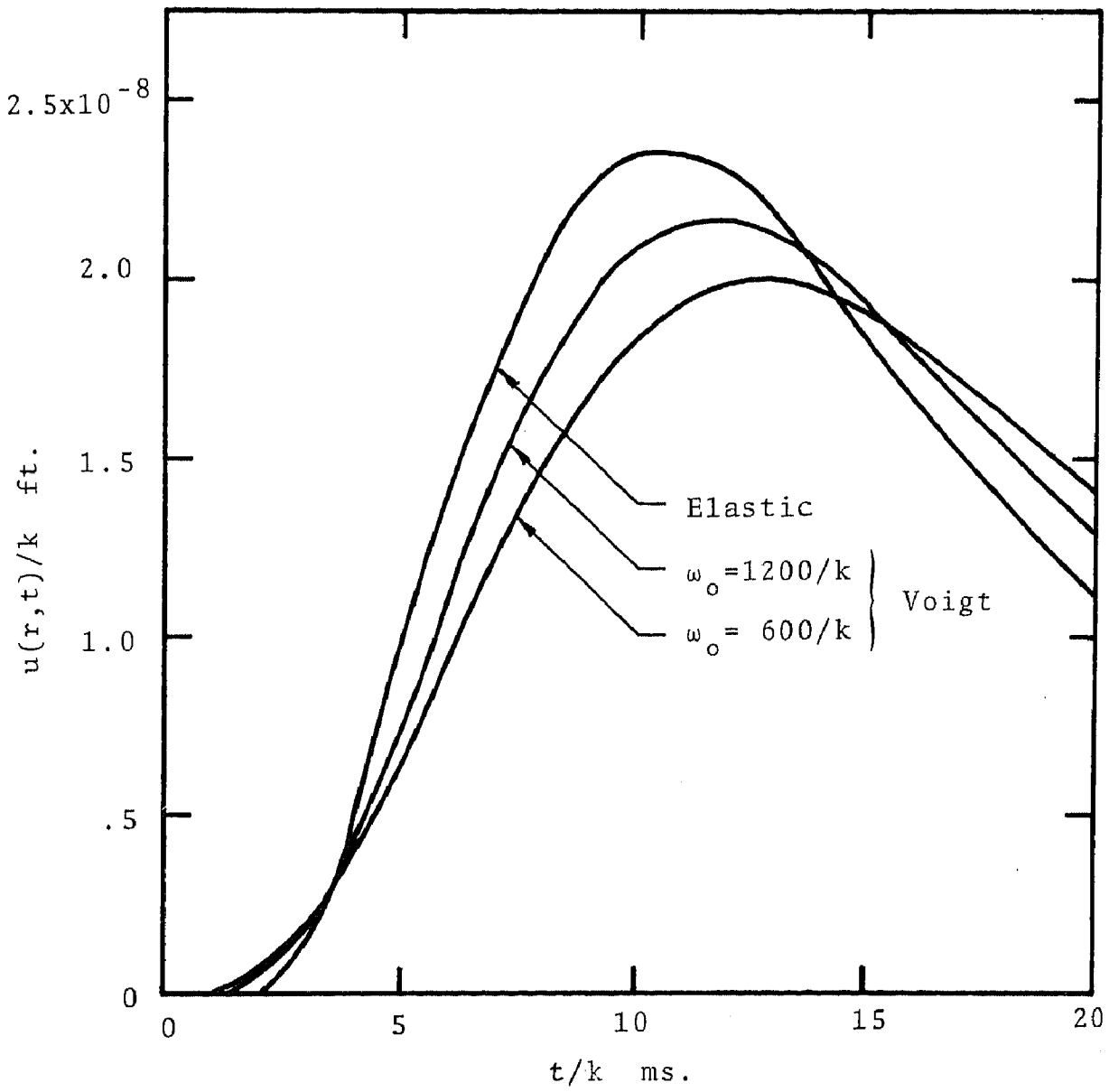

Figure 26. Displacement vs. time for spherical waves in Voigt and elastic granite media for a normalized dual exponential pressure pulse, $a\alpha=3,000$, $\beta/\alpha=4$, $r=1.5a$, $k=60/\alpha$.

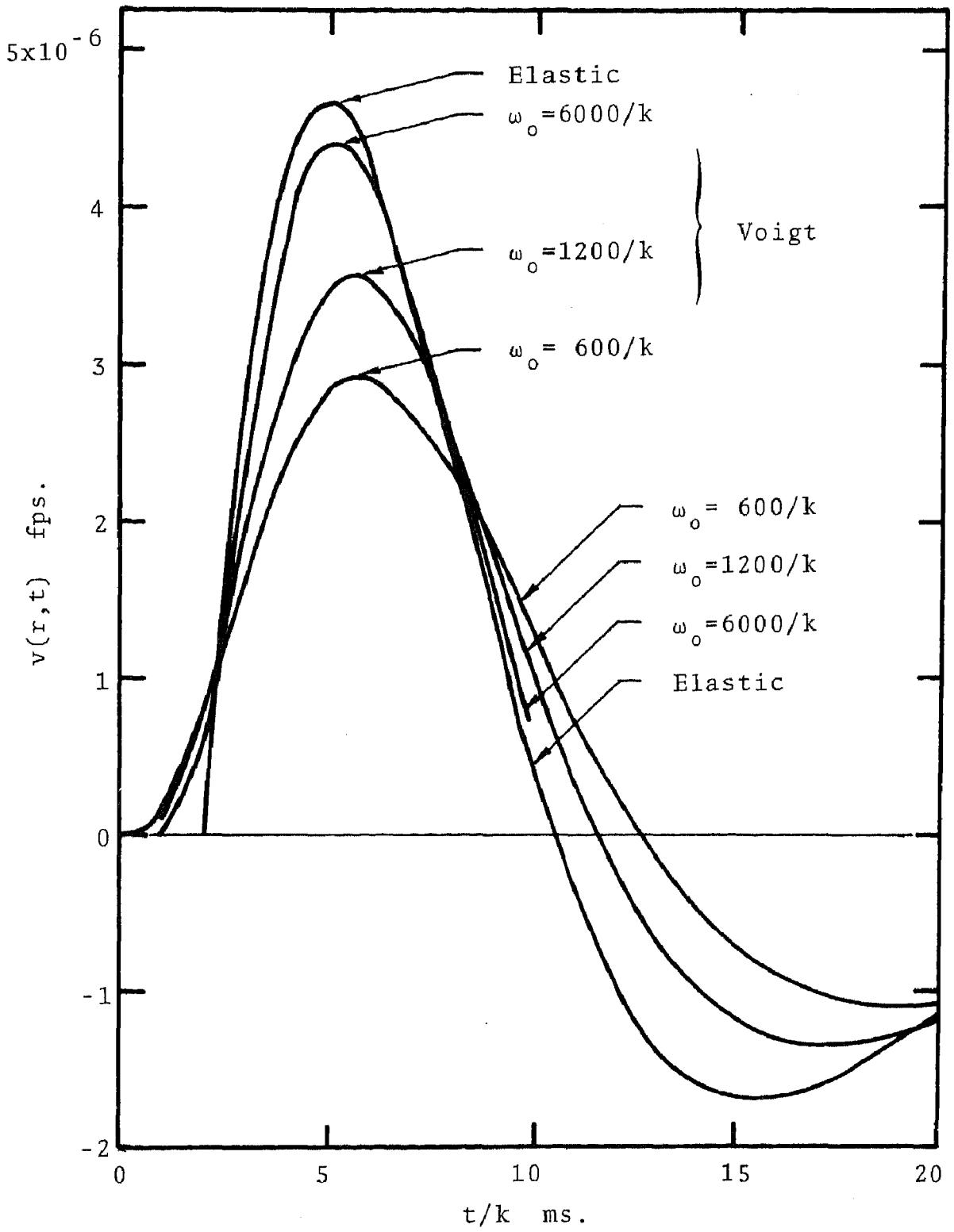

Figure 27. Particle velocity vs. time for spherical waves in Voigt and elastic granite media for a normalized dual exponential pressure pulse, $a\alpha=3{,}000$, $\beta/\alpha=4$, $r=1.5a$, $k=60/\alpha$.

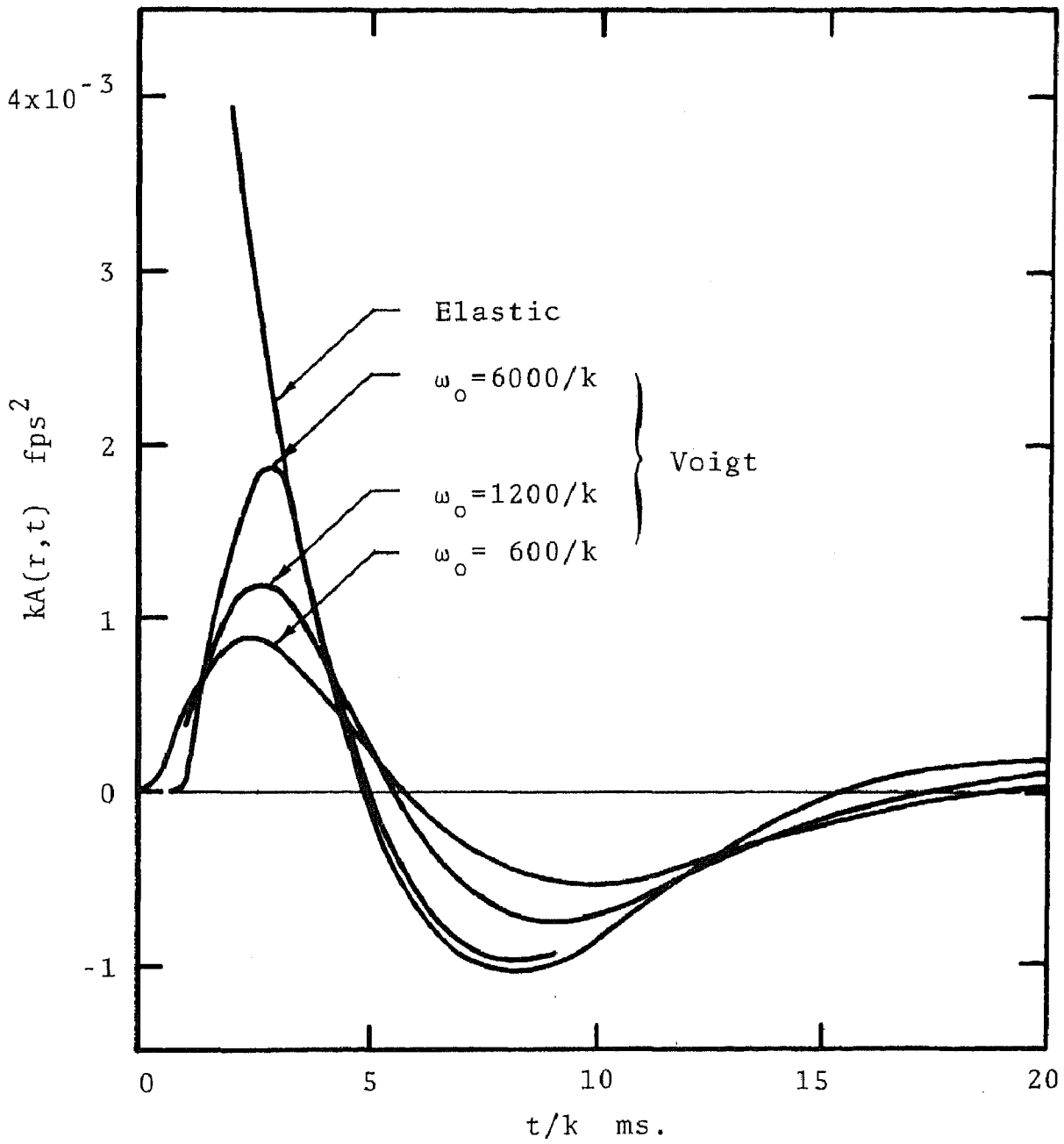

Figure 28. Acceleration vs. time for spherical waves in Voigt and elastic granite media for a normalized dual exponential pressure pulse, $a\alpha=3{,}000$, $\beta/\alpha=4$, $r=1.5a$, $k=60/\alpha$.

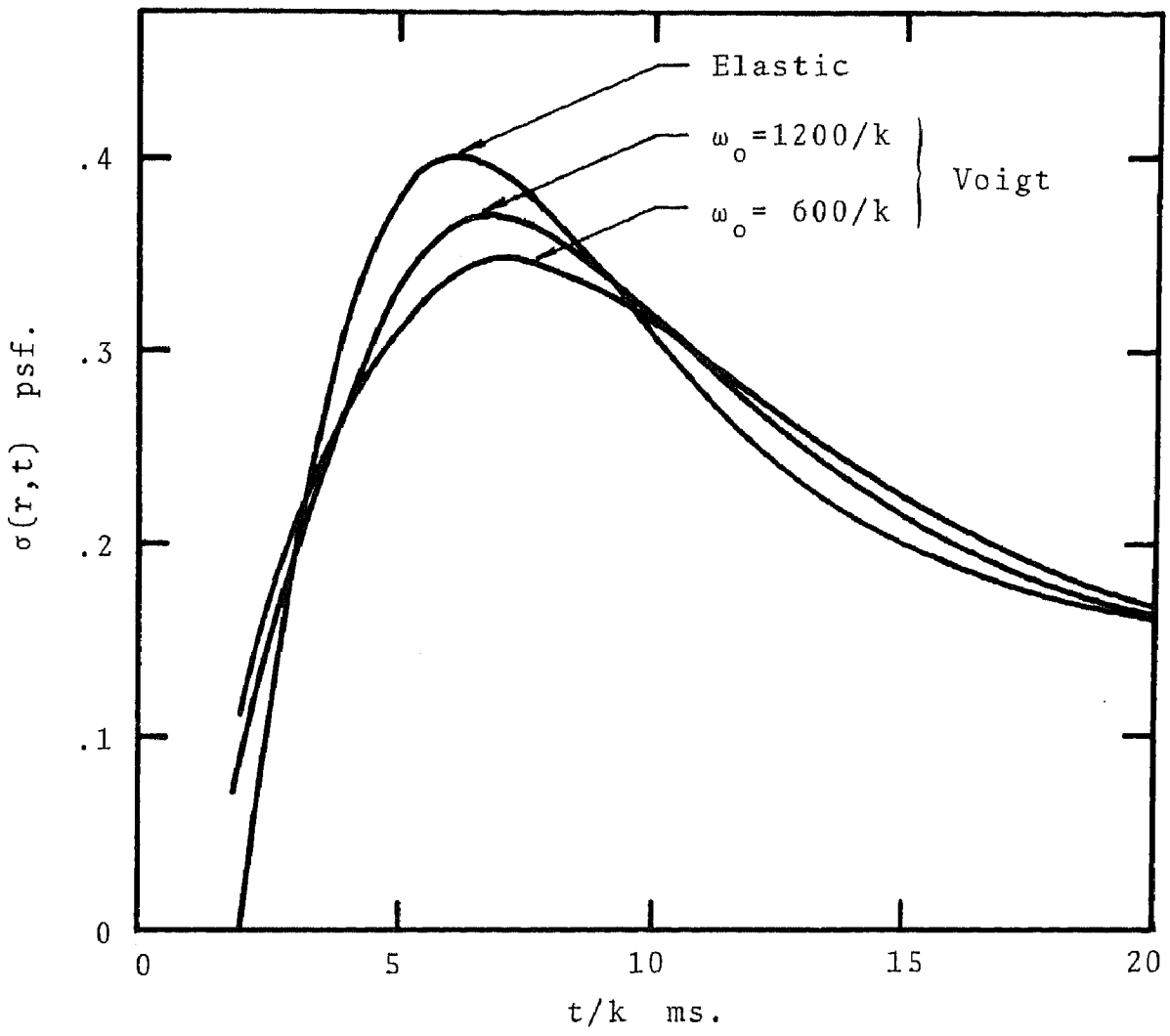

Figure 29. Stress vs. time for spherical waves in Voigt and elastic granite media for a normalized dual exponential pressure pulse, $a\alpha$=3,000, β/α=4, r=1.5a, k=60/α.

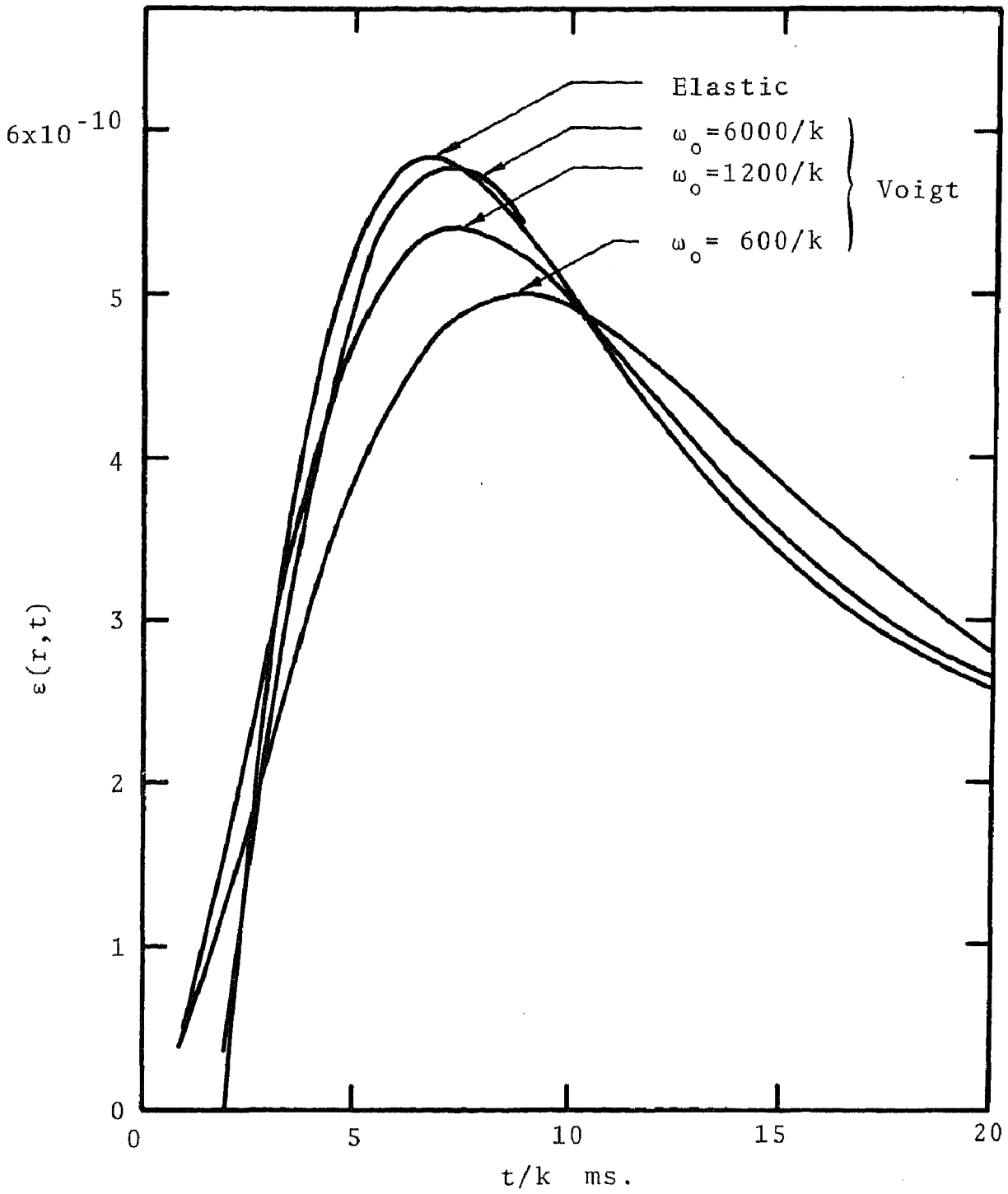

Figure 30. Strain vs. time for spherical waves in Voigt and elastic granite media for a normalized dual exponential pressure pulse, $a\alpha$=3,000, β/α=4, r=1.5a, k=60/α.

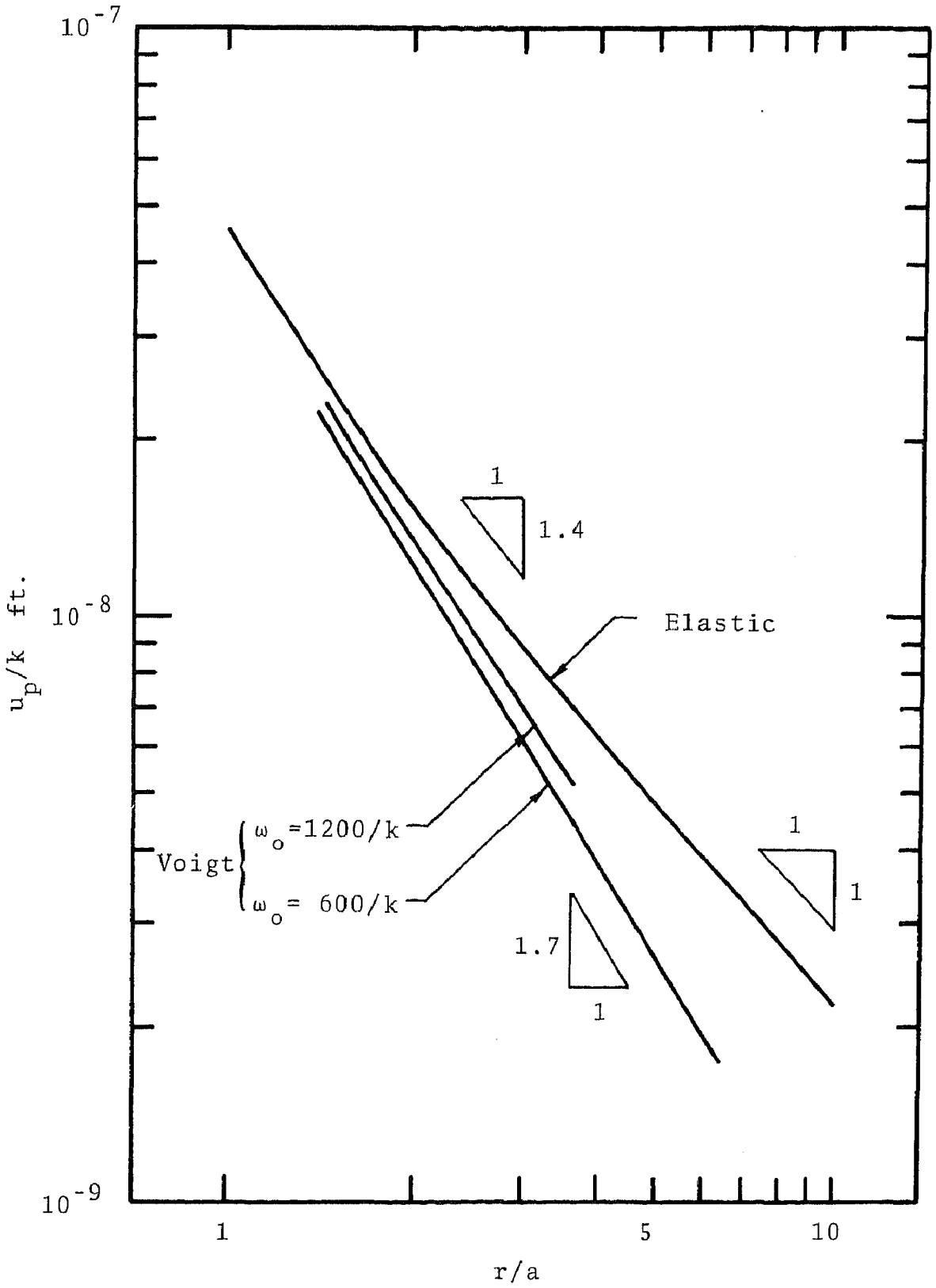

Figure 31. Peak displacement vs. radial distance for spherical waves in Voigt and elastic granite media for a normalized dual exponential pressure pulse, $a\alpha$=3,000, β/α=4, k=60/α.

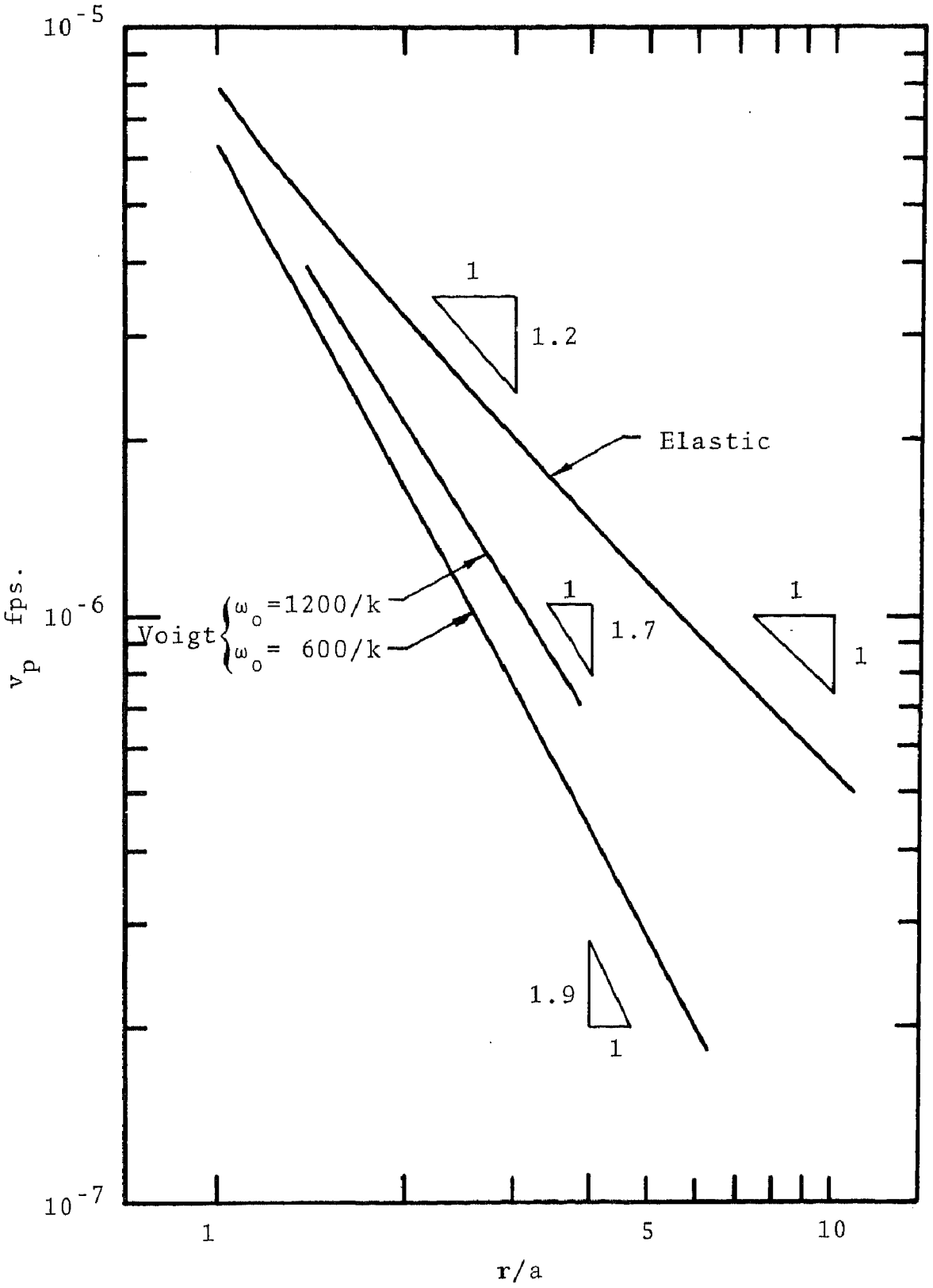

Figure 32. Peak particle velocity vs. radial distance for spherical waves in Voigt and elastic granite media for a normalized dual exponential pressure pulse, $a\alpha$=3,000, β/α=4, k=60/α.

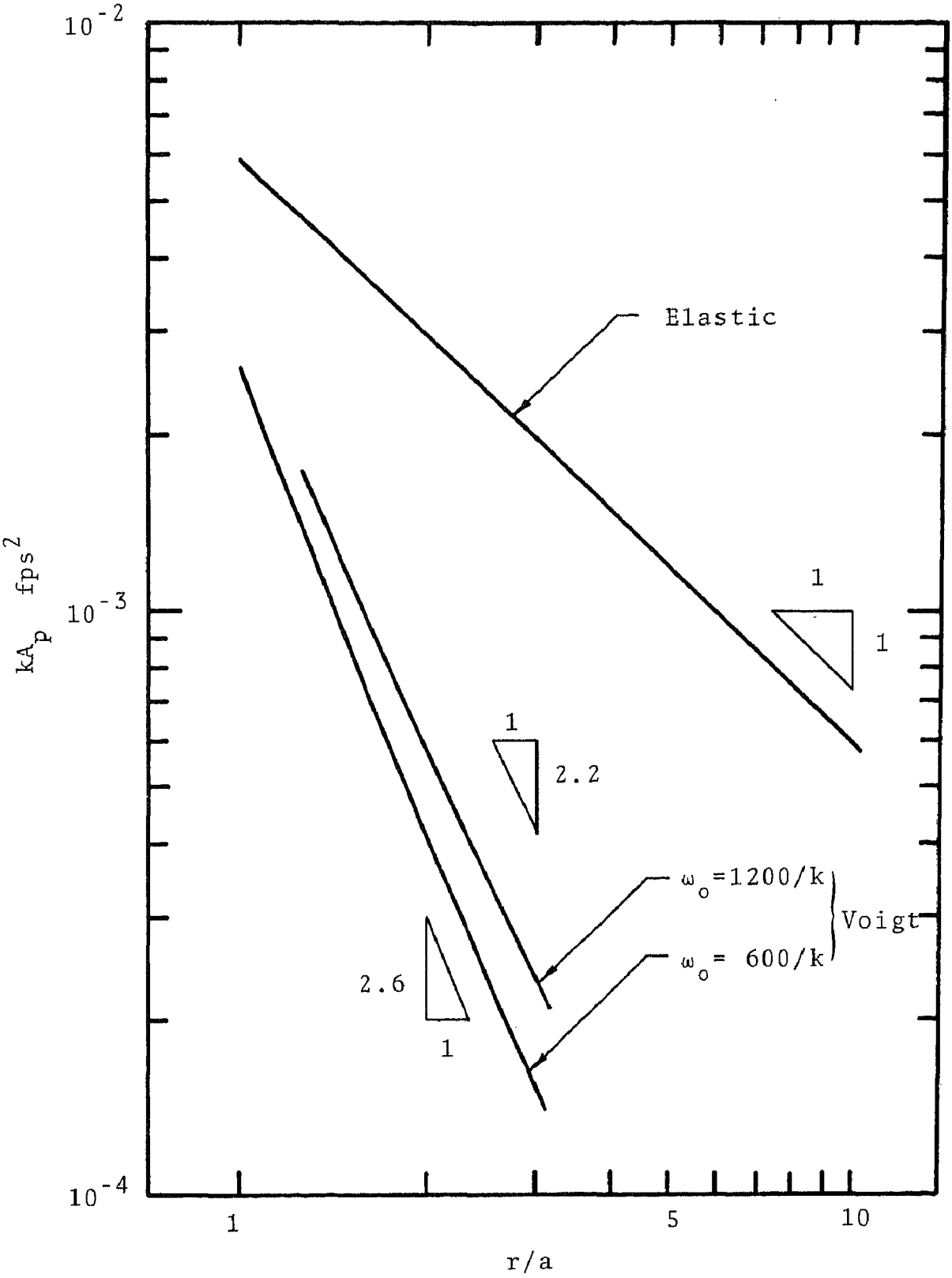

Figure 33. Peak acceleration vs. radial distance for spherical waves in Voigt and elastic granite media for a normalized dual exponential pressure pulse, $a\alpha$=3,000, β/α=4, k=60/α.

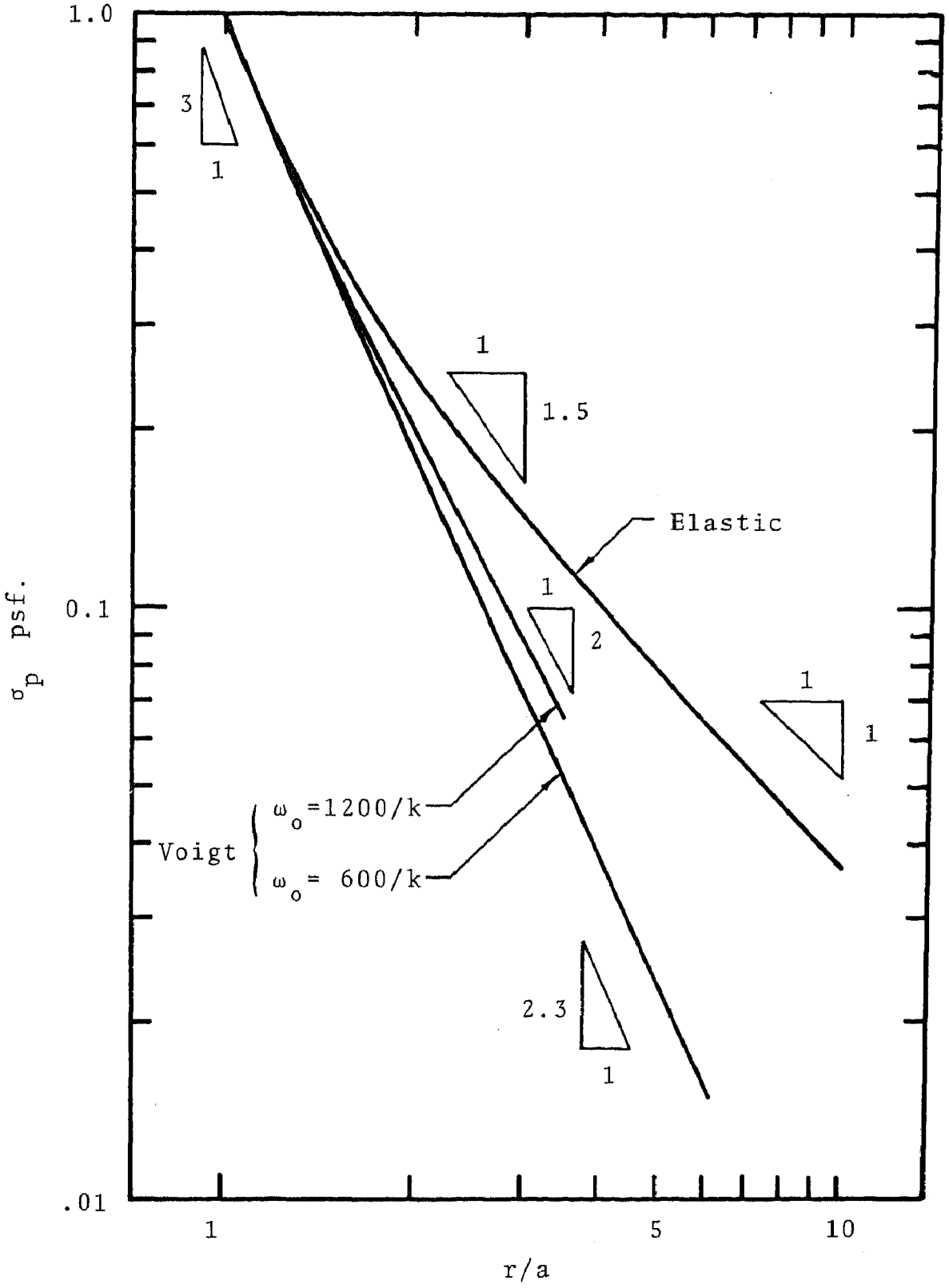

Figure 34. Peak stress vs. radial distance for spherical waves in Voigt and elastic granite media for a normalized dual exponential pressure pulse, $a\alpha$=3,000, β/α=4, k=60/α.

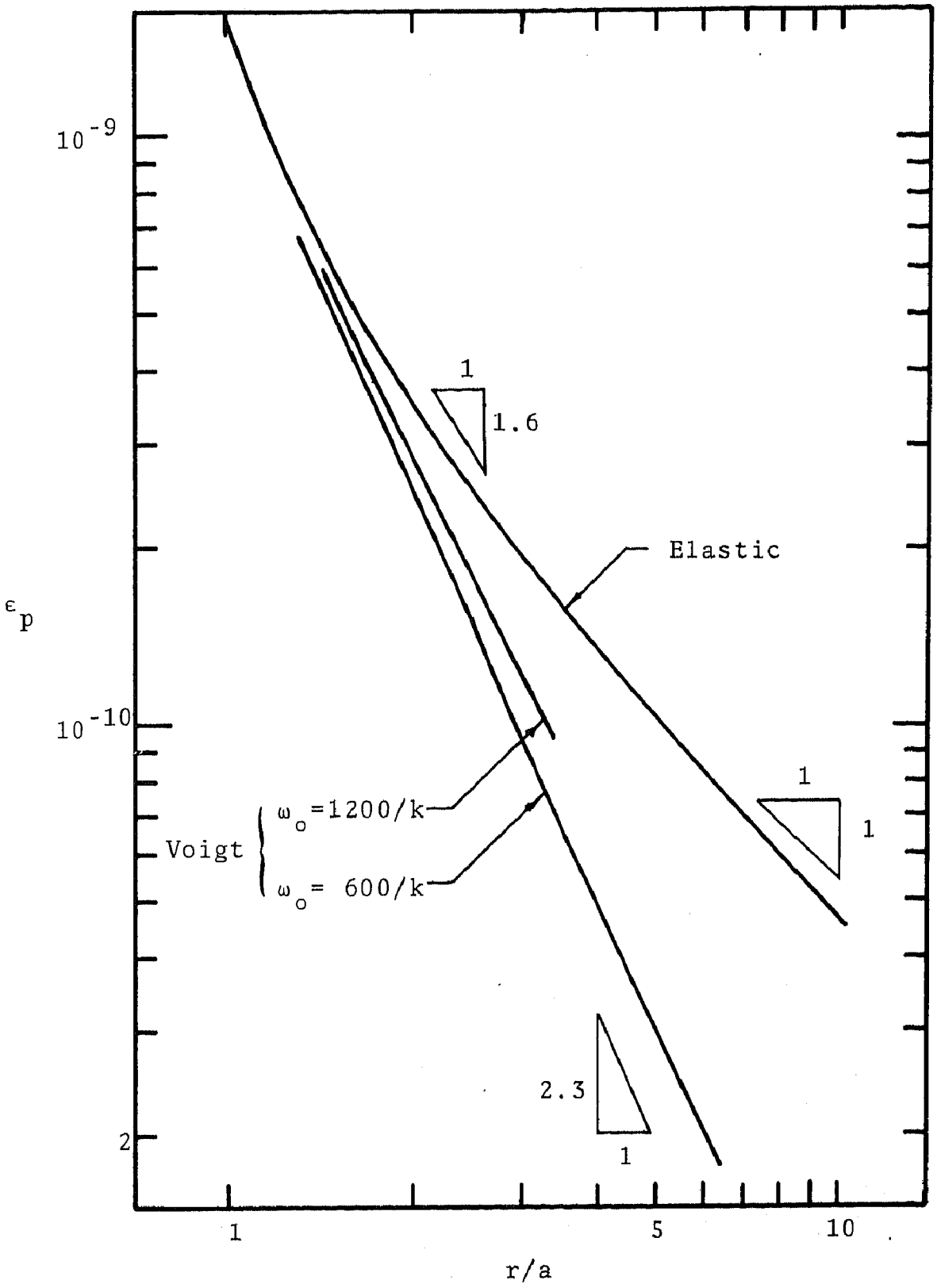

Figure 35. Peak strain vs. radial distance for spherical waves in Voigt and elastic granite media for a normalized dual exponential pressure pulse, $a\alpha$=3,000, β/α=4, k=60/α.

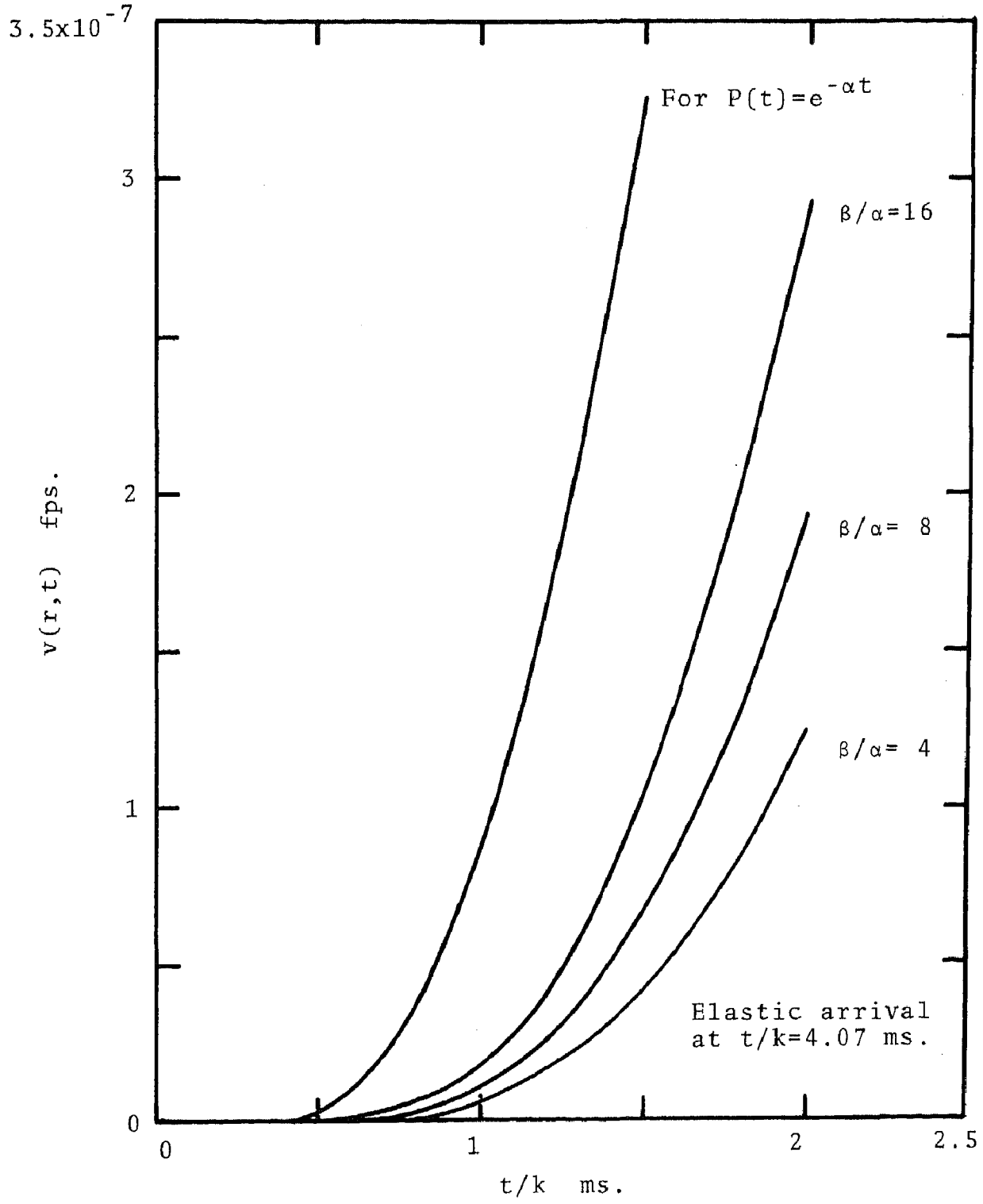

Figure 36. Velocity arrivals vs. time for spherical waves in a granite Voigt medium for single and normalized dual exponential pressure pulses, $a\alpha=3,000$, $\omega_o=600/k$, $r=2a$, $k=60/\alpha$.

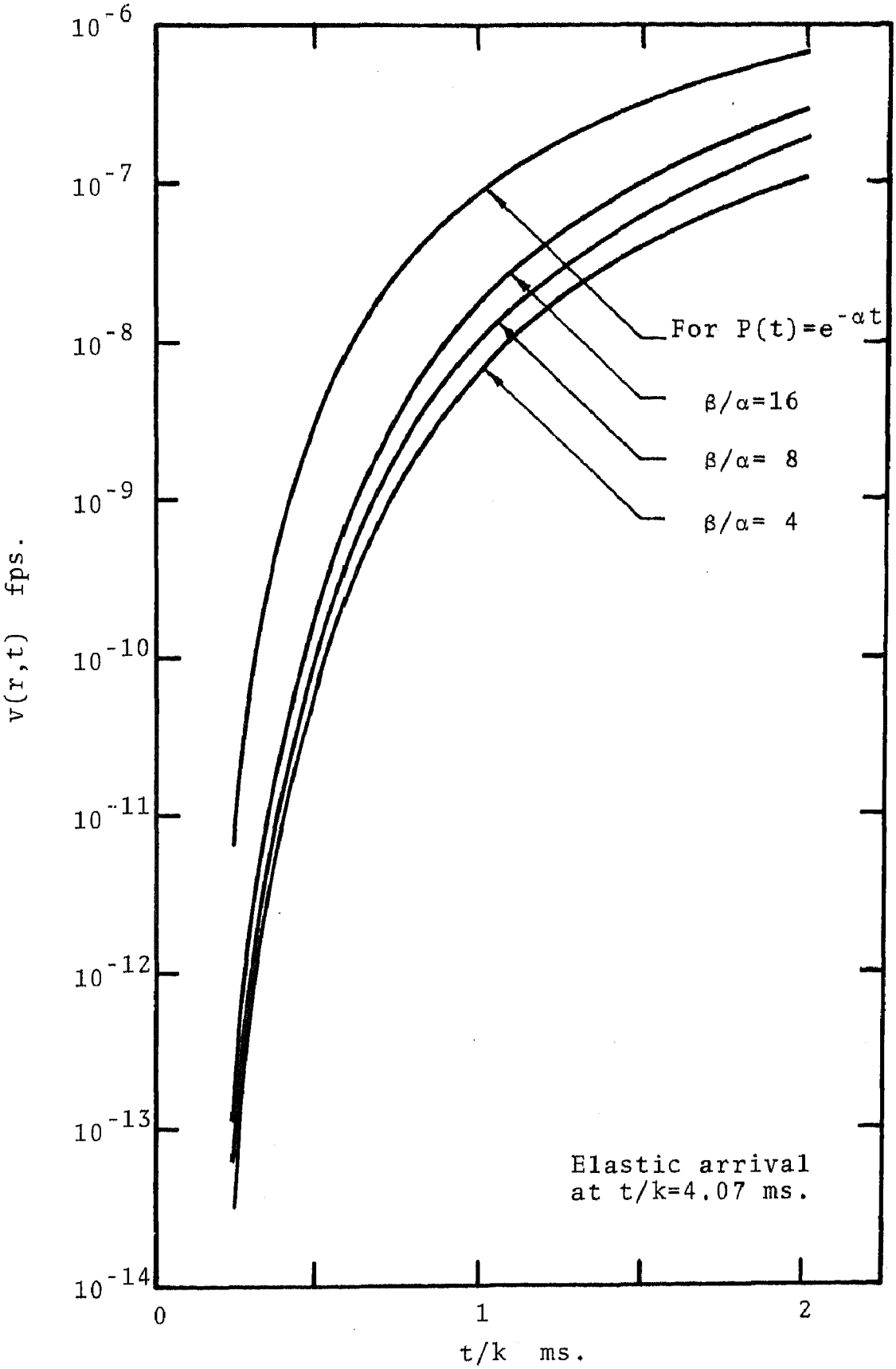

Figure 37. Logarithmic velocity arrivals vs. time for spherical waves in a granite Voigt medium for single and normalized dual exponential pressure pulses, $a\alpha=3,000$, $\omega_o=600/k$, $r=2a$, $k=60/\alpha$.

CHAPTER V

SERIES SOLUTIONS FOR PLANE WAVES IN A THREE-ELEMENT LINEAR VISCOELASTIC MEDIUM

Three-Element Models. There are four non-degenerate, three-element, linear viscoelastic models. Two of these are commonly called three-element elastic models, and they are equivalent. They are composed of an elastic element respectively in series with a Voigt model, and in parallel with a Maxwell model. The two remaining are the three-element viscous models which may be formed by adding a viscous element respectively, in series with a Voigt model, and in parallel with a Maxwell model.

Transient waves in a semi-infinite three-element rod were investigated in this research. The axial stress-strain relationship for both of the three-element elastic models is

$$\left[\frac{\partial}{\partial t} + p_o\right] \sigma = \left[q_1 \frac{\partial}{\partial t} + q_o\right] \varepsilon \tag{26}$$

where p_o, q_1, and q_o depend only on the elastic and viscous constants, and they take different forms for the two cases.

In this investigation, an elastic element of modulus E_1 in series with a Voigt model of elastic modulus E_2 and damping coefficient η_2 was assumed. The axial stress-strain relationship can be written

$$\left[\frac{\partial}{\partial t} + \frac{E_1+E_2}{\eta_2}\right] \sigma = \left[E_1 \frac{\partial}{\partial t} + \frac{E_1 E_2}{\eta_2}\right] \varepsilon. \tag{27}$$

Morrison (49) investigated both types of three-element viscoelastic media, and obtained integral solutions for the particle velocity and radial stress in a semi-infinite rod subjected to a unit step velocity pulse at the free end. Lee and Morrison (50) investigated the stress distribution in a semi-infinite rod subjected to a unit step velocity pulse and a unit step pressure pulse. Their investigations involved several models including the three-element viscoelastic, and their solutions were left in integral form. Both papers give numerical examples in the form of graphs. Arenz (51) also investigated the three-element model, but he used an extension of the Schapery collocation inversion method to obtain numerical results.

Series solutions for the particle velocity, acceleration, displacement, stress, and strain were derived. Three pressure pulses were utilized, the unit impulse, unit step, and the single decay exponential. The details of the derivation of the wave parameters are given only for the single decay exponential pressure pulse, since it is the most complex of the three, and since it utilizes all of the principles involved in obtaining solutions for the other two pressure pulses.

Transform Solutions. The strain displacement relationship is

$$\varepsilon = \frac{\partial u}{\partial x} \tag{28}$$

and the particle velocity is related to the displacement by

$$v = \frac{\partial u}{\partial t}. \tag{29}$$

Newtons second law is expressed as

$$\frac{\partial \sigma}{\partial x} = \rho \frac{\partial v}{\partial t} \tag{30}$$

where the stress-strain relationship is given by equation 27. It is convenient to make the substitutions

$$E_2 = E, \qquad E_1 = \chi E, \quad \text{and} \quad \eta_2 = E/\omega_o$$

and to re-write equation 27 in the form:

$$\left[\frac{1}{\omega_o}\frac{\partial}{\partial t} + (\chi+1)\right]\sigma = \chi E\left[\frac{1}{\omega_o}\frac{\partial}{\partial t} + 1\right]\varepsilon \tag{31}$$

The assumed initial and boundary conditions are

$$\sigma(0,t) = -P(t) \qquad t \geq o \tag{32}$$

$$\sigma(x,0) = 0 \qquad x > 0 \tag{33}$$

$$\varepsilon(x,0) = 0 \tag{34}$$

$$u(x,0) = 0 \tag{35}$$

$$v(x,0) = 0 \tag{36}$$

and

$$\lim_{x\to\infty} \sigma(x,t) = 0. \tag{37}$$

The Laplace transformations of equations 28 through 32 and equation 37, subject to the initial conditions given by equations 33 through 36 are, respectively:

$$\bar{\varepsilon} = \frac{d\bar{u}}{dx} \tag{38}$$

$$\bar{v} = s\bar{u} \tag{39}$$

$$\frac{d\bar{\sigma}}{dx} = \rho s\bar{v} \tag{40}$$

$$[s/\omega_o + (\chi+1)]\ \bar{\sigma} = \chi E\ [s/\omega_o + 1]\ \bar{\varepsilon} \tag{41}$$

$$\bar{\sigma}(0,s) = -P(s) \tag{42}$$

and

$$\lim_{\bar{x}\to\infty} \sigma\ (\bar{x},s) = 0 \tag{43}$$

Substitution of equation 39 into 40 gives

$$\frac{d\bar{\sigma}}{dx} = \rho s^2 \bar{u}, \tag{44}$$

and differentiation with respect to $\underline{x}$, and substitution of equation 38 yields

$$\frac{d^2\bar{\sigma}}{dx^2} - \rho s^2 \bar{\varepsilon} = 0. \tag{45}$$

Combining equations 41 and 45 gives the diffenential equation

$$\frac{d^2\bar{\sigma}}{dx^2} - \frac{\rho s^2\ [s/\omega_o + (\chi+1)]\ \bar{\sigma}}{\chi E\ [s/\omega_o + 1]} = 0. \tag{46}$$

The solution of equation 46 subject to the conditions of equations 42 and 43 is

$$\bar{\sigma}(x,s) = -P(s)\ \exp\left\{ - \frac{sx}{c_1} \left[\frac{s/\omega_o + (\chi+1)}{s/\omega_o + 1} \right]^{\frac{1}{2}} \right\} \tag{47}$$

where

$$c_1 = (\chi E/\rho)^{\frac{1}{2}}.$$

The transform equations for v, u, and ε can easily be obtained from equations 38, 39, and 40 in conjuction with equation 47.

Wave Equation. Equations 28 through 31 can be manipulated to give the wave equation

$$\frac{\partial^3 y}{\partial t^3} + (\chi+1)\omega_o \frac{\partial^2 y}{\partial t^2} = c_1^2 \frac{\partial^3 y}{\partial x^2 \partial t} + c_1^2 \omega_o \frac{\partial^2 y}{\partial x^2} \qquad (48)$$

where y can be any one of the parameters: u, v, A, σ, or ε.

The transform solutions could have been obtained from the wave equation, but it is simpler, when using Laplace transforms, to work directly with equations 28 through 31.

The transform solutions can also be obtained from the corresponding elastic solutions using the correspondence principle [Ref. Bland (52)].

Series Expansions. The pressure pulse was chosen to be the single decay exponential $P(t) = P_o e^{-\alpha t}$, whose Laplace transform is

$$P(s) = P_o/(s+\alpha). \qquad (49)$$

When s is replaced in equations 47 and 49 by $\omega_o s$, and equation 49 is substituted into 47 the result is

$$-\frac{1}{P_o}\sigma(x,t/\omega_o) = \frac{1}{(s+\alpha/\omega_o)} \exp\left\{-sX\left[1+\frac{\chi}{s+1}\right]^{\frac{1}{2}}\right\} \qquad (50)$$

where

$$X = \omega_o x/c_1.$$

The expansion of Mikusinski (53)

$$\left[\left\{1+\frac{\chi}{s+1}\right\}^{\frac{1}{2}} - 1\right]^n = n \sum_{\nu=o}^{\infty} \frac{(-1)^\nu (n+2\nu-1)!}{2^{n+2\nu}\,\nu!\,(n+\nu)!}\left[\frac{\chi}{s+1}\right]^{n+\nu} \quad n>o \qquad (51)$$

in conjunction with the exponential expansion

$$\exp\left\{-Xs\left[\left(1+\frac{\chi}{s+1}\right)^{\frac{1}{2}}-1\right]\right\} = 1+\sum_{n=1}^{\infty}\frac{(-1)^n X^n s^n}{n!}\left\{\left[1+\frac{\chi}{s+1}\right]^{\frac{1}{2}}-1\right\}^n \tag{52}$$

after replacing ν by ν-n, and changing the order of summation gives

$$\exp\left\{-Xs\left[\left(1+\frac{\chi}{s+1}\right)^{\frac{1}{2}}-1\right]\right\} = 1+\sum_{\nu=1}^{\infty}\sum_{n=1}^{\nu}\frac{(-1)^\nu(2\nu-n-1)!X^n s^n}{2^{2\nu-n}(n-1)!(\nu-n)!\nu!}\left[\frac{\chi}{s+1}\right]^\nu . \tag{53}$$

If the expansion

$$\frac{1}{s+\alpha/\omega_o} = \sum_{m=1}^{\infty}\frac{1}{s^m}(-\alpha/\omega_o)^{m-1} \tag{54}$$

is employed with equation 53, one can write

$$\frac{1}{(s+\alpha/\omega_o)}\exp\left\{-Xs\left[\left(1+\frac{\chi}{s+1}\right)^{\frac{1}{2}}-1\right]\right\} = \tag{55}$$

$$\frac{1}{(s+\alpha/\omega_o)}+\sum_{m=1}^{\infty}\sum_{\nu=1}^{\infty}\sum_{n=1}^{\nu}\frac{(-1)^\nu(2\nu-n-1)!(-\alpha/\omega_o)^{m-1}X^n\chi^\nu s^{n-m}}{2^{2\nu-n}(n-1)!(\nu-n)!\ \nu!\ (s+1)^\nu} .$$

Inverse Transformation. The series of terms involving the transform variable s in equation 55 can be inverted to the time plane by a term by term inversion using the relationships;

$$\left[s^i\left\{\frac{1}{s+1}\right\}^j\right] \doteq \begin{cases} \dfrac{d^i}{dt^i}\left[\dfrac{t^{j-1}e^{-t}}{(j-1)!}\right] + \delta(t) & i=j \\ \dfrac{d^i}{dt^i}\left[\dfrac{t^{j-1}e^{-t}}{(j-1)!}\right] & 1\leq i\leq j-1 \\ t^{j-1}e^{-t}/(j-1)! & i=0 \\ \int_0^t\int_0^{t_2}\cdots\int_0^{t_i} \dfrac{\tau^{j-1}e^{-\tau}}{(j-1)!}\, d\tau, dt_i, \ldots, dt_2 & i\leq -1 \end{cases} \tag{56}$$

where i and j are integers.

In order to simplify writing of the solutions, it is convenient to introduce the notation:

$$DE_{i,j}(t) = \begin{cases} D_{i,j}(t) = \dfrac{d^i}{dt^i}\left[t^{j-1}e^{-t}\right] & i>0 \\ D_{0,j}(t) = E_{0,j}(t) = t^{j-1}e^{-t} & \\ E_{|i|,j}(t) = \int_0^t\int_0^{t_2}\cdots\int_0^{t_i} \tau^{j-1}e^{-\tau}\, d\tau, dt_i, \ldots, dt_2 & i<0 \end{cases} \tag{57}$$

The DE notation allows the solutions to be written without breaking up the series. For computational reasons, however, the separate D and E notations are preferred, since the derivatives do not obey the same recursion relationship as the integrals.

In order to further shorten the notation, a factorial function is introduced:

$$F(\nu,n) = \frac{(-1)^\nu\,(2\nu-n-1)!}{2^{2\nu-n}(\nu-n)!(\nu)!(n-1)!(\nu-1)!} \tag{58}$$

The inverse transformation of the right side of equation 55 can be made term by term, employing the relationships given in equations 56. In the notation of equations 57 and 58 the inverse is

$$\frac{1}{(s+\alpha/\omega_o)} \exp\left\{-Xs\left[\left(1+\frac{\chi}{s+1}\right)^{\frac{1}{2}}-1\right]\right\} \doteq e^{-\alpha t/\omega_o} + \sum_{m=1}^{\infty}\sum_{\nu=1}^{\infty}\sum_{n=1}^{\nu} (-\alpha/\omega_o)^{m-1} F(\nu,n)\, X^n\, \chi^\nu\, DE_{n-m,\nu}(t). \tag{59}$$

After employing the 'cutoff theorem' $[e^{-bs} f(s) \doteq F(t-b)]$ to equation 59, it may be substituted into equation 50 to give the stress solution in the time plane. If t is replaced by $\omega_o t$, the solution is

$$-\frac{1}{P_o}\sigma(x,t) = e^{-\alpha Z/\omega_o} + \sum_{m=1}^{\infty}\sum_{\nu=1}^{\infty}\sum_{n=1}^{\nu} (-\alpha/\omega_o)^{m-1} F(\nu,n) X^n \chi^\nu DE_{n-m,\nu}(Z) \tag{60}$$

for $Z>0$, where

$$Z = T-X = \omega_o\,(t-x/c_1).$$

Equations 39 and 40 can be combined to give

$$u(x,t) \doteq \frac{1}{\rho s^2}\,\frac{\partial\sigma(x,s)}{\partial x}. \tag{61}$$

The displacement can be obtained in a manner similar to that used to obtain the stress solution. Multiplying equation 55 by $1/\rho s^2$, inverting term by term, employing the cutoff theorem, replacing t by $\omega_o t$, and substitution into equation 61 gives

$$\frac{\omega_o^2\rho}{P_o}\, u(x,t) = \frac{\partial}{\partial x}\left\{ -\left(\frac{\omega_o}{\alpha}\right)^2 + \frac{\omega_o Z}{\alpha} + \left(\frac{\omega_o}{\alpha}\right)^2 e^{-\alpha Z/\omega_o} \right.$$

$$\left. + \sum_{m=1}^{\infty} \sum_{\nu=1}^{\infty} \sum_{n=1}^{\nu} (-\alpha/\omega_o)^{m-1}\, F(\nu,n)\, X^n \chi^\nu DE_{n-m-2,\nu}(Z) \right\}. \qquad (62)$$

Differentiation of equation 62 with respect to x gives

$$\frac{\rho\omega_o c}{P_o} u(x,t) = \frac{\omega_o}{\alpha}\left\{1-e^{-\alpha Z/\omega_o}\right\} + \sum_{m=1}^{\infty} \sum_{\nu=1}^{\infty} \sum_{n=1}^{\nu} \chi^\nu (-\alpha/\omega_o)^{m-1}\, X^{n-1} F(\nu,n)$$

$$\left\{ X\, DE_{n-m,\nu}(Z) - 2nX^{n-1} DE_{n-m-1,\nu}(Z) + n(n-1) X^{n-2} DE_{n-m-2,\nu}(Z) \right\}. \qquad (63)$$

The particle velocity and acceleration can be readily obtained by differentiation of the displacement with respect to time, and the strain by differentiation of the displacement with respect to x. These differentiations are facilitated by the fact that

$$\frac{\partial}{\partial Z} DE_{i,j}(Z) = DE_{i+1,j}(Z). \qquad (64)$$

The radial wave parameter solutions for the unit impulse, unit step, and single decay exponential pressure pulses are:

Solutions for Unit Impulse Pressure Pulse (Z>o).

$$-\frac{1}{\omega_o}\, \sigma(x,t) = \sum_{\nu=1}^{\infty} \sum_{n=1}^{\nu} \chi^\nu\, X^n\, F(\nu,n)\, DE_{n,\nu}(Z) \qquad (65)$$

$$\rho c_1 u(x,t) = 1 + \sum_{\nu=1}^{\infty} \sum_{n=1}^{\nu} \chi^{\nu} X^{n-1} F(\nu,n) \left\{ X\, DE_{n-1,\nu}(Z) - n\, DE_{n-2,\nu}(Z) \right\} \tag{66}$$

$$\frac{\rho c_1}{\omega_o} v(x,t) = \sum_{\nu=1}^{\infty} \sum_{n=1}^{\nu} \chi^{\nu} X^{n-1} F(\nu,n) \left\{ X\, DE_{n,\nu}(Z) - n\, DE_{n-1,\nu}(Z) \right\} \tag{67}$$

$$\frac{\rho c_1}{\omega_o^2} A(x,t) = \sum_{\nu=1}^{\infty} \sum_{n=1}^{\nu} \chi^{\nu} X^{n-1} F(\nu,n) \left\{ X\, DE_{n+1,\nu}(Z) - n\, DE_{n,\nu}(Z) \right\} \tag{68}$$

$$-\frac{\rho c_1^2}{\omega_o} \varepsilon(x,t) = \sum_{\nu=1}^{\infty} \sum_{n=1}^{\nu} \chi^{\nu} F(\nu,n) \left\{ X^n\, DE_{n,\nu}(Z) - 2nX^{n-1} DE_{n-1,\nu}(Z) + n(n-1)\, X^{n-2}\, DE_{n-2,\nu}(Z) \right\} \tag{69}$$

Solutions for Unit Step Pressure Pulse (Z>o).

$$-\sigma(x,t) = 1 + \sum_{\nu=1}^{\infty} \sum_{n=1}^{\nu} \chi^{\nu} X^{n} F(\nu,n)\, DE_{n-1,\nu}(Z) \tag{70}$$

$$\rho c_1 \omega_o u(x,t) = Z + \sum_{\nu=1}^{\infty} \sum_{n=1}^{\nu} \chi^{\nu} X^{n-1} F(\nu,n) \left\{ X\, DE_{n-2,\nu}(Z) - nDE_{n-3,\nu}(Z) \right\} \tag{71}$$

$$\rho c_1 v(x,t) = 1 + \sum_{\nu=1}^{\infty} \sum_{n=1}^{\nu} \chi^{\nu} X^{n-1} F(\nu,n) \left\{ X\, DE_{n-1,\nu}(Z) - nDE_{n-2,\nu}(Z) \right\} \tag{72}$$

$$\frac{\rho c_1}{\omega_o} A(x,t) = \sum_{\nu=1}^{\infty} \sum_{n=1}^{\nu} \chi^{\nu} X^{n-1} F(\nu,n) \left\{ X\, DE_{n,\nu}(Z) - nDE_{n-1,\nu}(Z) \right\} \tag{73}$$

$$-\rho c_1^2\ \varepsilon(x,t) = 1 + \sum_{\nu=1}^{\infty}\sum_{n=1}^{\nu} \chi^{\nu} F(\nu,n) \Big\{ X^n\ DE_{n-1,\nu}(Z)$$

$$- 2nX^{n-1} DE_{n-2,\nu}(Z) + n(n-1)\ X^{n-2} DE_{n-3,\nu}(Z) \Big\} \qquad (74)$$

Solutions for Single Decay Exponential Pressure Pulse ($Z > o$).

$$-\frac{1}{P_o}\,\sigma(x,t) = e^{-\alpha Z/\omega_o} + \sum_{m=1}^{\infty}\sum_{\nu=1}^{\infty}\sum_{n=1}^{\nu} \chi^{\nu}\left(-\frac{\alpha}{\omega_o}\right)^{m-1} X^n F(\nu,n)\ DE_{n-m,\nu}(Z) \qquad (75)$$

$$\frac{\rho c_1 \omega_o}{P_o}\,u(x,t) = \frac{\omega_o}{\alpha}\left\{1 - e^{-\alpha Z/\omega_o}\right\} + \sum_{m=1}^{\infty}\sum_{\nu=1}^{\infty}\sum_{n=1}^{\nu} \chi^{\nu}\left(-\frac{\alpha}{\omega_o}\right)^{m-1} X^{n-1} F(\nu,n)$$

$$\Big\{X\ DE_{n-m-1,\nu}(Z) - n\ DE_{n-m-2,\nu}(Z)\Big\} \qquad (76)$$

$$\frac{\rho c_1}{P_o}\,v(x,t) = e^{-\alpha Z/\omega_o} + \sum_{m=1}^{\infty}\sum_{\nu=1}^{\infty}\sum_{n=1}^{\nu} \chi^{\nu}\left(-\frac{\alpha}{\omega_o}\right)^{m-1} X^{n-1} F(\nu,n)$$

$$\Big\{X\ DE_{n-m,\nu}(Z) - n\ DE_{n-m-1,\nu}(Z)\Big\} \qquad (77)$$

$$\frac{\rho c_1}{P_o \omega_o}\,A(x,t) = -\frac{\alpha}{\omega_o}\, e^{-\alpha Z/\omega_o} + \sum_{m=1}^{\infty}\sum_{\nu=1}^{\infty}\sum_{n=1}^{\nu} \chi^{\nu}\left(-\frac{\alpha}{\omega_o}\right)^{m-1} X^{n-1} F(\nu,n)$$

$$\Big\{X\ DE_{n-m+1,\nu}(Z) - n\ DE_{n-m,\nu}(Z)\Big\} \qquad (78)$$

$$-\frac{\rho c^2}{p_o}\,\varepsilon(x,t) = e^{-\alpha Z/\omega_o} + \sum_{m=1}^{\infty}\sum_{\nu=1}^{\infty}\sum_{n=1}^{\nu} X^{\nu}\left(-\frac{\alpha}{\omega_o}\right)^{m-1} F(\nu,n)$$

$$\left\{X^n\, DE_{n-m,\nu}(Z) - 2nX^{n-1} DE_{n-m-1,\nu}(Z) + n(n-1)X^{n-2} DE_{n-m-2,\nu}(Z)\right\} \tag{79}$$

Some Computational Details. For computational purposes it is desirable to separate the series solutions into those involving only derivative functions, and those involving only integral functions, since they obey different recursion relationships.

The $D_{i,j}$'s and the $E_{i,j}$'s can be calculated from the recursion relationships:

$$\begin{aligned} D_{0,j}(Z) &= E_{0,j}(Z) = Z^{j-1}e^{-Z} \\ D_{i,1}(Z) &= (-1)^i\, e^{-Z} \\ D_{i,j}(Z) &= (j-1)\, D_{i-1,j-1}(Z) - D_{i-1,j}(Z) \quad \begin{cases} i\geq 1 \\ j>1 \end{cases} \\ E_{i,1}(Z) &= \frac{Z^{i-1}}{(i-1)!} - E_{i-1,1}(Z) \end{aligned} \tag{80}$$

and

$$E_{i,j}(Z) = (j-1)E_{i,j-1}(Z) - E_{i-1,j}(Z) \quad \begin{cases} i\geq 1 \\ j>1 \end{cases}$$

The series solutions written in terms of the function DE can be broken into series involving only D functions and those involving only E functions. For example, the stress for the single decay exponential pressure pulse given by equation 54 can be re-written:

$$-\frac{1}{P_o}\sigma(x,t) = e^{-\alpha Z/\omega_o} + \sum_{\nu=1}^{\infty}\sum_{k=1}^{\infty}\sum_{n=1}^{\nu}\chi^{\nu}\left(-\frac{\alpha}{\omega_o}\right)^{k+n-1}\chi^{n}E_{k,\nu}(Z)\,F(\nu,n)$$

$$+\sum_{\nu=1}^{\infty}\sum_{n=1}^{\nu}\sum_{m=1}^{n}\chi^{\nu}\left(-\frac{\alpha}{\omega_o}\right)^{m-1}\chi^{n}\,D_{n-m,\nu}(Z)\,F(\nu,n) \qquad (81)$$

where k is a new summation index equal to m-n. Additional details are given in Appendix E.

Numerical Evaluation. The particle velocity for a dual exponential pressure pulse was investigated, employing superposition of the solutions for the single decay exponential pressure pulses: $P(t) = P_o\, e^{-\alpha t}$ and $P(t) = -P_o\, e^{-\beta t}$.

The particle velocity (Figures 38 and 39) was found to be relatively insensitive to large changes in ω_o and changes in radial distance, for $\chi = 1$. Smaller values of χ gave even less sensitive response to changes in ω_o.

The three-element model approaches an elastic model of modulus χE for large damping, and a modulus $\chi E/(\chi+1)$ as the damping approaches zero. Thus, the limiting response of the model is elastic, and there would therefore be a finite response at an infinite distance for any value of ω_o.

As χ becomes large the elastic element E_1 becomes rigid in comparison to the Voigt portion of the model for small to intermediate values of damping; therefore, the response should approach that of the Voigt model for large χ.

The series solutions obtained are apparently severely restricted as it was found that the series failed to converge

for $\chi=2$, and for $\alpha/\omega_o>1$. The series appeared to converge quite rapidly for $\chi\leq 1$, $\alpha/\omega_o<1$ and for small X and T.

The model was found to give a finite instantaneous response with the arrival of the wave front at $t = x/c_1$, for pressure pulses of instantaneous rise time. The single decay exponential pressure pulse, for example, gives an instantaneous response with the arrival of the wave front. The initial response is maximum for small ω_o. For larger values of ω_o the peak values occur some time after the arrival of the wave front (Figure 40).

Conclusions. It appears that the three-element elastic plane wave model is of little value as a model to represent real earth wave propagation. The attenuation is quite small for small values of χ, and for large values the model approaches the plane wave Voigt model. The Voigt model for plane wave propagation has been shown (References 6 through 9) to be insufficient to describe explosive generated waves in rocks.

The method of solution used on this model may offer aid in obtaining solutions to more complex models including the spherical wave problem with the three-element model.

The validity of the solutions (equations 65 through 79) is supported by the fact that the particle velocity approaches the appropriate elastic case as ω_o becomes large (Figures 38 and 40). Close agreement with the results obtained by numerical inversion also supportstheir validity (Appendix F).

The curves of Figures 38, 39, and 40 were obtained from equation 77.

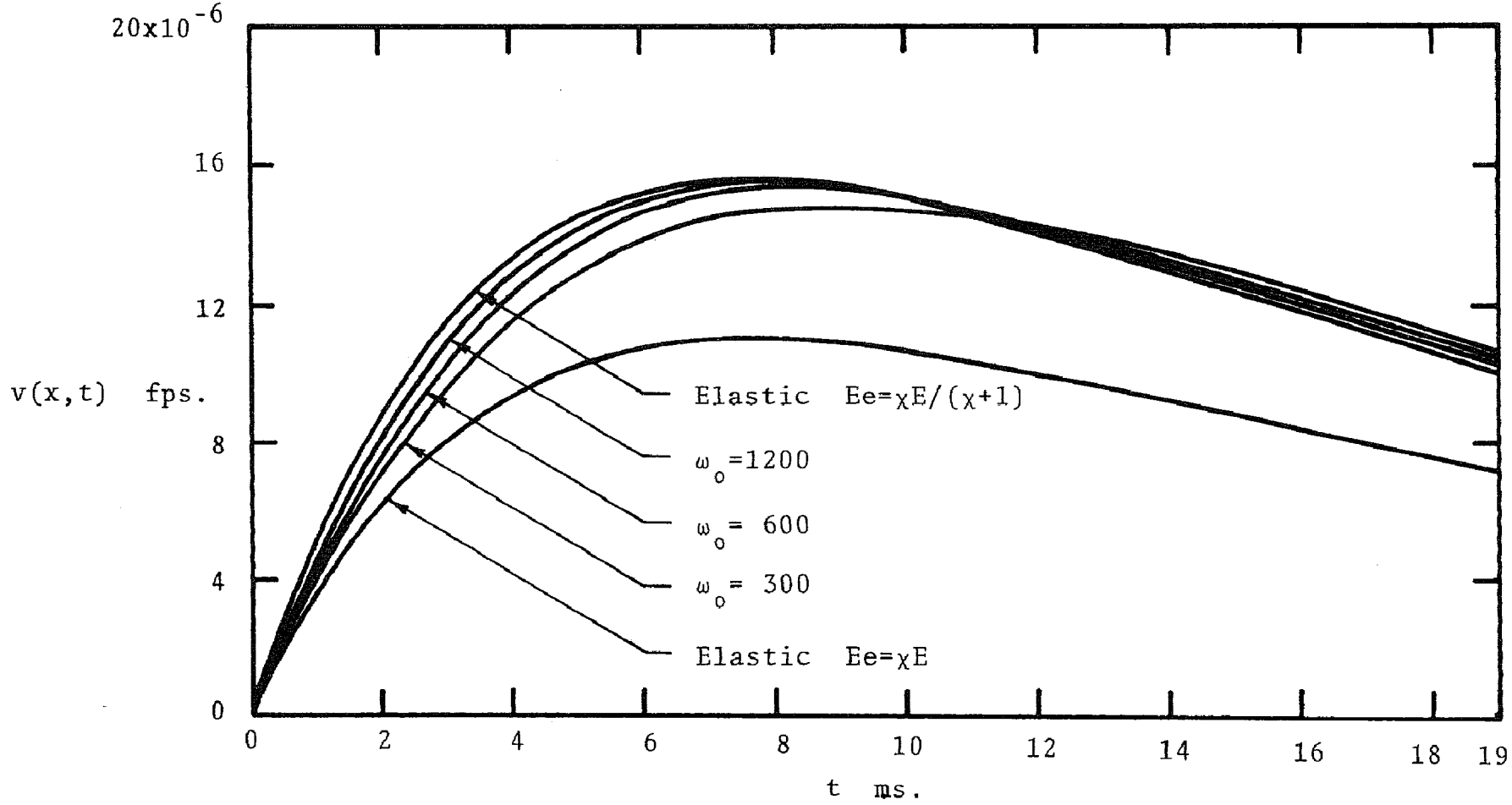

Figure 38. Particle velocity vs. time for plane waves in elastic and three-element viscoelastic granite media for a normalized dual exponential pressure pulse, x=0, α=60, β/α=4, χ=1.

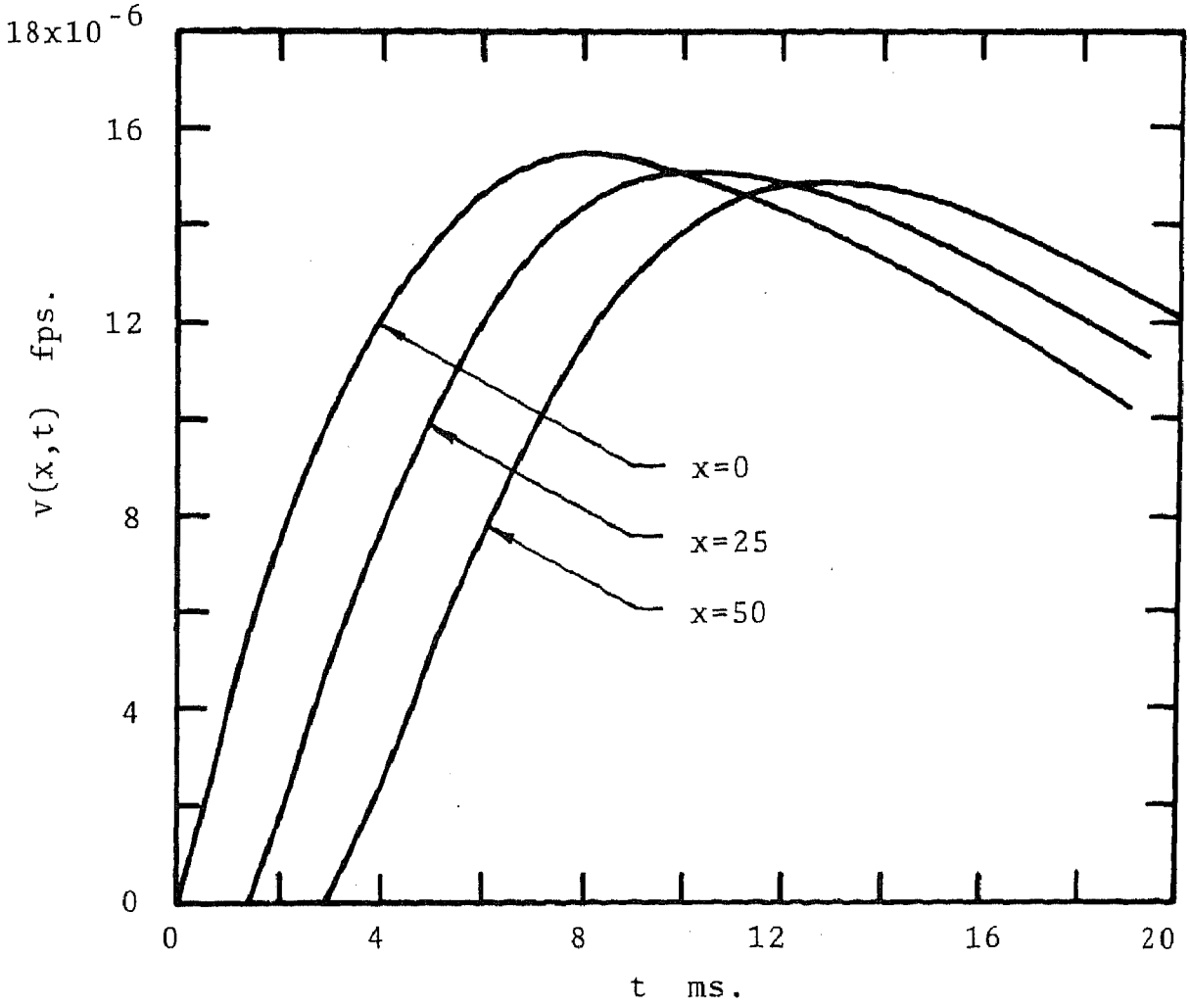

Figure 39. Particle velocity vs. time for plane waves in a three-element viscoelastic granite medium for a normalized dual exponential pressure pulse, $\alpha=60$, $\beta/\alpha=4$, $\chi=1$, $\omega_o=600$.

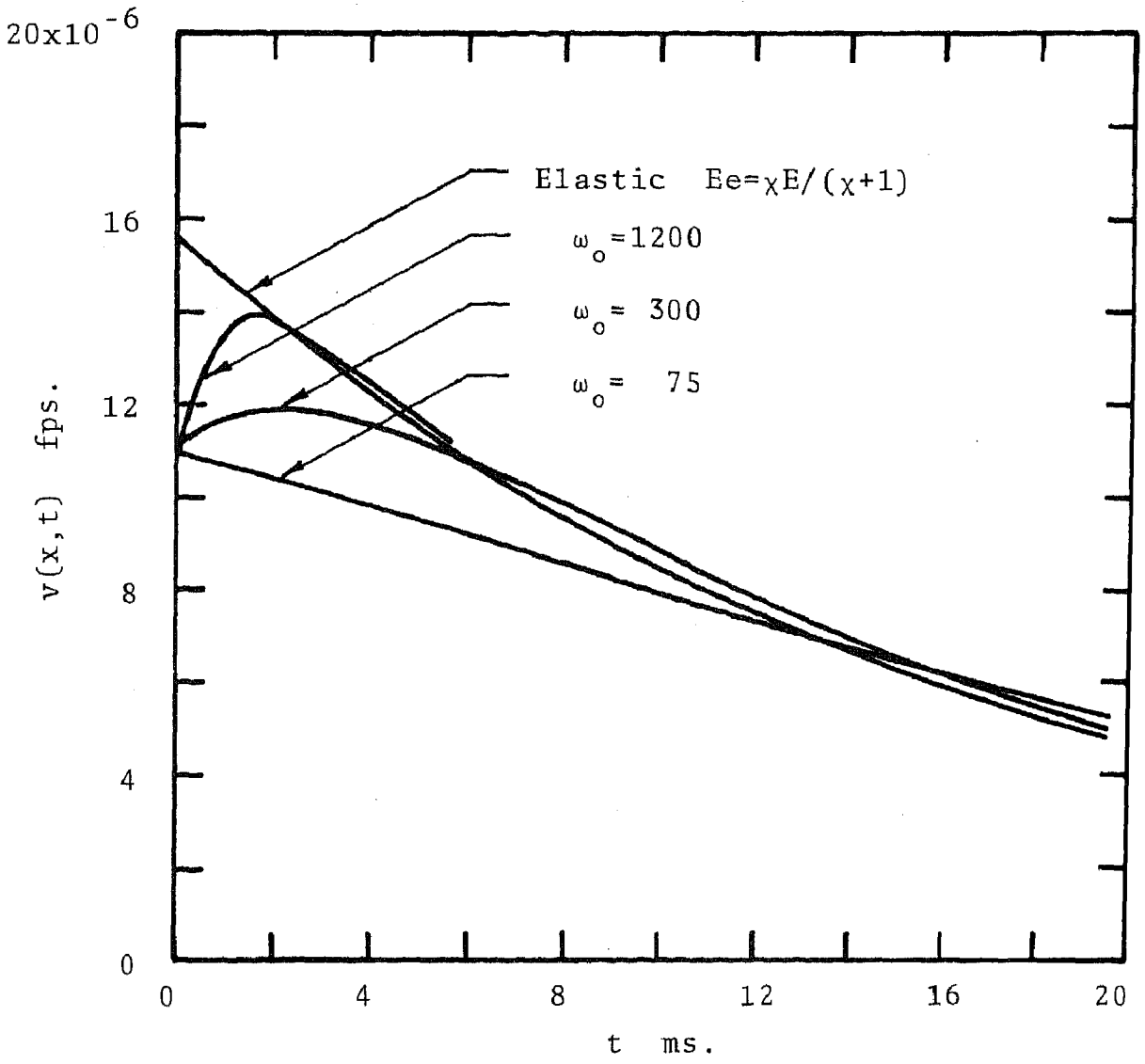

Figure 40. Particle velocity vs. time for plane waves in elastic and three-element viscoelastic granite media for a single decay exponential pressure pulse, x=0, α=60, χ=1.

CHAPTER VI

SUMMARY, CONCLUSIONS, AND RECOMMENDATIONS

Summary. A dual exponential pressure pulse of the form $P(t) = P_o (e^{-\alpha t} - e^{-\beta t})$ can be made to satisfactorily approximate explosive generated waves. The function is relatively simple, continuous, and easily scaled timewise.

It is difficult to compare theoretical wave propagation with real wave propagation because of insufficient knowledge about effective cavity radii. In spite of this difficulty, it has been shown that spherical elastic waves are not sufficient to to describe real waves in rock generated by an explosive source. Elastic waves do, however, exhibit attenuation rates for peak values of particle velocity and displacement which are in close agreement with attenutation rates for real waves at large radial distances. Elastic waves differ from real waves in several important respects. Real waves show pulse lengthening with travel distance and elastic waves exhibit pulse shortening. The attenuation rates for peak values of the wave parameters at small to intermediate distances are considerably greater for real waves than for elastic waves. Elastic wave arrivals are more abrupt than arrivals of real waves.

At intermediate distances Voigt spherical waves exhibit several significant correlations with real wave phenomena. At small radial distances the Voigt model would require a very large damping coefficient to give attenuation rates comparable

with those observed for real waves. At very large distances the Voigt model would have to approach the elastic model to give decay rates comparable with those of real waves.

For intermediate values of damping, Voigt waves exhibit pulse lenthening with travel distance, but this lengthening occurs both directions from the arrival time predicted by elastic theory or for real waves. The most significant difference between Voigt spherical and real waves, at intermediate travel distances is the early arrival of Voigt waves.

No simple scaling laws apply to a viscoelastic medium if the elastic and viscoelastic properties remain unaltered. If the damping coefficient is scaled and the elastic properties are held constant, viscoelastic waves obey the same scaling laws as elastic waves.

Series solutions were obtained for plane waves in a three-element, linear viscoelastic medium, for unit impulse, unit step, and single decay exponential pressure pulses. The investigation showed the model to be of little value as a model for real waves in rock. The response of the model is relatively insensitive to damping coefficient, for transient wave phenomena. The methods of solution used on this model may be an aid in obtaining solutions for other viscoelastic models, including spherical waves in a three-element viscoelastic medium.

Conclusions. The dual exponential pressure pulse gives theoretical wave phenomena which is in closer agreement with

real wave phenomena than that obtained employing a pressure pulse function with instantaneous rise or fall time. The improvements in wave parameter characteristics caused by the employment of a more realistic pressure pulse did not, however, satisfy many of the objections to the elastic and Voigt models reported by other investigators.

At best it appears that the elastic and Voigt models have very limited applications in predicting real wave phenomena. The Voigt model might be employed at intermediate distances and the elastic model at large radial distances, provided appropriate values of effective cavity radius and pressure pulse magnitude could be found. Predictions based on elastic or Voigt theory should be considered as order of magnitude approximations. In the presence of sufficient experimental data and empirical procedures, the use of these models is questionable.

Plane waves in a three-element viscoelastic medium offer little or no aid in the study of explosive generated waves in rock.

The results of this investigation and others cited in the literature raise serious doubts that explosive generated waves in rock can be accurately represented by linear viscoelastic models. One fundamental fault of all linear viscoelastic models is that they all tend ultimately to behave either as elastic or viscous models.

Recommendations. If further investigations of transient waves in viscoelastic media are undertaken, numerical inversion

techniques should be considered.

Since it appears that viscoelastic models are not sufficient to represent transient wave phenomena in rock; internal friction mechanisms other than, or in addition to, viscous damping should be investigated.

An investigation of effective cavity radii should be made, as information of that type would greatly facilitate correlation of theory and real wave phenomena.

REFERENCES

1. Sharpe, J. A. (1942). The Production of Elastic Waves by Explosion Pressures. I. Theory and Empirical Field Observations. Geophysics Vol. VII, No. 3, pp. 144-154.

2. Duvall, W. I. (1953). Strain-Wave Shapes in Rock Near Explosions. Geophysics Vol. XVIII, No. 2, pp. 310-323.

3. Goldsmith, W. (1953). Graphical Representation of the Spherical Propagation of Explosive Pulses in Elastic Media. Report No. 1, Institute of Engineering Research, U. of California, Berkeley.

4. Kolsky, H. (1963). Stress Waves in Solids. New York: Dover Publications, Inc., 117 pp.

5. Bland, D. R. (1960). The Theory of Linear Viscoelasticity. (Vol. 10 of International Series of Monographs on Pure and Applied Mathematics. General Editors I. N. Sneddon and S. Ulam. 10 Vols., New York: Pergamon Press.)

6. Clark, G. B. (1966). Blasting and Dynamic Rock Mechanics. Paper presented at the VIII Symposium on Rock Mechanics at the University of Minnesota, August 1966.

7. Collins, F. (1960). Plane Compressional Voigt Waves. Geophysics Vol. XXV, No. 2, pp. 483-504.

8. Rupert, G. B. (1964). A Study of Plane and Spherical Compressional Waves in A Voigt Viscoelastic Medium. (unpublished Ph.D. thesis, U. of Missouri at Rolla, Rolla, Missouri. 46 pp.)

9. Clark, G. B. and Rupert, G. B. (1966). Plane and Spherical Waves in a Voigt Medium. Journal of Geophysical Research, Vol. 71, No. 8, pp. 2047-2053.

10. Clark, G. B., Rupert, G. B., and Jamison, J. E. (1967). A Comparison of Plane and Spherical Transient Voigt Waves with Explosion Generated Waves in Rock Masses. (unpublished report of Rock Mechanics Research Center, U. of Missouri at Rolla, Rolla, Missouri. 98 pp.)

11. Lee, E. H. and Kanter, I. (1953). Wave Propagation in Finite Rods of Viscoelastic Material. Journal of Applied Physics, Vol. 24, No. 9. pp. 1115-1122.

12. Hanin, M. (1956). Propagation of an Aperiodic Wave in a Compressible Viscous Medium. Journal of Math. and Physics, Vol. 36, pp. 234-249.

13. Morrison, J. A. (1956). Wave Propagation in Rods of Voigt Material and Visco-Elastic Materials with Three-Parameter Models. Quarterly of Applied Math., Vol. 14, No. 2, pp. 153-169.

14. Glauz, R. D. and Lee, E. H. (1954). Transient Wave Analysis in a Linear Time-Dependent Material. Journal of Applied Physics, Vol. 25, No. 8, pp. 947-953.

15. Lee, E. H. and Morrison, J. A. (1956). A Comparison of the Propagation of Longitudinal Waves in Rods of Viscoelastic Materials. Journal of Polymer Science, Vol. 19, pp. 93-110.

16. Arenz, R. J. (1964). Uniaxial Wave Propagation in Realistic Viscoelastic Materials. Journal of Applied Mechanics, Transactions of the ASME, March, pp. 17-21.

17. Berry, D. S. and Hunter, S. C. (1956). The Propagation of Dynamic Stresses in Visco-Elastic Rods. Journal of the Mechanics and Physics of Solids, Vol 4, pp.72-95.

18. Allen, D. E. and Robison, A. R. (1966). Interaction of Plane Stress Waves with a Spherical Cavity in Elastic and Viscoelastic Media. Civil Engineering Studies, Structural Research Series No. 302, University of Illinois, Urbana, Illinois, 123 pp.

19. Lee, T. M. (1964). Spherical Waves in Viscoelastic Media. The Journal of the Acoustical Society of America, Vol. 36, No. 12, pp. 2402-2407.

20. Berry, D. S. (1958). Stress Propagation in Visco-Elastic Bodies. Journal of the Mechanics and Physics of Solids, Vol. 6, pp. 177-185.

21. Lockett, F. J. (1961). Interpretation of Mathematical Solutions in Viscoelasticity Theory Illustrated by a Dynamic Spherical Cavity Problem. Journal of Mech. and Physics of Solids, Vol. 9, pp. 215-229.

22. Cole, R. H. (1948). Underwater Explosions. Princeton Univ. Press., Princeton, New Jersey, 437 pp.

23. Collins, op. cit., p. 487 .

24. Tse, F. S., Morse, I. E., and Hinkle, R. T. (1963). Mechanical Vibrations. Boston: Allyn and Bacon Inc. p. 294.

25. Churchill, R. V. (1958). Operational Mathematics. New York: McGraw Hill, pp. 5-7 and 25-28.

26. Sharpe, op. cit., pp. 149-150.

27. Goldsmith, op. cit., p. 1.

28. Duvall, op. cit., p. 311.

29. Wuerker, R. G. (1956). Annotated Tables of Strength and Elastic Properties of Rocks, U. of Illinois, Urbana, Ill., Published by Petroleum Branch, AIME, Paper No. 663-G.

30. Johnson, G. W., Higgins, G. H., and Violet, C. E. (1959). Underground Nuclear Detonations, U. of California, E. O. Lawrence Radiation Lab. Report. pp. 5-8.

31. Sharpe, op. cit., pp. 146-150.

32. Duvall, op. cit., pp. 310-323.

33. Rupert, op. cit., pp. 31-33.

34. Hubbert, M. K. (1937). Theory of Scale Models as Applied to the Study of Geologic Structures. Bull. Geol. Soc. of Am., Vol 48, pp. 1459-1520.

35. Clark, op. cit., p-32.

36. Cole, op. cit., p. 7.

37. Duvall, op. cit., p. 313-314.

38. Sauer, F. M., et al., (1964). Empirical Analysis of Ground Motion and Cratering, Nuclear Geoplosics, Pt. IV, DASA-1285(IV).

39. Clark, Rupert, and Jamison, op. cit., p. 24.

40. Clark, Rupert, and Jamison, op. cit., pp. 16-22, 45-49.

41. Collins, op. cit., pp. 500-501.

42. Kolsky, op. cit., pp. 112-113.

43. Sauer, et al., op. cit., p. 48.

44. Sauer, et al., op. cit., p. 46.

45. Sauer, et al., op. cit., p. 44.

46. Sauer, et al., op. cit., p. 37.

47. Clark, Rupert, and Jamison, op. cit., p. 28.

48. Clark, Rupert, and Jamison, op. cit., pp. 24-28.

49. Morrison, loc. cit.

50. Lee and Morrison, loc. cit.

51. Arenz, loc. cit.

52. Bland, loc. cit.

53. Mikusinski, J. (1959). Operational Calculus, Gen. Editors Sneddon, I. N., and Ulam S., v-8, Int. Series of Monographs on Pure and Applied Mathematics, Translated from the second Polish edition v-30, 1957, p. 177. MacMillan Co., New York.

54. Collins, op. cit., pp. 500-501.

55. Abramowitz, M., and Stegun, I. A., (1965). Handbook of Math. Functions, National Bureau of Standards., Applied Math. Series 55, pp. 297-298.

56. Clark, Rupert, and Jamison, op. cit., p. 23.

57. Perret, W. R., (1963). Operation Nougat, Shot Hard Hat, POR, Project 3.3, Free-Field Motion in Granite, Sandia Corp., POR-1803 (WT-1803), pp. 48-50.

58. Perret, loc. cit.

59. Clark, Rupert, and Jamison, op. cit., p. 85.

60. Weart, W. D., (1962). Project Gnome, Particle Motion Near a Nuclear Detonation in Halite, Sandia Corp., PNE-108P, p. 60.

61. Day, J. D., and Murrell, D. W., (1966). Operation Long Shot, Ground and Water Shock Measurements, POR, Project 1.01, U.S.A. Waterways Exp. Sta.,

62. Sauer, et al., op. cit., p. 37.

63. Sauer, et al., op. cit., p. 46.

64. Allen and Robinson, op.cit., pp. 39-43.

APPENDICES

APPENDIX A

VISCOELASTIC MODELS AND THEIR UNIAXIAL STRESS-STRAIN RELATIONSHIPS

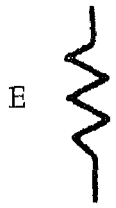

Elastic $\qquad \sigma = E\varepsilon \qquad (82)$

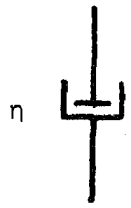

Viscous $\qquad \sigma = \eta \frac{\partial \varepsilon}{\partial t} \qquad (83)$

Maxwell $\qquad \left[\frac{1}{E}\frac{\partial}{\partial t} + \frac{1}{\eta}\right]\sigma = \frac{\partial \varepsilon}{\partial t} \qquad (84)$

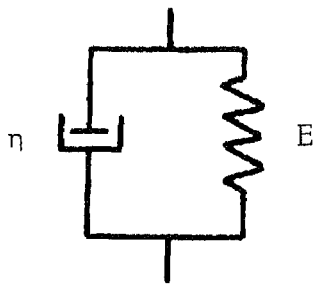

Voigt $\qquad \sigma = \left[E + \eta\frac{\partial}{\partial t}\right]\varepsilon \qquad (85)$

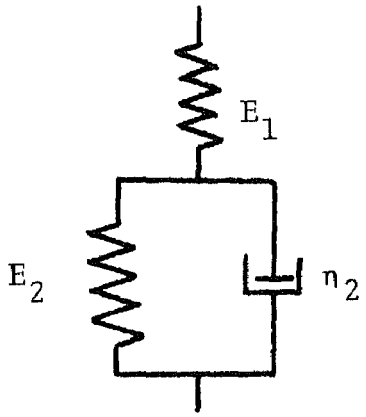

$$\left[\frac{\partial}{\partial t} + \frac{E_1+E_2}{\eta_2}\right]\sigma = \left[E_1\frac{\partial}{\partial t} + \frac{E_1E_2}{\eta_2}\right]\varepsilon \qquad (86)$$

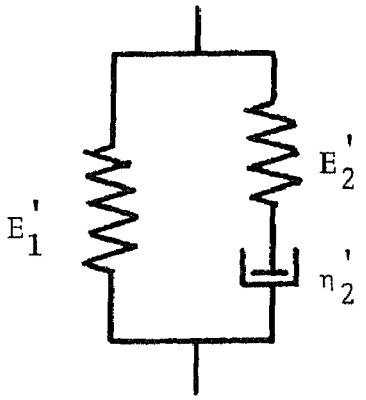

$$\left[\frac{\partial}{\partial t} + \frac{E_2'}{\eta_2'}\right]\sigma = \left[(E_1'+E_2')\frac{\partial}{\partial t} + \frac{E_1'E_2'}{\eta_2'}\right]\varepsilon \qquad (87)$$

Equivalent representations of the three-element elastic model.

APPENDIX B

DISPLACEMENT POTENTIAL FOR SPHERICAL ELASTIC WAVES

The wave equation for spherical elastic waves is

$$\frac{\partial^2(r\phi)}{\partial r^2} = \frac{1}{c^2}\frac{\partial^2(r\phi)}{\partial t^2} . \tag{88}$$

The imposed boundary conditions are

$$(\lambda+2\mu)\frac{\partial^2\phi}{\partial r^2} + \frac{2\lambda}{r}\frac{\partial\phi}{\partial r} = -\sigma_r = -P(t) \qquad r=a,\ t>o \tag{89}$$

$$\frac{\partial(r\phi)}{\partial t} = o \qquad r>a,\ t=o \tag{90}$$

$$r\phi = o \qquad r>a,\ t=o \tag{91}$$

and

$$\lim_{r \to \infty} r\phi = o \tag{92}$$

The Laplace transformations of equations 88,89, and 92 subject to the conditions of equations 90 and 91 are respectively

$$\frac{d^2(r\bar{\phi})}{dr^2} - \frac{s^2}{c^2}(r\bar{\phi}) = o \tag{93}$$

$$(\lambda+2\mu)\frac{d^2\phi}{dr^2} + \frac{2\lambda}{r}\frac{d\bar{\phi}}{dr} = -P(s) \qquad r=a \tag{94}$$

$$\lim_{r \to \infty} r\bar{\phi} = o \tag{95}$$

The solution of equation 93 subject to the condition given by equation 95 is

$$r\bar{\phi} = Ae^{-sr/c} \tag{96}$$

When equation 96 is substituted into equation 94 it yields the constant A:

$$A = \frac{-aP(s)\ e^{as/c}}{\left[(\lambda+2\mu)\ \frac{s^2}{c^2} + \frac{4\mu s}{ac} + \frac{4\mu}{a^2}\right]} \tag{97}$$

Substitution of the constant A into equation 96 yields

$$r\bar{\phi} = \frac{-P(s)\ a\ e^{-s(r-a)/c}}{\left[(\lambda+2\mu)\ \frac{s^2}{c^2} + \frac{4\mu s}{ac} + \frac{4\mu}{a^2}\right]} \tag{98}$$

If the dual exponential pressure pulse $P(t) = P_o\ (e^{-\alpha t} - e^{-\beta t})$ is chosen, the transform pressure pulse is

$$P(s) = P_o \left[\frac{1}{s+\alpha} - \frac{1}{s+\beta}\right] \tag{99}$$

From equations 98 and 99 it becomes quite obvious that superposition can be employed and that the solutions for the dual exponential pressure pulse can be obtained by superimposing the solutions for $P(t) = P_o\ e^{-\alpha t}$ and $P(t) = -P_o\ e^{-\beta t}$.

If the pressure pulse is the single decay exponential $P(t) = P_o\ e^{-\alpha t}$, the displacement potential in the transform plane can be written:

$$r\bar{\phi} = \frac{-aP_o \left[c^2/(\lambda+2\mu)\right] e^{-s(r-a)/c}}{(s+\alpha)\left[s+\frac{2c\left[\mu+i\sqrt{(\lambda+\mu)\mu}\right]}{a(\lambda+2\mu)}\right]\left[s+\frac{2c\left[\mu-i\sqrt{(\lambda+\mu)\mu}\right]}{a(\lambda+2\mu)}\right]} \qquad (100)$$

The inversion of equation 100 by the method of Heaviside gives

$$-\frac{\rho r\phi}{aP_o} = \frac{\exp\left[-\alpha(t-\frac{r-a}{c})\right]}{\left[\alpha^2 - \frac{4\alpha c\mu}{a(\lambda+2\mu)} + \frac{4c^2\mu}{a^2(\lambda+2\mu)}\right]}$$

$$+ \frac{\exp\left[\frac{-2c(\mu+i\sqrt{(\lambda+\mu)\mu})\ (t-\frac{r-a}{c})}{a(\lambda+2\mu)}\right]}{\left[\frac{8c^2\mu i\sqrt{(\lambda+\mu)\mu}}{a^2(\lambda+2\mu)^2} - \frac{8c^2\mu(\lambda+\mu)}{a^2(\lambda+2\mu)^2} - \frac{4c\alpha i\sqrt{(\lambda+\mu)\mu}}{a(\lambda+2\mu)}\right]}$$

$$+ \frac{\exp\left[\frac{-2c(\mu-i\sqrt{(\lambda+\mu)\mu})(t-\frac{r-a}{c})}{a(\lambda+2\mu)}\right]}{\left[\frac{-8c^2\mu i\sqrt{(\lambda+\mu)\mu}}{a^2(\lambda+2\mu)^2} - \frac{8c^2\mu(\lambda+\mu)}{a^2(\lambda+2\mu)^2} + \frac{4c\alpha i\sqrt{(\lambda+\mu)\mu}}{a(\lambda+2\mu)}\right]} \qquad (101)$$

After rearrangement and simplification the displacement potential can be written in the form given by equation 9 of Chapter III.

APPENDIX C

COMPUTATIONAL DETAILS FOR SPHERICAL VOIGT WAVES

The wave parameters for spherical Voigt waves generated by the dual exponential pressure pulse were obtained by superposition of the solutions for $P(t) = P_o e^{-\alpha t}$ and $P(t) = -P_o e^{-\beta t}$. The two solutions were carried along simultaneously in the computer program in order to take advantage of the time saving permitted where calculations independent of α and β were required [eg. in the calculation of $\operatorname{erfc}(R/2\sqrt{T})$ and $D_{-n}(R/\sqrt{2T})$].

In order to facilitate computation, the series

$$\sum_{n=o}^{\infty} \sum_{m=o}^{\infty} \frac{b_m R^n}{n!} \, 2^{(m+n+z)/2} \, T^{(m+n+z-1)/2} D_{-m-n-z}(R/\sqrt{2T}) \qquad (102)$$

was expressed as the Cauchy product

$$\sum_{n=o}^{\infty} \sum_{m=o}^{n} \frac{b_m R^{n-m}}{(n-m)!} \, 2^{(n+z)/2} \, T^{(n+z-1)/2} \, D_{-n-z}(R/\sqrt{2T}) \qquad (103)$$

The b_m's follow a simple recursion pattern. They are functions of the constants in the product

$$(s-\gamma)\,[A] = s^3 + A_1 s^{5/2} + A_2 s^2 + \cdots + A_5 s^{1/2} + A_6. \qquad (104)$$

The recursion for the b_m's is

$$\begin{aligned} b_o &= 1 \\ b_1 &= -A_1 b_0 \\ b_2 &= -A_1 b_1 - A_2 b_0 \\ b_3 &= -A_1 b_2 - A_2 b_1 - A_3 b_0 \end{aligned} \qquad (105)$$

$$\vdots$$

$$b_k = -\sum_{i=1}^{6} A_i\, b_{k-i} \qquad k \geq 6$$

The parabolic cylinder functions can be calculated from the recursion [Ref. Collins (54)]

$$(n+1)\, D_{-n-2}(Y) = -Y\, D_{-n-1}(Y) + D_{-n}(Y) \tag{106}$$

where

$$D_o(Y) = e^{-Y^2/4}$$

$$D_{-1}(Y) = \sqrt{\pi/2}\; e^{Y^2/4}\; \mathrm{erfc}(Y/\sqrt{2})$$

The complimentary error function was computed from the error function (erfc = 1.0 - erf) for arguments less than 3.6. The error functions can be calculated from any of several series expansions [Ref. (55)]. For arguments equal to or greater than 3.6, the complimentary error function was calculated directly from an asymptotic expansion. The value of the argument of 3.6 was chosen because the two methods give approximately equal accuracy for that value. The accuracy of both methods is least for arguments near 3.6.

The order and manner of multiplication is very important in the evaluation of the double series since some terms become very large and some very small (out of the range of the computer). Frequent checks of size of components and appropriate corrective actions were required throughout the computer program. [Ref. Clark, et. al. (56)].

GENERALIZED COMPUTER FLOW DIAGRAM FOR VOIGT SPHERICAL WAVES

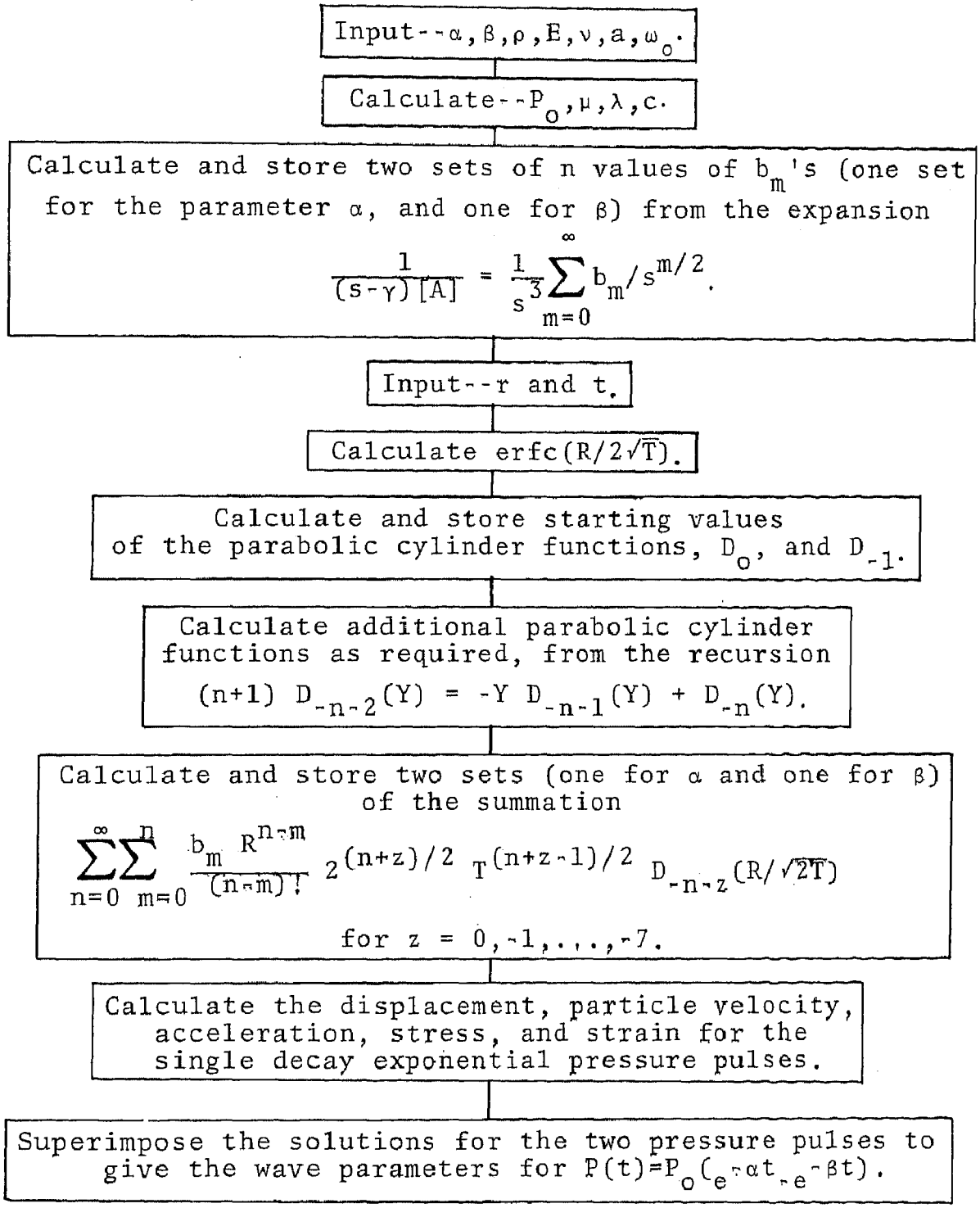

APPENDIX D

EXAMPLES OF REAL EARTH WAVES

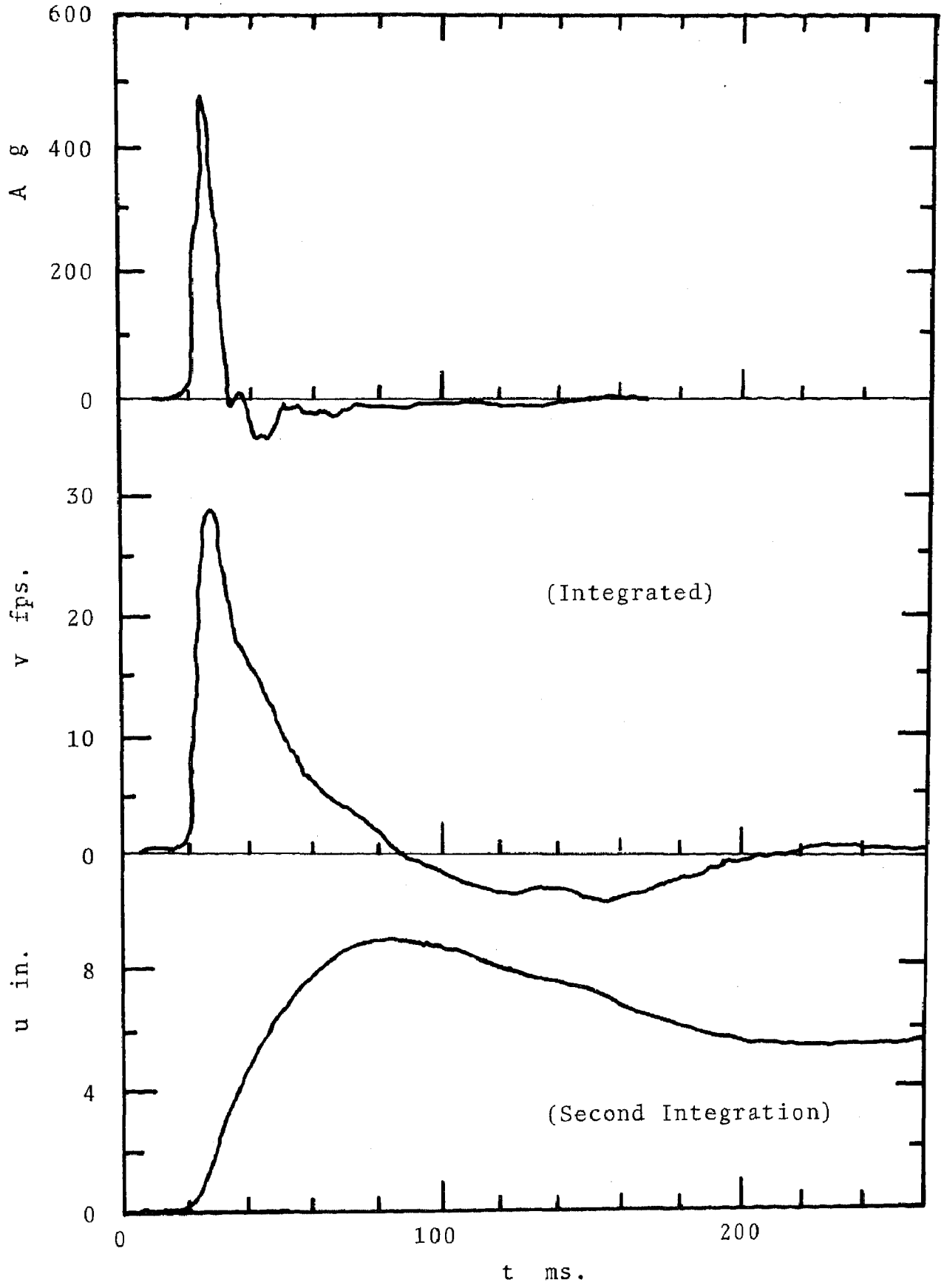

Figure 41. Example of free-field radial motion from an underground explosion in NTS granite, gage 8-a, Hard Hat, range 369 ft. {Ref. Perret (57)}

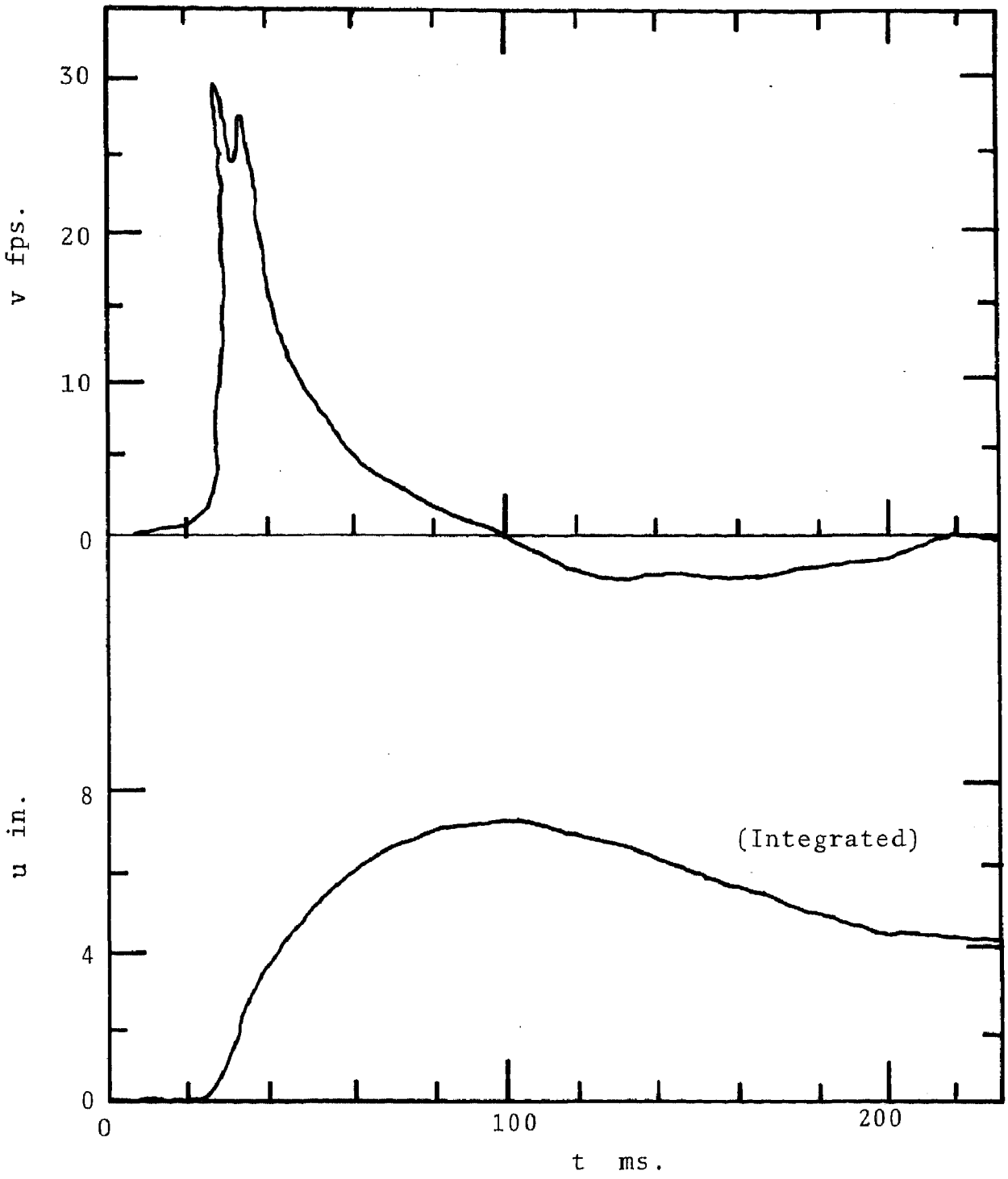

Figure 42. Example of field-free radial motion from an underground explosion in NTS granite, gage 8-u, Hard Hat, range 369 ft. {Ref. Perret (58)}

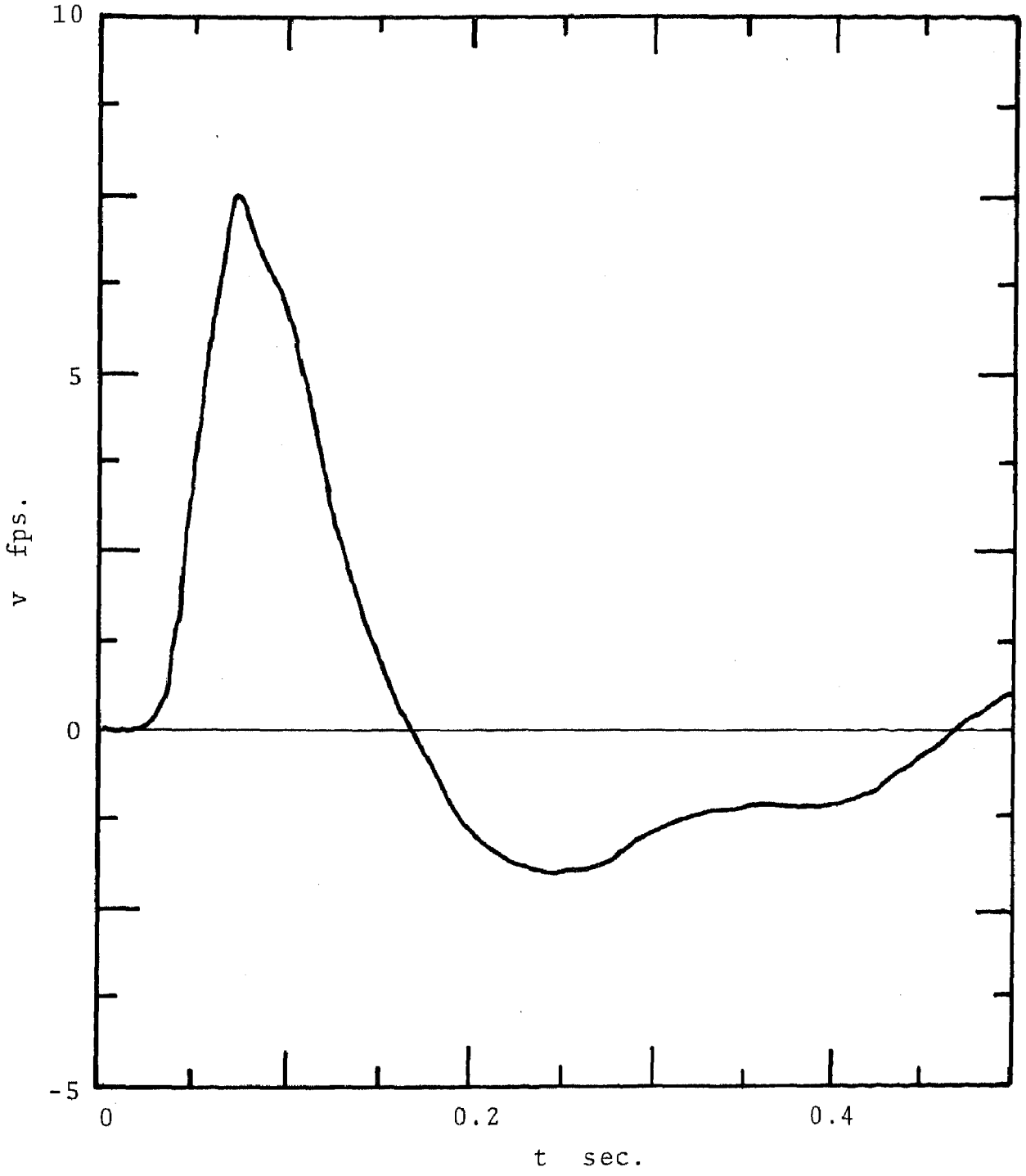

Figure 43. Particle velocity vs. time, Project Airvent, gage 60u. {Ref. Clark et al. (59)}

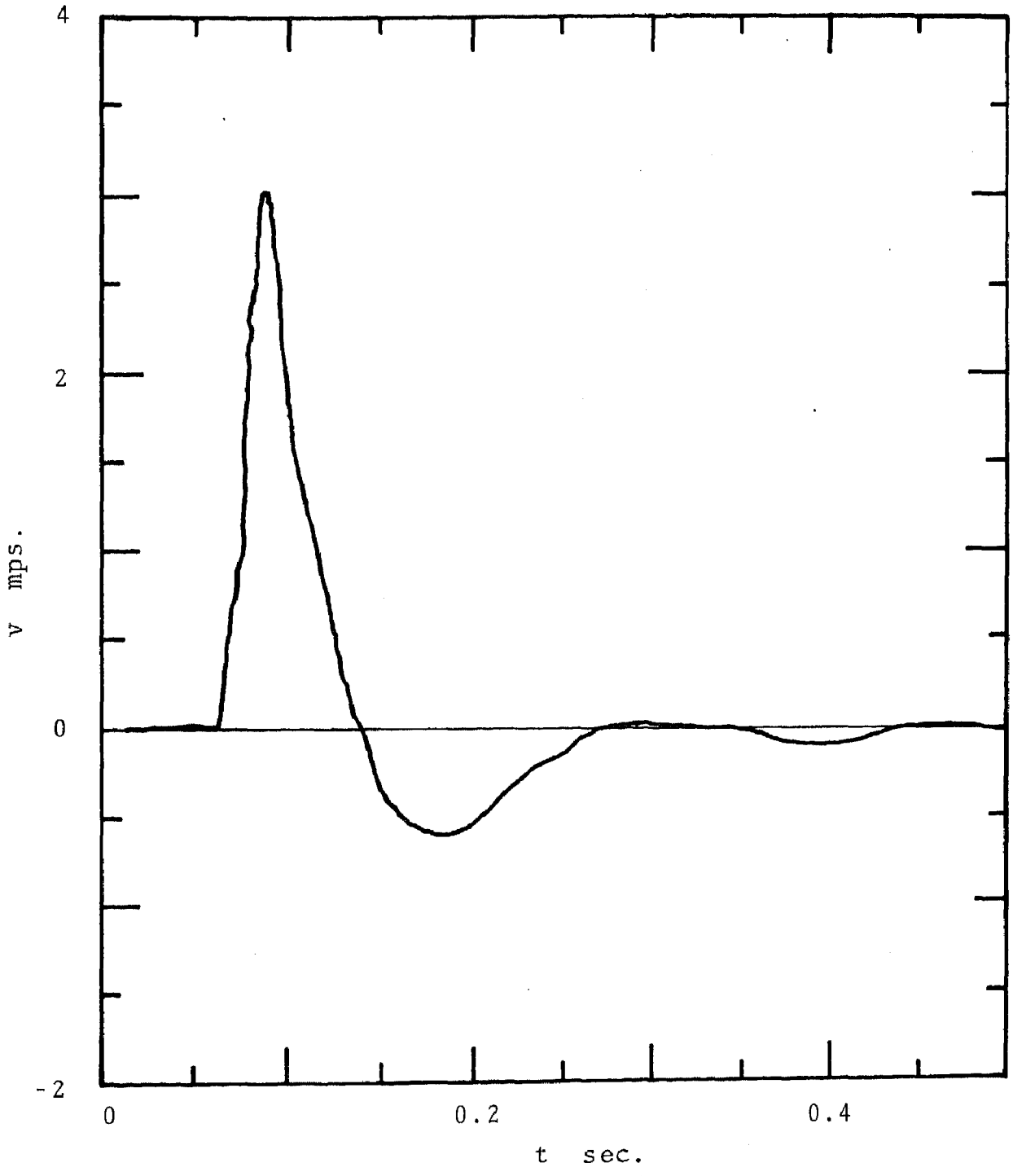

Figure 44. Particle velocity vs. time in salt, Project Gnome, range 298 meters, 7-u1H. {Ref. Weart (60)}

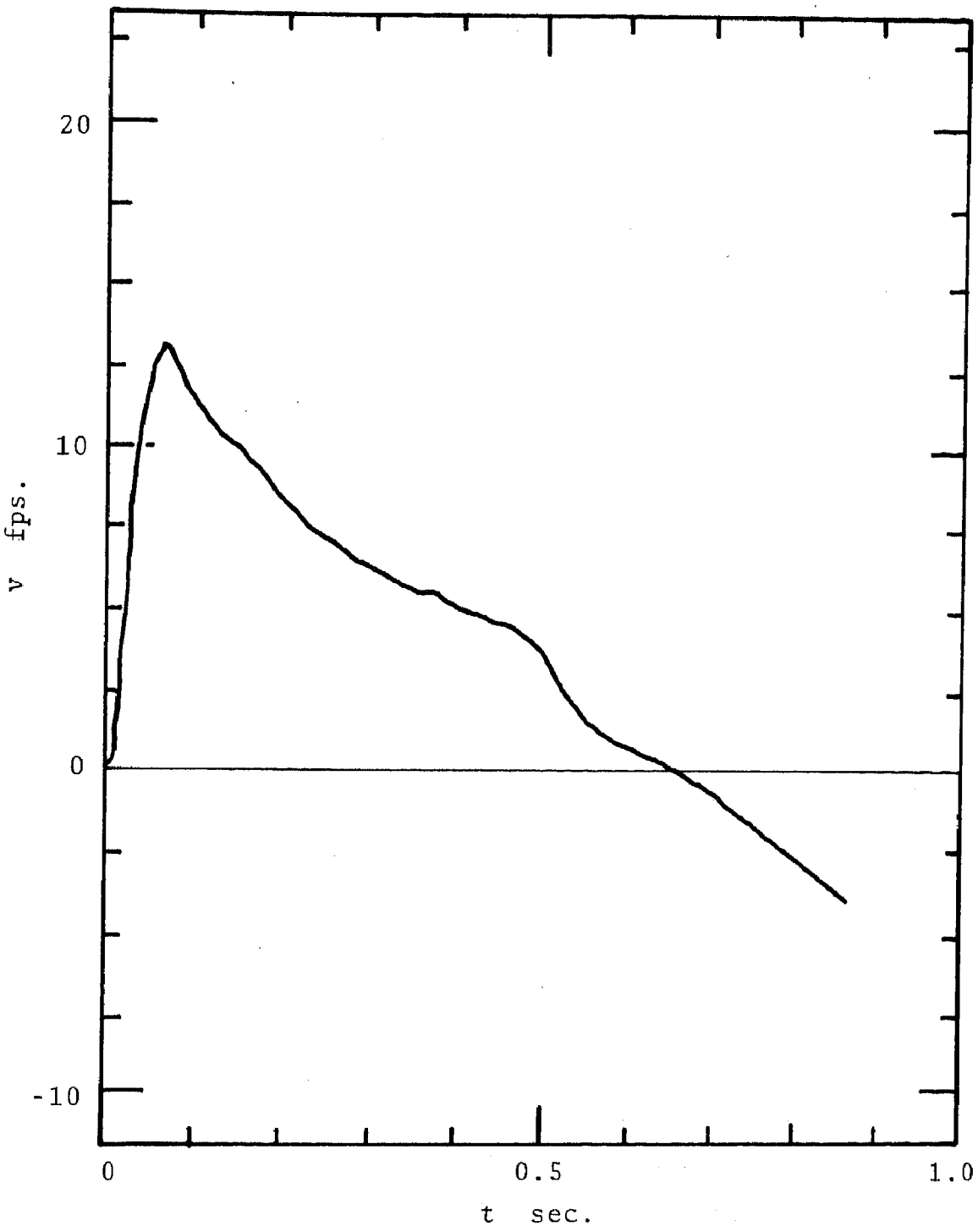

Figure 45. Particle velocity vs. time in andesite, Project Longshot, 80 KT, slant range 2281 ft., gage 8-H, EH-3. {Ref. Day and Murrell (61)}

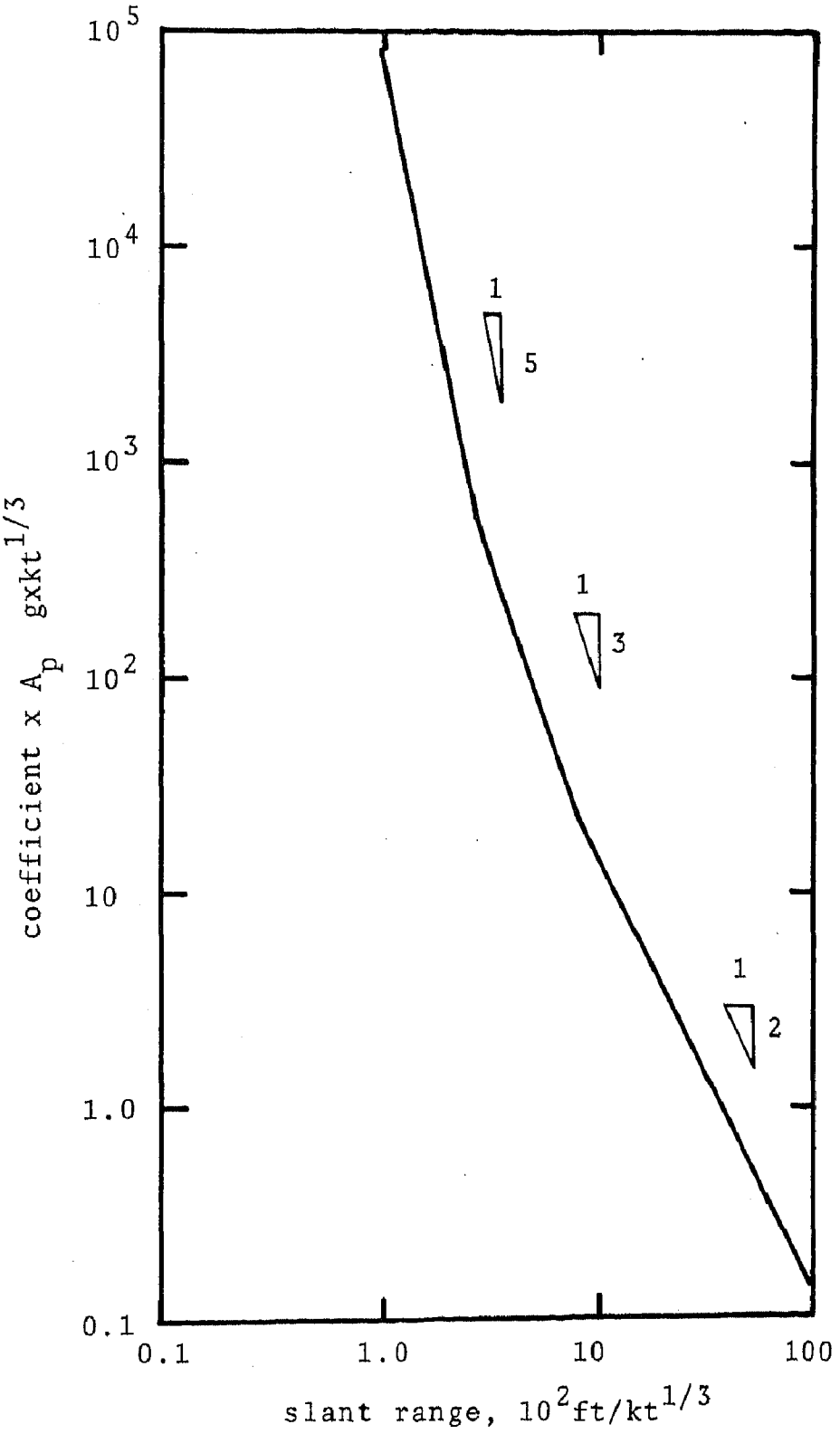

Figure 46. Composite correlation of first radial acceleration peak, scaled to 1 KT, for detonations in salt, NTS granite, tuff, and alluvium. {Ref. Sauer et al. (62)}

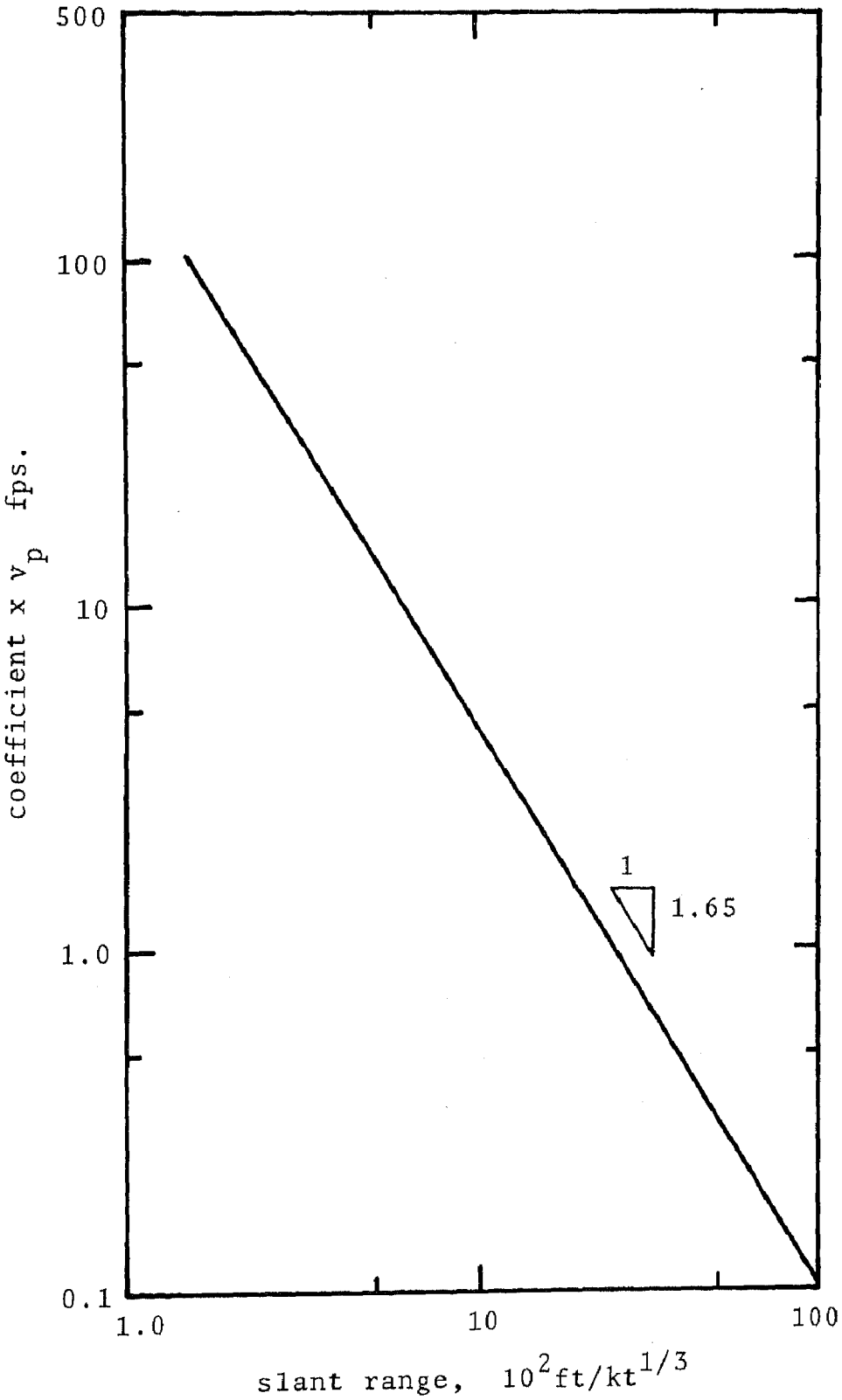

Figure 47. Composite correlation of first particle velocity peaks, scaled to 1 KT, for detonations in salt, NTS granite, and tuff. {Ref. Sauer et al. (63)}

APPENDIX E

COMPUTER FLOW DIAGRAM FOR THREE-ELEMENT PLANE WAVES

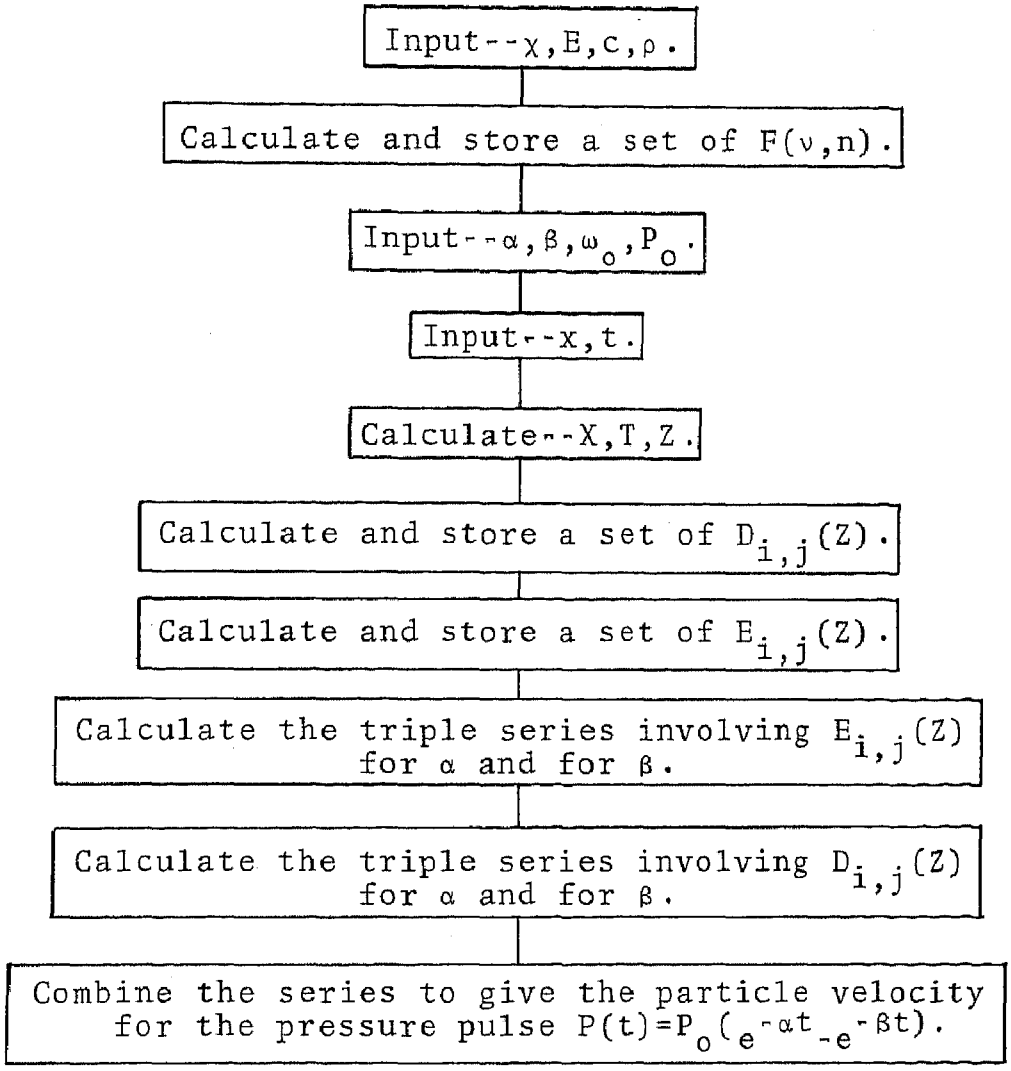

APPENDIX F

SOLUTIONS BY NUMERICAL INVERSION

One check on the validity of the series solutions of Chapters IV and V was that they approach the appropriate elastic cases as ω_o becomes large. In order to obtain an additional check on their validity, a numerical inversion technique was employed. Particle velocity curves were obtained for the elastic and Voigt spherical, and plane three-element models.

The numerical inversion technique employed was that reported by Allen and Robinson (64). A summary of their method follows.

The one-sided Laplace transformation of a function f(t) is given by

$$F(s) = \int_0^\infty e^{-st} f(t)\, dt. \tag{107}$$

It is assumed that F(s) is known and that it is required to find f(t). If one substitutes

$$t = (1/\sigma)\ \ln(1/\sin r) \tag{108}$$

into equation 107, the result is

$$F(s) = (1/\sigma) \int_0^{\pi/2} \cos r\ (\sin r)^{s/\sigma - 1}\ g(r)\, dr \tag{109}$$

where

$$g(r) = f\left[(1/\sigma)\ \ln(1/\sin r)\right] .$$

If s/σ is allowed to take on integral values of 2k, where k is an integer, equation 109 can be rewritten:

$$F(2k\sigma) = (1/\sigma) \int_0^{\pi/2} \cos r \, (\sin r)^{2k-1} \, g(r) \, dr. \qquad (110)$$

The function g(r) defined on the interval $(0,\pi/2)$ is expanded in a sine series

$$g(r) = \sum_{n=1}^{\infty} c_n \sin 2nr. \qquad (111)$$

In order to obtain the coefficients c_n, the product $\cos r \, (\sin r)^{2k-1}$ is also expanded in a sine series

$$\cos r \, (\sin r)^{2k-1} = \qquad (112)$$
$$(1/2^{2k-1}) \sum_{j=0}^{k-1} (-1)^{k-j-1} \left[\binom{2k-1}{j} - \binom{2k-1}{j-1} \right] \sin 2(k-j)r$$

where

$$\binom{2k-1}{-1} = 0.$$

Substitution of equations 111 and 112 into 110 and integration, by orthogonality gives

$$2^{2k-1} \sigma F(2k\sigma) = \pi/4 \sum_{j=0}^{k-1} (-1)^{k-j-1} \left[\binom{2k-1}{j} - \binom{2k-1}{j-1} \right] c_{k-j} \qquad (113)$$

The constants c_n can be obtained from equation 113 by substituting k = 1, 2, ..., n:

$$c_1 = (4/\pi) \, 2\sigma \, F(2\sigma)$$
$$c_2 = (-4/\pi) \, 2^3 \sigma \, F(4\sigma) + 2c_1$$

and

$$c_k = (-1)^{k-1} \, (4/\pi) \, 2^{2k-1} \sigma \, F(2k\sigma) + \qquad (114)$$
$$\sum_{j=1}^{k-1} (-1)^{j-1} \left[\binom{2k-1}{j} - \binom{2k-1}{j-1} \right] c_{k-j}.$$

The inverse function f(t) can be found for any value of time t by substituting

$$r = \sin^{-1} (e^{-\sigma t}) \tag{115}$$

into equation 111, where f(t) = g(r).

Although the choice of σ is arbitrary, the rate of convergence of the sine series (equation 111) depends on its magnitude. Allen and Robinson found that approximately 0.8n significant figures were required to compute n of the c_n coefficients. In all of the numerical inversions of Figures 48, 49, and 50, the series was carried to twenty terms since a double precision routine on the IBM 360 computer permitted sixteen significant figures to be carried. It was thus necessary to choose a value of σ which would give rapid convergence.

Since one of the primary objects of performing the numerical inversion was to check the series solutions of Chapters IV and V, a choice of σ was made by comparing the numerical solutions with the closed form solutions for the spherical elastic problem. Sigma was chosen to be 13.5, since that value appeared to give the best agreement with the spherical elastic particle velocity (at r=1.5a) of Figure 7. That value was arrived at by choosing the value of σ which, of the several values investigated, gave a minimum sum of the absolute values of the differences between the exact solution and the numerical inversion. Any choice of σ between 10 and 16 gave acceptable results, but the optimum choice appeared to lie between 13 and 14.

In Figures 48, 49, and 50, the particle velocity curves of Figures 7, 27, and 39 are compared with the results obtained by numerical inversion. The overall agreement is excellent, with differences generally less than two or three percent. The differences which do exist may well be attributed largely to errors in the numerical inversion since only twenty terms were taken.

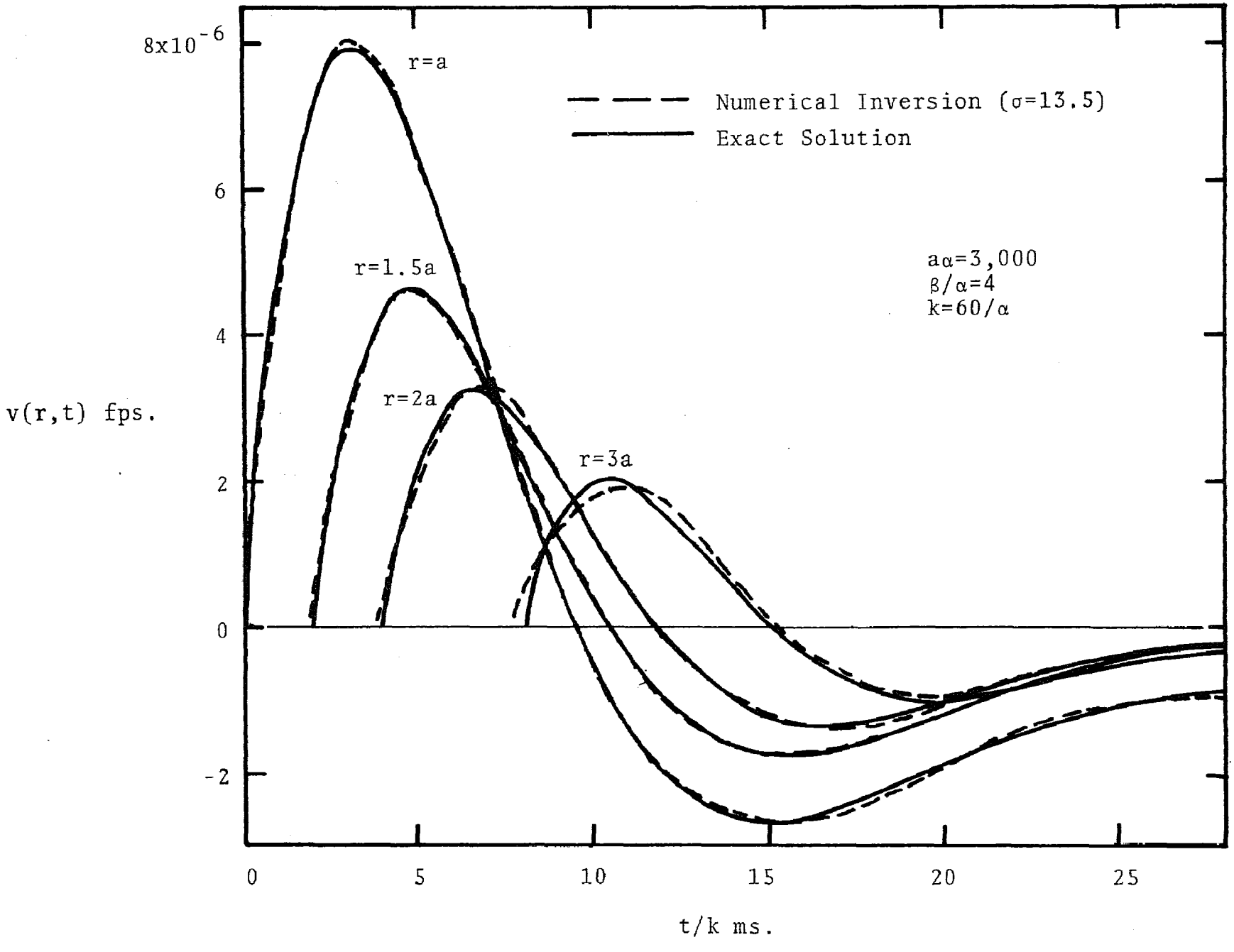

Figure 48. Elastic spherical particle velocity obtained from the exact solution and by numerical inversion.

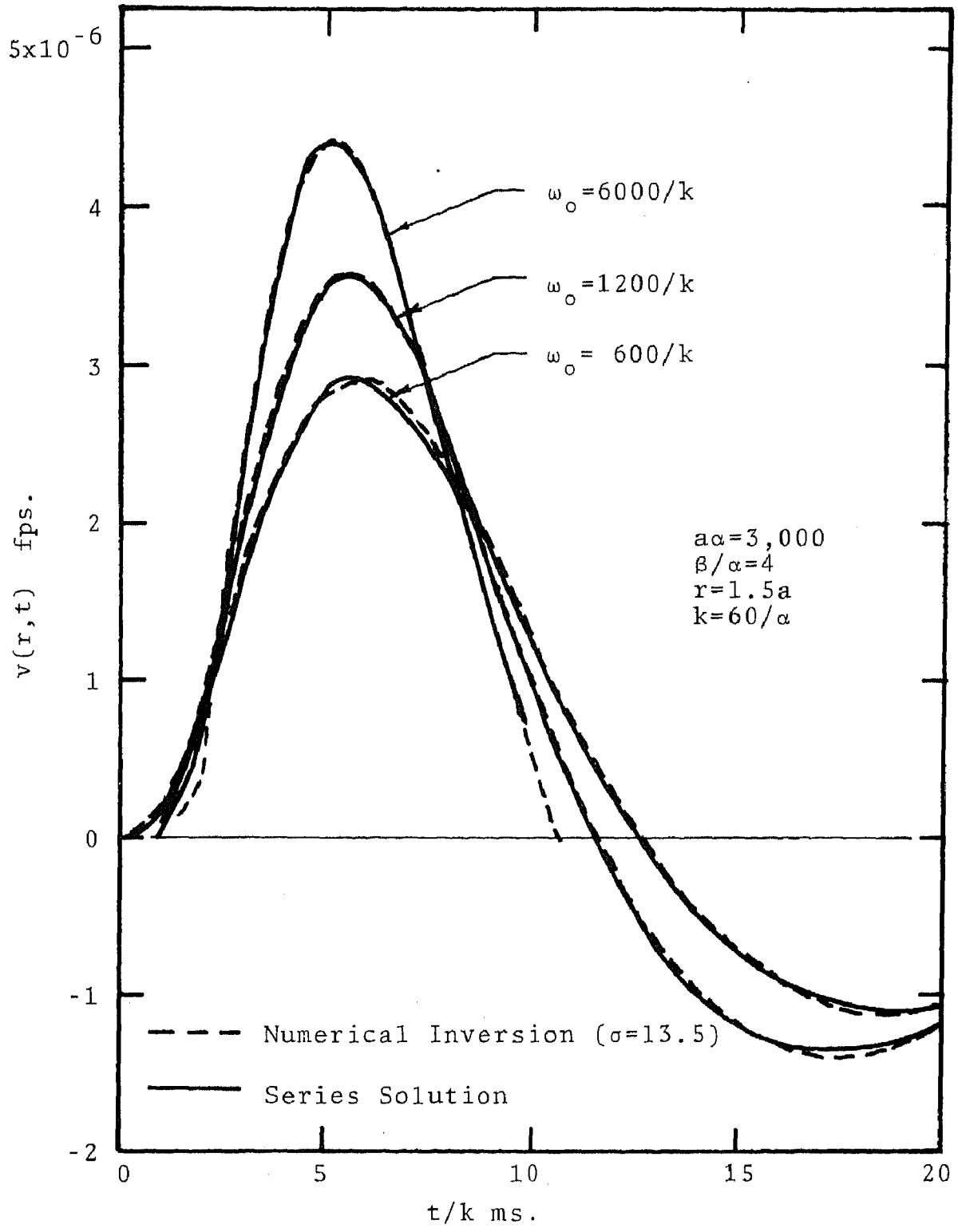

Figure 49. Voigt spherical particle velocity obtained from the series solution and by numerical inversion.

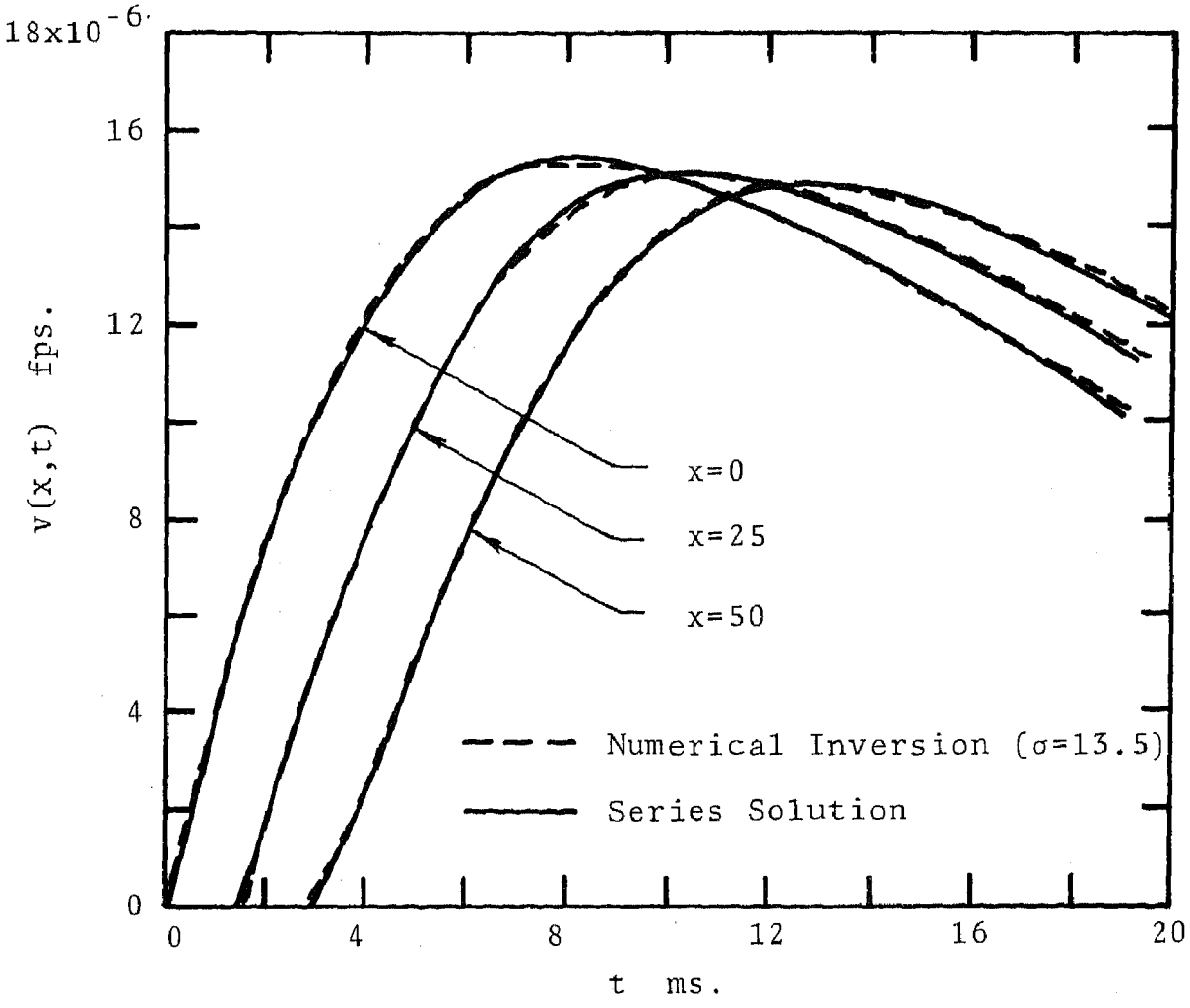

Figure 50. Three-element viscoelastic particle velocity obtained from the series solution and by numerical inversion.

VITA

Edward Eugene Hornsey, son of Lewis E. and Dorothy L. Hornsey, was born May 31, 1937, in Potosi, Missouri. He attended the Potosi public schools and graduated from high school in May 1955. In September 1955 he entered the Missouri School of Mines and Metallurgy from which he received the degrees, Bachelor and Master of Science in Mining Engineering, in May 1959 and 1961, respectively. During his undergraduate work he was the recipient of a four year St. Joseph Lead Co. Scholarship. During the school year 1959-60 he was employed as a graduate assistant in the Mining Department.

From September 1960 until June 1962 and September 1963 to the present time he has been employed as an Instructor of Engineering Mechanics at this institution. Throughout his teaching career he has continued graduate studies on a part-time basis. From June 1962 until September 1963 he was employed as a Mining Methods Research Engineer with the Rock Mechanics Research Group, Applied Physics Research Laboratory of the U.S. Bureau of Mines at College Park, Maryland. His summer experience includes research work in rock mechanics at this institution, geophysical investigations with the St. Joseph Lead Co., and a summer institute in aero-space mechanics at the University of Arizona, Tucson.

On November 26, 1959, he was married to the former Joyce Lorina Albert of Ferdinand, Indiana.